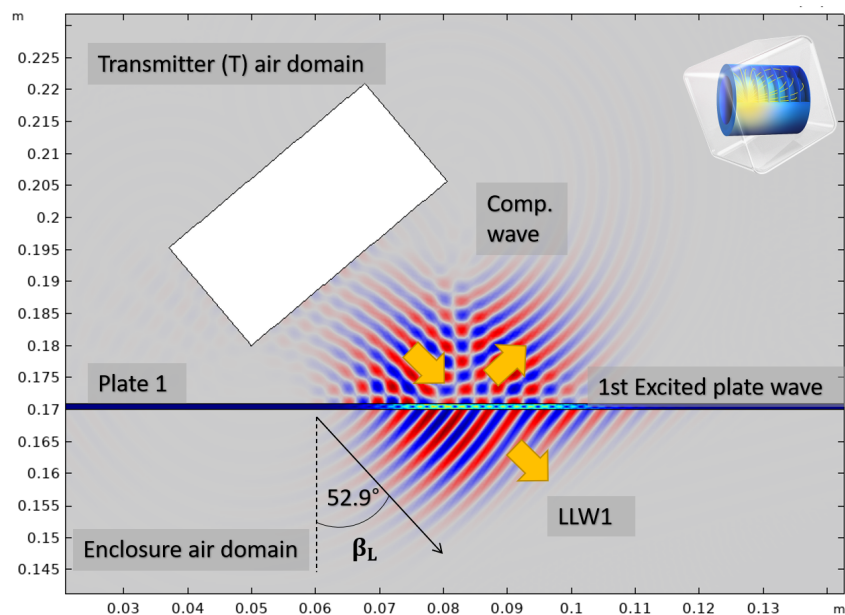FMH606 Master's Thesis 2021
Electrical Power Engineering

Non-intrusive ultrasonic sound detection of internal arc fault in medium voltage switchgear

Tonje Tollefsen

Faculty of Technology, Natural Sciences and Maritime Sciences

Campus Porsgrunn

University of South-Eastern Norway

www.usn.no

Course: FMH606 Master's Thesis 2021
Title: *Non-intrusive ultrasonic sound detection of internal arc fault in medium voltage switchgear*
Pages: *136*
Keywords: *<Switchgear, Internal arc fault detection, Ultrasound, NDT, Sound velocity, Rayleigh-Lamb wave, Snell's Law, COMSOL Multiphysics®>*

Student: *Tonje Tollefsen*
Supervisor: *Elin Fjeld*
External partner: *ABB Electrification Norway AS*

Summary:

Arc fault protection is becoming ever more critical for all power systems to maintain the safety of personnel and reduce damage to expensive equipment. An internal arc fault is an unintentional event within an enclosed power system where the released energy from the arc causes a rapid rise in temperature and pressure. The fast-acting arc fault detection sensors used today require access to the switchgear compartment.

It has become a topic of interest to investigate alternate arc fault detection, which utilizes other means of sensor technology that may prove similar in performance but are non-intrusive. Since an internal electric arc will generate high temperature at a fast rate, and the speed of sound is affected by temperature, the objective of this thesis is to investigate the feasibility of using non-intrusive ultrasonic transducers to detect an internal arc fault within medium voltage switchgear.

This thesis gives a theoretical understanding of the generation of electric arc in the air, limiting systems used in medium voltage switchgear, and how the theory of ultrasound, the speed of sound, and Lamb waves can be used for non-intrusive ultrasonic sound detection of internal arc fault in medium voltage switchgear. Simplified models of the theory were developed and simulated through 5 test cases in COMSOL Multiphysics ® with different parameters and conditions. The results from the simulations showed potential in non-intrusive ultrasonic detection of arc fault using Lamb waves, but should be further investigated with more detailed modeling and actual physical experiments to draw a decisive conclusion.

Preface

This thesis is completed during the spring of 2021 as the final work of the four-semester Master's degree in Electrical Power Engineering at the University of South-Eastern Norway (USN), campus Porsgrunn. The topic of this thesis was suggested by the R&D department of ABB Electrification Norway AS, Skien.

The project description for this thesis is attached in Appendix A. The topic of this thesis is about investigating the feasibility of non-intrusive ultrasonic sound detection of internal arc fault in medium voltage switchgear. The work presented in this thesis will consist of a literature study on the concept of non-intrusive ultrasonic sound transmission through solid materials, the generation and the limiting systems of an internal arc fault, and how the speed of sound changes by the heat generated from an arc fault. After that, several test cases will be conducted to see if the concept can be applied as an arc fault detection technique in medium voltage switchgear. The initial plan for this master project was to investigate the topic by conducting physical experiments with an ultrasonic transducer given by ABB. However, due to some instrumental limitations of the ultrasonic transducer that was provided, it was decided to change the task description, and investigate the topic by conducting the experiments with COMSOL Multiphysics ® simulations instead.

I would like to thank my supervisor Elin Fjeld for her great guidance and assistance for the work and the writing of this thesis. I would also like to thank Shailendra Singh and Magnus Bjerkely for providing me with this thesis problem, and giving me great input upon investigating this very interesting topic. Last but not least, I am immensely grateful for my loving family, and would like to thank them for supporting me and my time as a student.

The picture used on the title page is a simulation snapshot of one of the test cases that was conducted in the COMSOL Multiphysics ® with tags.

Porsgrunn, 19th May 2021

Tonje Tollefsen

Contents

Contents

x

List of Figures

List of Tables

Nomenclature

t_g	ultrasonic Lamb wave transit time between plate 1 and plate 2	[s]
t_L	ultrasonic sound wave transit time between plate 1 and plate 2	[s]
t_R	ultrasonic sound wave transit time between plate 2 and receiver	[s]
t_T	ultrasonic sound wave transit time between transmitter and plate 1	[s]
α_R	Receiver angle	[deg]
α_T	Transmitter angle	[deg]
β_L	Excitation angle of plate Lamb wave	[deg]
λ	wavelength	[m]
ω	angular frequency	[rad/s]
$\vec{\mathrm{E}}_f$	electric field	[V/m]
$\vec{\mathrm{F}}$	force in the direction of the electric field	[N]
ρ	density	[kg/m^3]
θ_1	angle of incident wave in material 1	[deg]
θ_2	angle of incident wave in material 2	[deg]
a	acceleration	[m/s^2]
C	material elastic constant	[N/m^2]
c	wave velocity	[m/s]
c_ideal	wave velocity in ideal gas	[m/s]

Nomenclature

c_a	Compressional wave velocity in ambient air domain	[m/s]
c_g	wave group velocity	[m/s]
c_L	compressional wave velocity in enclosure domain	[m/s]
c_p	wave phase velocity	[m/s]
c_{Long}	longitudinal wave velocity	[m/s]
c_{Trans}	transverse wave velocity	[m/s]
D	distance between plates	[m]
d	plate thickness	[m]
E	Young's modulus	[N/m^2]
e	electron charge	[C]
E_{arc}	electric input energy / arc energy	[J]
f	frequency	[Hz]
F_s	spring force	[N]
G	Shear modulus	[N/m^2]
h	planck's constant	[Js]
i	momentary arc current	[A]
K	bulk modulus	[N/m^2]
k	spring constant	[N/m]
k_B	boltzmann's constant	[J/K]
L	propagation path between plate 1 and plate 2	[m/s]
M	molar mass	[kg/mol]
m	mass	[kg]
p	pressure	[Pa]

R	molar gas constant	$[\mathrm{mol^{-1}}]$
R_h	Receiver height	$[\mathrm{m}]$
r_R	distance between receiver and plate 2	$[\mathrm{m}]$
R_s	specific gas constant	$[\mathrm{kg/m^3}]$
r_T	distance between transmitter and plate 1	$[\mathrm{m}]$
R_w	Receiver width	$[\mathrm{m}]$
T	temperature	$[\mathrm{K}]$
T_h	Transmitter height	$[\mathrm{m}]$
T_w	Transmitter width	$[\mathrm{m}]$
t_{delay}	total time delay between sent and received ultrasonic signal	$[\mathrm{s}]$
u_{arc}	arc duration	$[\mathrm{s}]$
u_{arc}	momentary arc voltage	$[\mathrm{V}]$
V	volume	$[\mathrm{m^3}]$
V_i	ionization potential energy needed for ionization	$[\mathrm{V}]$
V_{L_1}	longitudinal wave velocity in material 1	$[\mathrm{m/s}]$
V_{L_2}	longitudinal wave velocity in material 2	$[\mathrm{m/s}]$
x	spring displacement	$[\mathrm{m}]$
x_g	distance between Lamb wave inlet and outlet in plate 2	$[\mathrm{s}]$
x_L	tangent distance of L	$[\mathrm{s}]$
x_{in}	Lamb inlet	$[\mathrm{m}]$
x_{out}	Lamb outlet	$[\mathrm{m}]$
xp	Lamb wave inlet-outlet seperation	$[\mathrm{m}]$
Z	acoustic impedance	$[\mathrm{kg/m^2 s}]$

xx

1 Introduction

1.1 Background

ABB Electrification Norway is a large producer that offers a wide-ranging portfolio of products, digital solutions, and services that improves and innovates today's electrification technology to be safe, reliable, sustainable, and energy-efficient.

An internal arc fault is an unintentional event within an enclosed power system installation where a large amount of electrical energy gets released in the form of an electric discharge arc. The energy released from the arc is supplied continuously from the available short circuit current flowing through the arc. The consequence from an internal arc fault is temperature- and pressure rise within the enclosure.

Arc fault protection is becoming ever more critical for all power system and process industries to maintain the safety of personnel and reduce damage to expensive equipment. Although the occurrence of an arc fault is rare, it is one of the most severe faults within a power system. The amount of released arc flash energy is a function of time. Due to these reasons, it is critical to develop fast-acting arc fault detection and mitigation technology that can reduce the above mentioned-consequences.

Through the years, the innovation of arc fault detection technology has led to the development of protection system which earths the fault very quickly (less than 10s of ms). Usually, these methods use light detecting diode fed through a glass fiber network to detect internal arc fault. The limitation of such a detection system is that the switchgear compartment must be accessible for installing the fiber or a diode. This brings some challenges when a sealed gas tank (GIS) is involved as important factors like accessibility, leakage, reliability of the electronics, cost, etc, has a significant influence when developing such equipment. Therefore, it has become a topic of interest to investigate alternate arc fault detection, which utilizes other means of sensor technology that may prove similar in performance without the limitations mentioned above.

1.2 Objective

The proposal for the thesis is as follows. An internal electric arc will generate high temperature at a fast rate, and the theory is to utilize this temperature rise as a condition for arc fault detection, and is it possible to do so in a non-intrusive method. Since the sealed enclosure has its large thermal capacitance, it needs a much longer time to detect the temperature rise by a thermal sensor. The speed of sound, however, is affected by temperature. Therefore, the proposal is to use the variation in speed of sound to detect a few 10s or 100s degrees of temperature rise when the temperature of the arc can elevate into a few thousand Kelvins. Through the utilization of ultrasonic sound sensors, investigate if an increase in temperature inside an enclosure will shorten the time delay between sent and received ultrasonic sound signal, and if this is a potentially fast and cost-effective sensor technology that can be stationed outside the enclosure/switchgear as a non-intrusive arc fault detection system.

1.3 Previous work

There seem to be hardly any published studies done on the specific concept of using non-intrusive ultrasonic transducers for internal arc fault detection in medium voltage switchgear. For this reason, the work presented in this thesis will be based on published studies on ultrasonic transducers used in the process industry. This thesis will investigate the feasibility of internal arc fault detection based on the knowledge from the process industry, and implement the ultrasound transmission techniques used in gas flow metering for internal arc fault detection.

Non-intrusive ultrasonic transducers are a practical testing technique used in many industrial applications like material inspection, examination, and dimensional measurements. Ultrasonic transducers is also applicable in the process industry, where the time delay between sent and received ultrasonic signal can be used to measure the gas flow, tank level, etc. Ultrasonic transducers have the benefit in the industry of being installed as a clamp-on ultrasonic flow meter equipment, that does not require pipe/tank modification nor disturb (non-contact) the process fluid, thus making it a non-intrusive measuring technique. There are many types of ultrasonic transducers available for the process industry today. However, these transducers are mainly intended for processes involving liquid fluids, where it is uncomplicated to transmit ultrasound through the tank/pipe walls. Yet, for processes consisting of gas fluids, the transmission of ultrasound through the tank/pipe walls is complex and nearly unachievable. Thus, making the application for internal arc fault detection by transmitting sound through switchgear walls immensely challenging, due to the key problem that sound waves will reflect at a gas-solid interface.

In 2018, z. Fan, W. Jian, W. M. D. Wright did a study on "Non-contact ultrasonic gas flow metering using air-coupled leaky Lamb waves" where they described and developed a model for a completely non-contact ultrasonic sound method using leaky Lamb waves for gas flow metering [1]. It was shown that through careful orientation of the transducer's angle, and strategic selection of the ultrasound frequency, it was possible to transmit sound through an gas-solid interface. The solid is excited by a special type of wave mode called a Lamb wave, which leaks energy into the adjacent air. The leaky Lamb wave ultrasonic transducer technique described in the article will be used in this thesis, and further extended to see if it can be applied as an alternative method for internal arc fault detection. The investigations will be carried out by COMSOL Multiphysics simulations, which will provide a way to visualize and analyze the feasibility of the concept.

1.4 Scope

The scope of this thesis is as follows:

1. Survey on internal electric arc fault generation and limiting systems used in medium voltage switchgear

2. Survey on ultrasound propagation and applications

   - How ultrasound is used for non-destructive testing (NDT)

   - How temperature affects the speed of sound

   - Generation and propagation of Lamb waves (a type of ultrasonic sound wave) in solid plates

3. Develop a simplified model for internal arc fault detection by non-intrusive ultrasonic transducers

   - Analytical model for the time delay between sent and received ultrasonic signal at a constant temperature

   - Analytical model for the time delay between sent and received ultrasonic signal when temperature increases

   - COMSOL Multiphysics model for simulating test cases (with polycarbonate material and steel material)

4. Discuss the test results and the overall feasibility for utilizing non-intrusive ultrasonic transducers for internal arc fault detection in medium voltage switchgear.

1.5 Limitations

- The models developed are simplified, and the gas conditions are considered ideal, in order to avoid excessive complex modelling.

- The dimensions for the models are minuscule compared to the real dimensions of a switchgear, this is to save the immensely long computation time in COMSOL (12-15 hours for the minuscule models, instead of 4-5 days for the real dimensions).

- The simulated tests are not confirmed by real physical experiments, due to lack of available instrumental equipment.

- No testing of SF6 or other pressurized gas used in GIS switchgear

- The temperature increase is based on average values and are non-specific.

1.6 Report structure

Chapters 2, 3, and 4 will cover the fundamental theory necessary to understand the concept used in the simulation tests conducted in this thesis. Chapter 2 will introduce the reader to the electric arc and the conditions/factors that lead to an electrical breakdown in gas. Chapter 3 describes the basic operation of medium voltage switchgear, and the causes and consequences in the event of an internal arc fault. A short summarization of the passive and active limiting systems used today to mitigate the effects of an internal arc fault is shown. Afterward, the reader will be introduced to the fundamental theory behind ultrasonic propagation and applications. Chapter 5 explains the general concept of how ultrasonic transducers can be used to detect an internal arc fault of a medium voltage switchgear using leaky Lamb waves. A simplified model for analytically calculating the time delay between send and received signal during an arc fault temperature rise is presented. The approach for developing the COMSOL Multiphysics® models is shown in chapter 6. Chapter 7 presents the different simulation test cases, where the results from the simulations and analytically calculations are analyzed and discussed. Discussion about the feasibility of utilizing non-intrusive transducers for internal arc fault detection in medium voltage switchgear will place in chapter 8. Finally, the conclusion of the Master's Thesis and recommendations for further work is shown in chapter 9.

2 Electric arc

This chapter covers the basic theory of how an electric arc can be generated in gas, some of the different mechanisms and conditions contributing to forming the electric arc, and how the arc can be regarded as a heat emitting energy source.

2.1 Electrical conduction

When a material is subjected to an electric field, a flow of electrically charged particles will arise. The electric field is typically produced by a voltage potential difference applied between each end of the material. The movement of electrically charged particles along the material's conducting path is commonly known as an electric current. The charged particles can be described as charge carriers, and their conducting properties depend on the state of the material (i.e., solid, liquid, and gas). In solids like metals, the cloud of free electrons acts as the charge carriers because they are capable of moving freely within the conducting crystal structure of the solid. In electrolytes (liquid) and plasma (gas), the charged carriers are free electrons and ions (which are atoms or molecules that have acquired or removed electrons, making them electrically charged). [2].

Materials with a considerably large concentration of charge carriers, such as solid metals, can conduct a high amount of electric current with a given electric field. A material with high conducting ability is regarded as an electrical conductor. A material with few charge carriers will conduct a smaller amount of current with a given electric field and is regarded as an electrical insulator. But it is important to note that the conducting abilities of the material may vary when the conditions surrounding the material change (like temperature or electric field). Present work in this thesis will focus on how electrical conduction in gases may occur when influenced by conditions like the temperature or the electric field. [2].

Gases are generally regarded as effective insulators against electrical conduction. However, this is highly dependent on the magnitude of available charge carriers in the gas. Several different causes can increase the magnitude of charge carriers, and consequently decrease the insulating properties of the gas. As a result, the gas may become an electrical conductor. In this case, we have an electrical breakdown of the gas, and the current flowing through the gas is commonly known as an electric arc. The electrical breakdown in gas forming an electric arc between to electrodes is shown in figure 2.1 [2]

Figure 2.1: An electric arc formed in the gas gap between two electrodes [3]

2.2 Breakdown mechanisms in gas

The mechanism by which the conductivity of a material change from insulating to conductive is called an electrical breakdown. The breakdown mechanisms in gas consists mainly of ionizing the gas molecules so that the number of charge carriers (electrons and ions) is increased. When the gas contains a sufficiently high amount of ionized molecules and atoms, the gas has reached the so-called plasma state. The Plasma state can be achieved by thermally heating the gas, thereby initiating several ionization mechanisms, or exposing it to a strong electric field, where an electron avalanche (Townsend discharge) may occur in the electric field. Therefore, an electrical breakdown happens in the normally non-conductive gas when the plasma state has been established by ionization, and an electric current flows through it. [4]

2.2.1 Ionization mechanisms

The most common types of ionization mechanisms that can occur in a gas are listed as follows: [4]

- Photoionization

- Thermal ionization

- Collision ionization

Photoionization   A gas molecule that is exposed to electromagnetic radiation at a given frequency can cause ejection of electrons of that molecule. A Photon is the quantum of light and energy associated with the electromagnetic field, which can be expressed with the following equation: [4]

$$W_f = h \cdot f \tag{2.1}$$

where f : frequency of the photon   [**Hz**]
        h : Planck's constant $= 6.626 \cdot 10^{-34}$ [**Js**]

Photoionization to molecules happens at random. From the equation, we can see that an increase in frequency can lead to an increase in photon energy, which means that the chance of photoionization may increase. However, photoionization is still a rare occurrence in air, and is thereof little importance in practical terms. [4].

Thermal ionization   Molecules flying in gas are in a constant motion, and have an average kinetic energy. The average kinetic speed of molecules in gas can be expressed with the following equation: [4].

$$W_t = \frac{3}{2} k_B T \tag{2.2}$$

where T : Temperature   [K]
        k_B : Boltzmann's constant $(= 1.381 \cdot 10^{-23})$ [J/K]

A molecule in gas may ionize when it is exposed to energy above a certain threshold. This is known as the ionization energy of the gas, and it can be accomplished with an increase in temperature. An increase in temperature causes the kinetic energy of particles to rise, which can consequently lead to particles becoming ionized if the kinetic energy of

the particle exceeds the thermal ionization energy threshold. [4]. The degree of thermal ionization in gas can be explained with the Saha equation: [5]

$$\frac{x^2}{1-x^2} \cdot p = 3.16 \cdot 10^{-7} \cdot T^{\frac{5}{2}} \cdot e^{-\frac{eV_i}{k_B T}} \tag{2.3}$$

where x : degree of ionization
 p : atmosphere pressure [Pa]
 T : temperature [K]
 V_i : ionization potential energy needed for ionization [V]
 e : electron charge $(= 1.602 \cdot 10^{-19})$ [C]
 k_B : Boltzmann's constant $(= 1.381 \cdot 10^{-23})$ [J/K]

The Saha equation describes that the degree of ionization increases fast with temperature. Consequently, the conductivity of air increases with temperature. The conductivity of air as a function of temperature, where the arc is at atmospheric pressure, is illustrated in figure 2.2. Thus, it is reasonable to argue that gas changes its ability from being a reasonably good insulator to a conductor by raising the temperature of the gas by a few thousand Kelvin . [5]
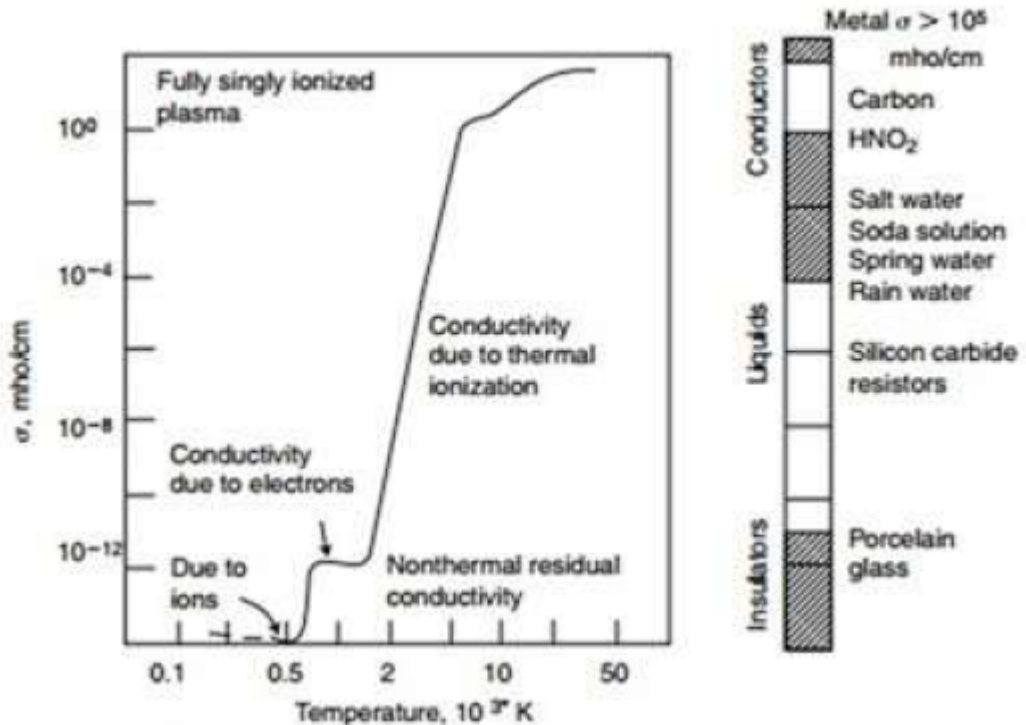
Figure 2.2: The conductivity of air as a function of temperature [5]

Collision ionization   Since molecules in a gas are in constant motion, they will often collide with one another. The velocity of the molecules is associated with kinetic energy. If the kinetic energy exceeds the ionization energy threshold of the molecule during a collision, it may result in electrons breaking free from the molecule. The kinetic energy of the gas molecule can be expressed with the following equation: [4]

$$W_k = \frac{1}{2}mv^2 \tag{2.4}$$

where m : Mass of the molecule   [kg]
           v : Speed of the molecule   [m/s]

It is important to note that the molecule velocity is not constant and may vary with temperature. Therefore, the velocity of the molecule is generally given statistically around a mean value. [4]

2.2.2 Townsend discharge/Electron avalanche

The electric field between the two conductors depend on distance and applied voltage. The free electrons and ions between the gap will be subjected to an electric field which causes a force to be exerted on the particles, as expressed in the following equation: [4]

$$\overrightarrow{\mathrm{F}} = q \cdot \overrightarrow{\mathrm{E}_f} \tag{2.5}$$

where $\overrightarrow{\mathrm{F}}$: force in the direction of the electric field   [N]
           e : Charge of the particle (= - 1.602 $\cdot 10^{-19}$)   [C]
           $\overrightarrow{\mathrm{E}_f}$: Electric field   [V/m]

The force will accelerate the electrons in the opposite direction of the electric field (from cathode to anode). The strength of the electric field is determined by the applied voltage, which also defines the electron's speed. Electrons in movement may collide with other atoms on their way to the anode. If the speed of an electron is significantly high when it collides with an atom, it may initiate collision ionization, which is an ionization mechanism, as was previously explained above. The collision may result in additional free electrons being released, which will also be accelerated by the applied electric field, and may once again collide with other atoms. Because of this, frequent repetition of molecule collision will cause an ionization mechanism called the electron avalanche. This phenomenon was discovered by John Sealy Townsend, hence why the electron avalanche is commonly called the Townsend discharge. Over time, Townsend discharge in gas will

lead to the gas reaching the so-called plasma state, where the gas contains more charged particles than neutral gas. Eventually resulting in an electric current flowing through the plasma, thus bridging the gap between the conductors with an electric arc. The avalanche mechanism is illustrated in figure 2.3. [4][6]

2.3 Electric input energy

An electric that burn between two electrodes generates energy that leaks to its surrounding. The energy from the arc is transferred through different energy transferring mechanisms like conduction, radiation and convection. Therefore, the arc can be regarded as an energy source. The total energy from the electric can be calculated by the electric energy input to joule heating, which the following equation can express: [7]

$$E_{arc}(t) = \int_0^t i(\tau)u_{arc}(\tau)d\tau \qquad (2.6)$$

where E_{arc} :   electric input energy / arc energy   [J]
        t :   arc duration after arc initiation   [s]
        i :   momentary arc current   [A]
        u_{arc} :   momentary arc voltage   [V]

This expression is for a single phased arc. For a three-phase arc, the energy dispersed in each phase must be added together in the expression. the arc voltage depend on: [7]

- Fault current

- Cooling of the arc

- Arc length

- Electrode material

- Melting and vaporization of electrode material affect the arc length

- Electrode erosion from the electrodes increases the gap, thereby increases the arc length

- magnetic forces extends the arc length. The magnetic forces changes over time, which creates erratic movement of the arc.
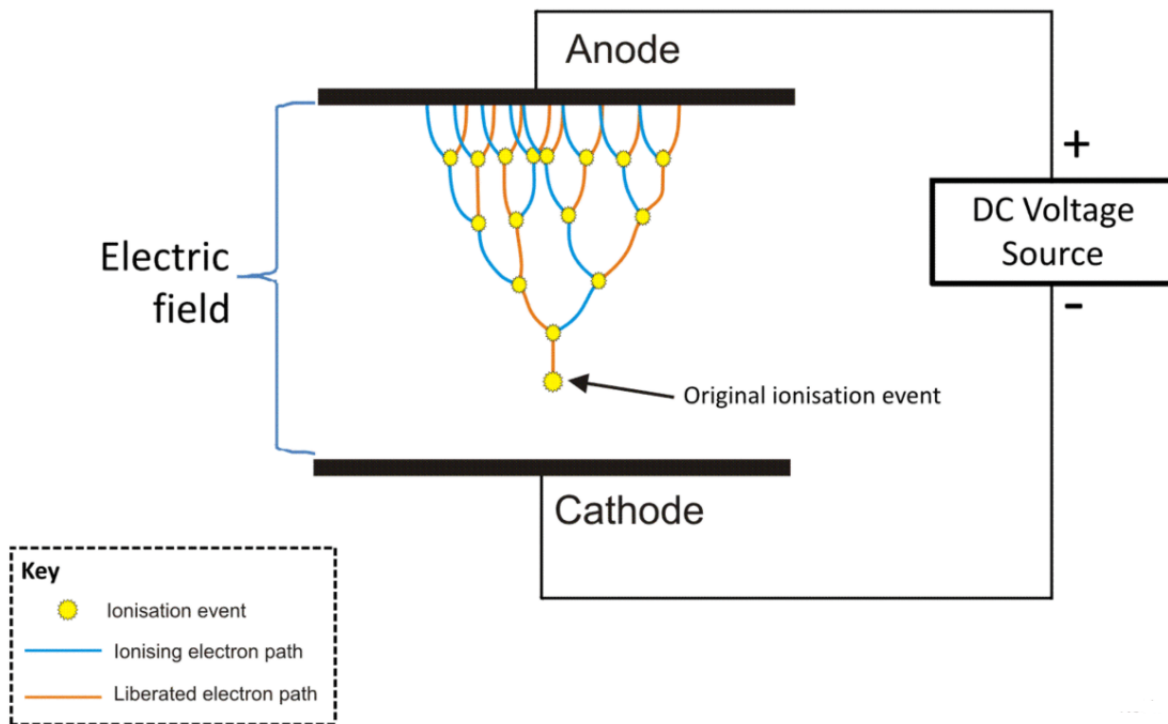
Figure 2.3: This figure illustrates how the Townsend avalanche effect starts with ionisation of an atom where one electron is liberated. The electron will collide with other atoms and each successive collision will further liberate more electrons. Eventually, there will be a full-blown electron avalanche in the gas, where there are more charged particles than neutral gas. [6]

2.4 Plasma state

Plasma is the state of a gas which contains a great number of charge carriers consisting of free electrons and charged ions. The plasma state can be achieved by increasing the temperature in the gas, or by exposing it to a strong electric field. An increase of temperature of or a strong electric field will initiate several ionization mechanisms in the gas, as described in the previous chapters. Ionization in the gas increases the conducting abilities of the plasma gas, and a continuous arc may flow between two electrodes. The electric arc is formed between the electrodes with a luminous glow. As the arc flows between the electrodes there are continuously ongoing processes of ionization, dissociation and ion recombination, as shown in figure 2.4. [5]

In order for the arc to burn in the air continuously, it needs an electron path that are constantly replenishing itself. Due to the high resistance in air, the current path where the arc is burning will generate a substantial amount of heat. Hence why the electric arc can be generally regarded as an energy source. This will ionize the surrounding air even further, thus replenishing the plasma with more ionized gas. As described earlier, the increased temperature from the burning arc will increase the kinetic energy and speed of the particles, which will consequently rapidly collide with other particles, further ionizing the air and maintaining the plasma state in the gas. Therefore, an electric arc may continue to burn by the self replenishing plasma, unless it is interrupted by external forces, for example an interruption/earthing device. [5]
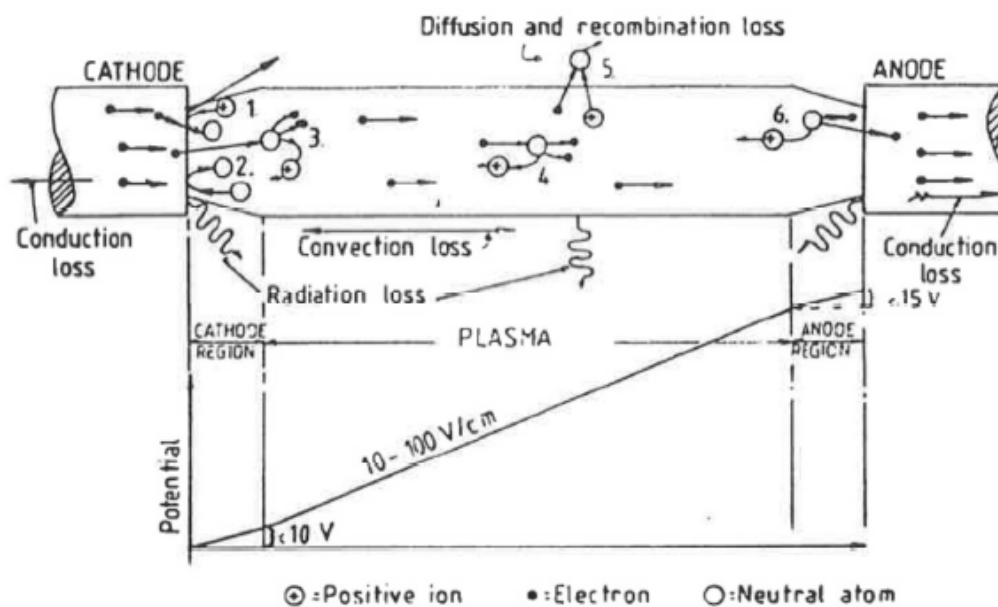
Figure 2.4: Electric arc conduction by plasma gas between two electrodes. The forces involved with transporting electrons from cathode to anode initiates ionization, dissociation and also recombination of ions in the air. [5]

2.5 Electrical discharge

It has been theoretically established that an electric arc is the transmission of electricity through a normally non-conductive material, such as gas. Sufficiently high temperature can cause the gas to transform into a plasma state, containing an abundance of free electrons and molecules as charge carriers. Once the gas is in a plasma state, a current is allowed to flow through it, as an electrical discharge current. The electric arc can be continuous as long as the electric arc's releases heating energy to contribute in creating more free electrons from the surrounding neutral air. The electric arc is visually recognizable as a bright flash, and omit hot gases, which exposes the plasma to a buoyancy that bends the current into an upward arc shape, hence the name electric arc. Electric discharge takes on many different forms, and the electric arc is the special kind of electrical discharge that conducts currents typically from 1 A up to more than 100 kA, with a voltage ranging from 10 to 1000 volts. The different electric discharge regimes are illustrated in figure 2.5, where the electric arc can be seen on the-right hand side of the figure. [4][5][7]
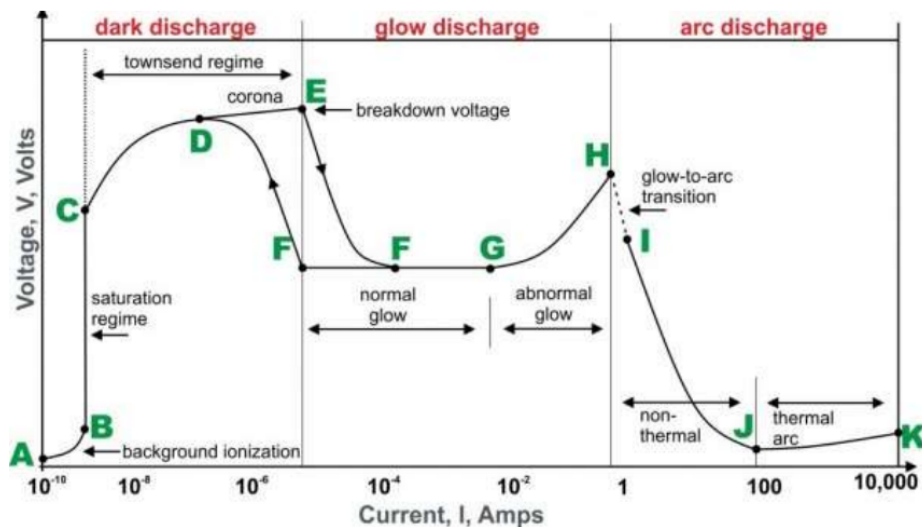
Figure 2.5: Electrical discharge regimes [5]

From the figure, we can see the variation in voltage drop, and that the Townsend avalanche occurs on C-E slope. Beyond E, ionization is sustained and partial discharges occurs in air, otherwise known as corona effect, which is recognized by a glow at the most concentrated electric field geometric point. After H, the partial discharge transitions to a full bridged arc. It is important to note that an arc may be initiated without a preliminary Townsend discharge. For example when conducting contacts separates, which is common and unavoidable in some switching operations. However, this thesis will focus on electric arc caused by an internal fault in a medium voltage switchgear. [5].

3 Medium voltage switchgear

This chapter covers the basic theory of medium voltage switchgear design and functions. The different causes and consequences for an internal arc fault, and how one can limit the consequences with passive and active limiting systems. Further on, a list of the different electric arc detection sensors will is shown. A simplified method for calculating the temperature rise and pressure rise from an electric arc is established.

3.1 Electricity distribution system

The power grid is an essential and extensive infrastructure in our society that makes it possible to transfer electricity between the producer and the consumer in an efficient and secure way. The Norwegian power grid consists of three levels: the Central grid, Regional grid, and Distribution grid. [8] Each grid level with each associated voltage range is shown in figure 3.1. Medium voltage is a voltage class that traditionally range between 1000 volt and 52 kilo volt. Medium voltage switchgear is typically used in transformer stations between the regional grid and distribution grid, as depicted in figure 3.2. [9]
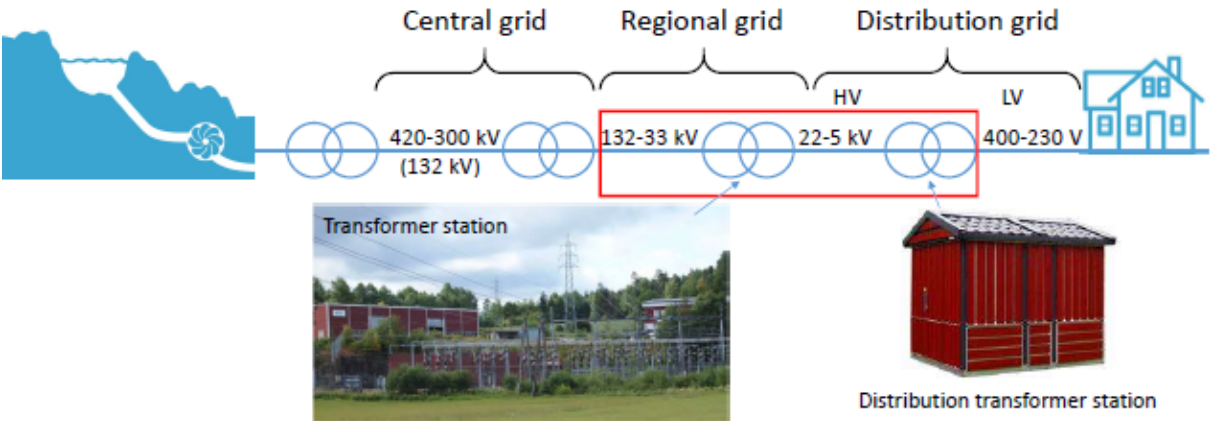
Figure 3.1: The Norwegian power grid illustrated with the associated voltage of the Central grid, the Regional grid, and the distribution grid. Medium voltage switchgear is typically found in transformer stations between the regional grid and distribution grid. [9]
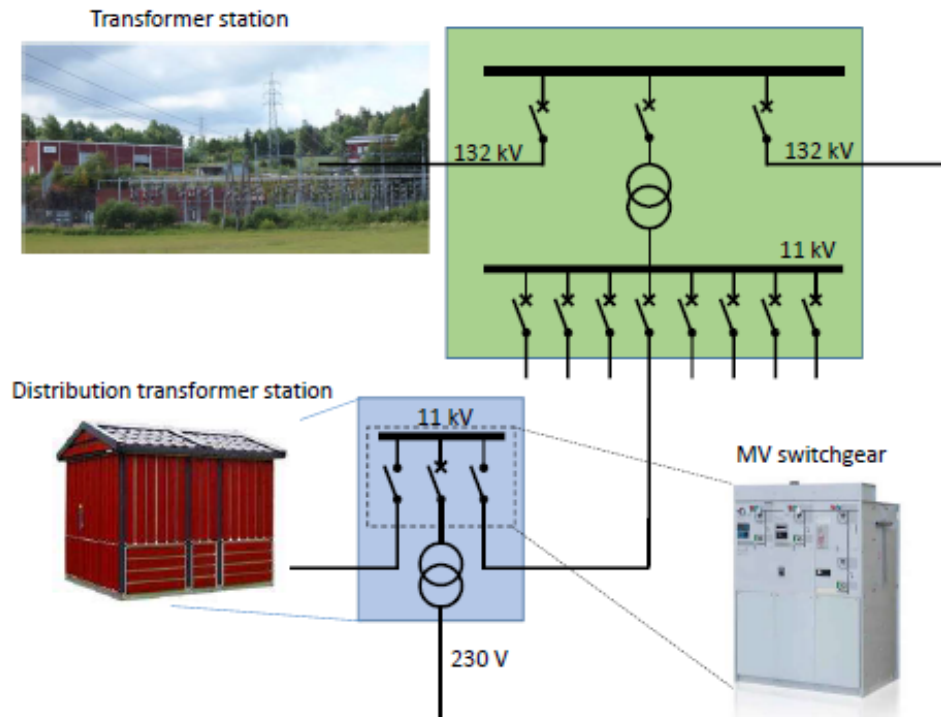
Figure 3.2: Medium voltage switchgear is typically used in distribution transformer stations because it consists of the necessary electric protection equipment and switching devices. [9]

Figure 3.2 shows that a transformer station distributes the power supplied from the central grid busbar over several lines. From there, the power gets additionally distributed over the distribution grid with several distribution transformer stations. In order to control, isolate and protect the lines, most lines are installed with switching devices (disconnectors, grounding switches, circuit breakers) and other components for electricity transmission and protection (voltage transformers, power compensation reactors and capacitor banks, surge arrestors, etc.). Most of the switching devices involving protection and isolating operations for distribution lines are collected inside the medium voltage switchgear, as shown in bottom right corner of figure 3.2. The configuration of a transformer station may vary depending on the trade-off between redundancy and cost. The so-called ring configuration is often used in particularly populated areas, where the distribution transformers are referred to as ring main units (RMU). Ring main units offer the great advantage of isolating faulty parts of the ring while still maintaining service to the remaining parts of the ring. These operations are controlled and accomplished with the electrically insulated switchgear. [9]

3.2 Switchgear

Switchgear is one of the main electrical protection equipment in a high voltage electric power system because it is a centralized collection of switches, fuses, circuit breakers, and more. Switchgear is used in distribution systems, transformer stations, and power-demanding industrial facilities. The main purpose of the switchgear is to reliably isolate, control and protect high voltage equipment connected to the power system. Switchgear is intentionally designed to handle the high-power short circuit currents or overloads that may occur while also maintaining service to the unaffected parts of the circuit. Switchgear is also used to de-energize parts of the circuit to enable safe work and maintenance conditions. The compact metal encapsulated structure of the switchgear makes it suitable for indoor and outdoor installations and presents a high rate of personnel safety. Figure 3.3a displays the front panel of typical gas-insulated compact switchgear from ABB. Figure 3.3b shows the insides of a gas-insulated switchgear containing the primary parts of power conduction (busbar, cable-connections) and switches (disconnector, circuit breaker (Vacuum circuit breaker VCB), earthing switch), which will be briefly described with the following text below. [10]
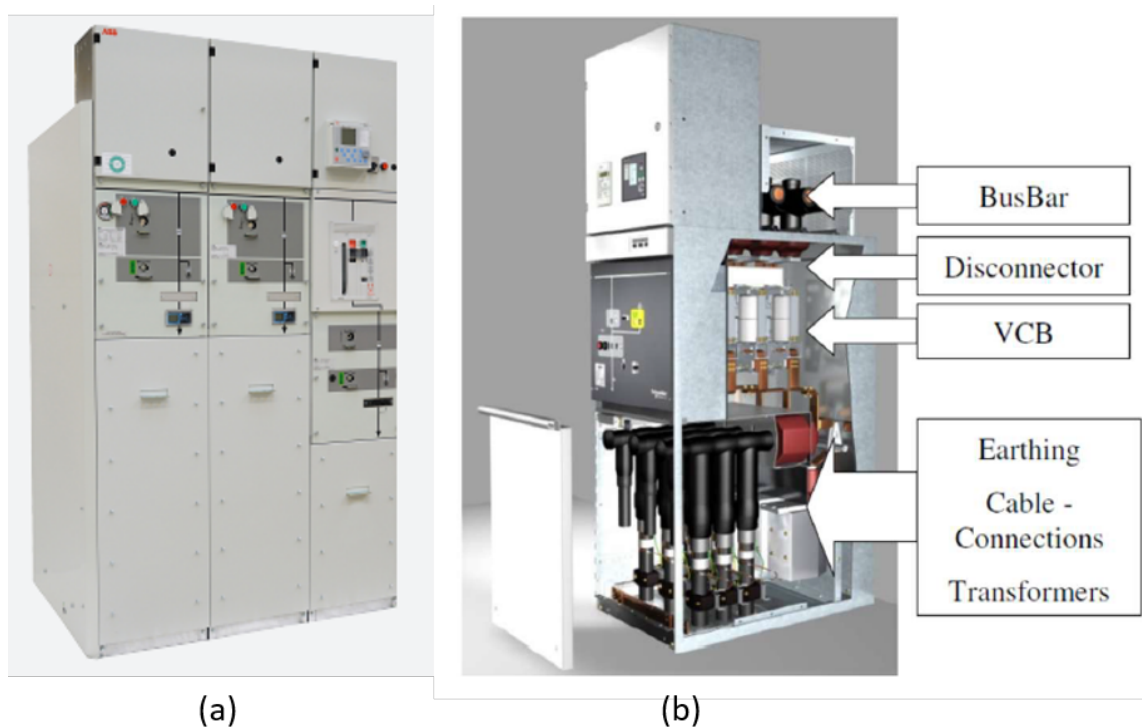
Figure 3.3: (a) Front panel of a gas-insulated compact switchgear from ABB (SafePlus 36) [11] (b) The insides of a medium voltage GIS showing the main components for power transmission and protection equipment (switches) [10]

There are several types of switchgear designs, but the two most commonly used are the gas-insulated switchgear (GIS) and air-insulated switchgear (AIS): [9]

- ***Gas-Insulated switchgear (GIS)***, is shown in figure 3.3a. GIS switchgear houses the electrical components and switching devices inside a hermetically sealed pressurized tank filled with insulating gas. The insulating gas can consist of Sulfur Hexafluoride (SF6) or a mixture of other insulating gases similar to SF6. This type of switchgear is quite space-efficient due to the excellent insulating and cooling properties of SF6, which allows the switchgear to have a reduced distance between the electrical components. [9]

- ***Air-insulated switchgear (AIS)***, houses the power components and switching devices inside enclosed tanks are not necessarily pressurized or hermetically sealed because it uses atmospheric air as the insulating gas. Air as an insulation medium has lower dielectric strength than SF6. Therefore, the switchgear requires more distance between the electrical components. They may be equipped with ventilation openings to enhance the cooling conditions. [9]

Switchgear is equipped with the following primary switching components, which are used to isolate, protect and control different parts in a power system. Some of the primary parts are shown in figure 3.3b. [10] [12]

- ***Earthing switches***, is closed when maintenance work is needed. The equipment is isolated from all sources of electrical energy when the earthing switch is closed. In addition, it directs any residual static discharge to earth, effectively making the contacts safe for personnel to touch. An earthing switch is also used as an "arc-killer" when an internal arc fault occurs. The arc is interrupted by cutting every source of energy supply. [12]

- ***Disconnector switches***, are used to isolate a part of the switchgear. The distance between the separated contacts defines the withstand voltage. Disconnector switches are incapable of breaking load currents and short circuit currents because they can only be opened when the loads are already disconnected from the switchgear. [12]

- ***Load break switches***, must be capable of carrying and interrupting load current under normal operating conditions, including a specified overload condition over a specified time. It is required that a load break switch can handle a short circuit current over a short amount of time, but it is not expected to break it. Breaking a short circuit current is executed by the circuit breakers. [12]

- ***Circuit breakers***, are made to withstand and break currents in both normal and abnormal circuit situations, such as short circuits currents. They have a crucial role in clearing faults that may occur in the circuit. A circuit breaker is the most expensive switching device of switchgear and the most important to ensure a safe and reliable power transmission. [12]

3.3 Internal arc fault consequences and possible causes

An internal arc fault occurring inside a switchgear enclosure causes an extremely rapid rise in temperature and pressure. Over time, the accumulated energy can result in the temperature reaching levels as high as 20 000 K. The rapid pressure rise is caused by the gas volume inside the switchgear expanding from the temperature increase. The pressure rise can get so violent that the resulting forces can cause irreversible mechanical damage to the switchgear equipment and may even puncture the enclosure of the switchgear. This poses as a huge threat to the safety of working personnel in close proximity to the switchgear. If the switchgear walls are punctured from the intense pressure surge or temperature rise, flying debris projectiles, flames, and hot gases can occur from the switchgear. The release of hot gas and flames from an internal arc fault is shown in figure 3.4. [13] [14]

The possible causes of an internal arc fault inside a switchgear may be as follows: [13] [14]

- Faulty equipment (e.g. mounting faults leading with poor connections)

- Insulation material degradation (e.g. ageing of insulation due to electrical stress, gradually leading to arc ignition)

- Underdimensioned and wrong rating of equipment

- Thermal stress, Electrical stress, mechanical stress, pollution, humidity, corrosion

- Faulty human operation, accidents during work (e.g. the operator is inattentive when doing non-permissible work under live conditions that may lead to accidental contacts)

- Intrusion of rodents, reptiles and insects, or foreign objects inside the switchgear (e.g. forgotten/mislaid tools)

- Poorly executed cable connections leading to partial discharges between the contacts.

- Use of equipment that has exceeded its rated service life.

- Inadequate routines for maintenance and cleaning.

Figure 3.4: The potential consequence of an internal arc fault if the switchgear is not capable of handling the pressure and temperature increase [13]

3.4 Systems for limiting the consequences of internal arc faults

Although the occurrence of an internal arc fault in switchgear is extremely rare, it must not be neglected due to the consequences being so severe. To limit the consequences mentioned above, switchgear manufacturers have developed many internal arc fault limiting systems to improve personnel safety and reduce damage to equipment. The limiting systems can be subdivided into two subgroups, which are the passive systems and active systems. [14]

3.4.1 Passive limiting systems

Passive limiting systems reduce hot gases and pressure surges in a passive manner. Passive systems do not need any circuit board or intelligent system for the limiting mechanisms to have an immediate effect on an internal arc fault occurrence. [14]

Pressure relief openings - bursting disc   The purpose of pressure relief openings is to alleviate the pressure build-up from an internal arc fault and avoid any erratic puncture or explosion of the switchgear enclosure. Pressure relief openings are also commonly called bursting discs and are designed to open when the pressure rise exceeds a specific threshold. Hot gases and pressure are allowed to be released through the opening of the

bursting disc. Figure 3.5a shows a photograph of a bursting disc, and figure 3.5b shows hot gases from the arc being released through the bursting disc opening. [15]

Figure 3.5: (a) bursting disc (b) pressure and hot gases released through the pressure relief openings [15]

Switchgear enclosure design Switchgear enclosure is designed and tested to withstand the pressure surges, and the temperature rises to some degree, deforming as little as possible, as the hot gases and pressure rise is released from the switchgear enclosure in a controlled manner. Manufacturers must prove that their switchgear is safe in the event of an arc fault, through IEC tests. The IEC standard 62271-200 is for metal-enclosed switchgear up to 52 kV, and consists of several pass-fail criteria considering the switchgear pressure and temperature rise withstand capability. To pass the requirement, several tests must be performed with positive results from the following criteria: [14][15]

- Doors, covers, and walls must remain closed and intact.

- Fragmentation projectiles cannot exceed an individual mass of 60 gram.

- Arc flames must not burn holes through an accessible part of the switchgear any lower than 2 meters.

- Cotton indicators must not be damaged or ignite from flames and hot gases.

- Ground point connection to the enclosure must remain intact.

Ventilation ducts   In addition to pressure relief openings, switchgear may be designed with ducts that evacuate the pressure and hot gases to controlled areas. Leading the gases away from the switchgear room improves personnel safety and reduces damage to electrical equipment. The duct may be constructed by using an existing conduit in the floor or through walls or by placing the switchgear with a defined distance from the back wall. [14] Figure 3.6 shows two example configurations for ventilation from ABB SafePlus switchgear catalog, where the hot gases and pressure waves are lead through ventilation, as shown by the red arrows. [11]
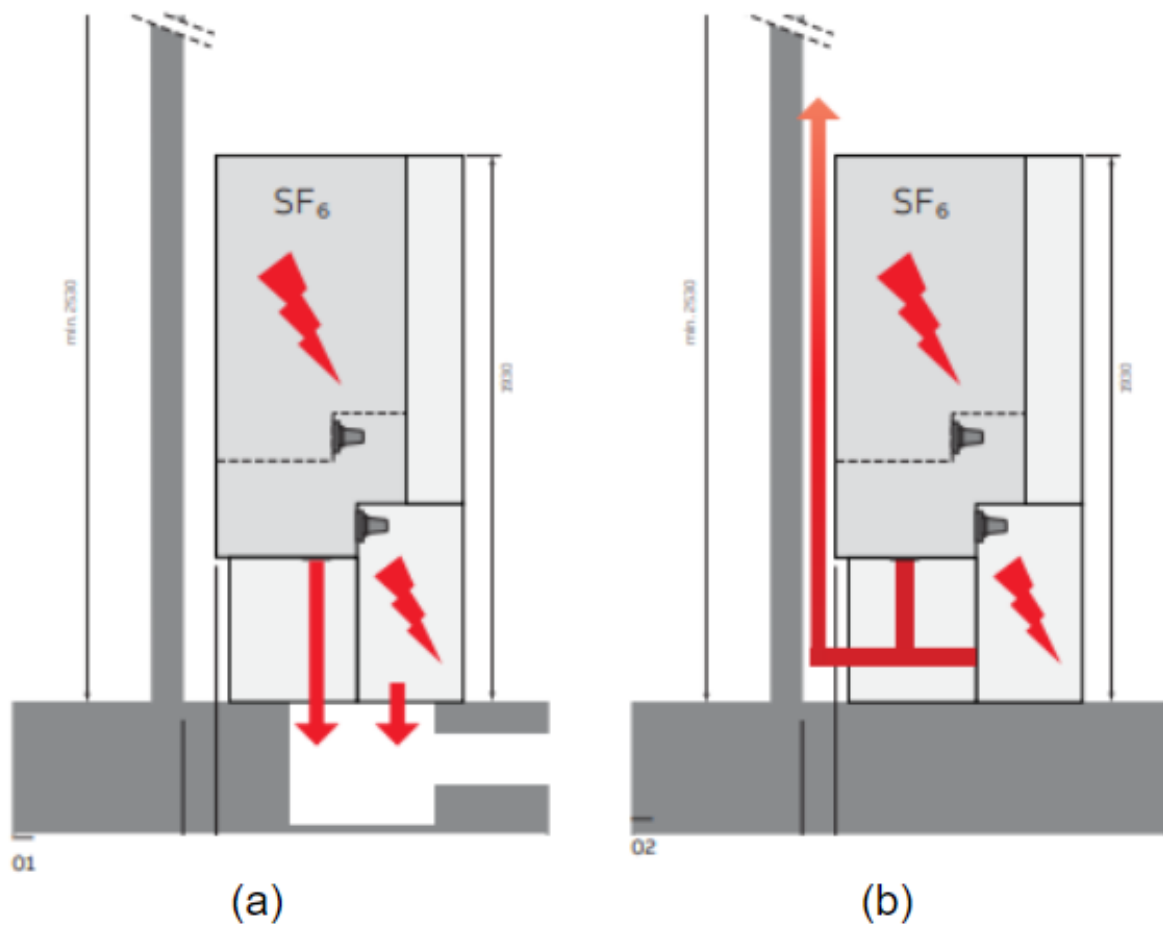
Figure 3.6: ABB Catalog for SafePlus 36 Switchgears ventilation illustrations. (a) hot gasses and pressure are evacuated downwards in the cavity in the floor. (b) hot gasses and pressure are evacuated behind the switchgear and upwards. [11]

3.4.2 Active limiting systems

The electric arc inside the enclosure is regarded as an energy source that converts electrical energy into heat and pressure. The total electric input energy was defined by equation (2.6) as function of momentary arc current *i* and momentary arc voltage u_{arc} over arc duration *t* after arc initiation. We cannot efficiently control the arc fault voltage or arc current to limit the total arc energy. The best option for restricting the dissipated energy is to limit the duration of the arc fault. In order to limit the duration of an arc fault and interrupt it we need an intelligent system that can detect the conditions of an arc fault. Once the intelligent system detects an arc fault condition, it immediately sends a tripping signal to an interruption device that will take action to cut the energy supply, hence the name active limiting system. [14].

The active limiting system for interrupting an internal arc fault can consist of breaking elements combined with protection relays or short-circuiting elements. The breaking elements can be any circuit breaker which trips on command from a protection relay, thereby extinguishing the arc. The protection relay detects a fault depending on the calibration of the relay. Short-circuiting elements are typically fast-acting earthing switches "arc-killer," which short-circuits the arc by connecting all the power supply phases to earth. Tripping of the earthing switch may be initiated with a detection system that detects arc fault conditions (pressure rise, temperature rise, arc light flash). The following text describes the different electric arc detection sensors and how they detect an arc fault condition. [14]

Over current sensors Current sensors are standard equipment included in most switchgears because they provide current reading information. A current sensor can detect the current associated with an arc fault, which can be used as a tripping signal for circuit breakers to interrupt the fault. However, the time required for a current sensor to detect the fault and for a circuit breaker to extinguish the arc is a minimum of 50 ms. This is might be too slow to limit the effects of the arc, as the pressure will have already reached substantial high amounts by that time. Therefore, over current sensors are rarely used as the only sensor in an arc detection system, but may be used as an additional equipment to confirm the signals sent from the following detection sensors. [16][17]

Flash light sensors   A flash light sensor uses optical sensors such as point-sensor or loop-sensors to detect the bright flash of light from an electric arc forming in gas. The point-sensors or loop-sensors are placed inside the switchgear enclosure to monitor the typical locations where an arc fault can occur. The signals from the flash light sensors are sent to a processing unit which evaluates if the signal exceeds a defined threshold, and sends a tripping signal to the earthing switch. These sensors are often combined with over current sensors in order to avoid false alarm tripping caused by light sources other than the arc. The over current sensors provide redundancy and confirmation for arc fault detection. Fiber optic point-sensor and loop sensor are shown in figure 3.7. [16][17]

Figure 3.7: market standard point sensor and fiber optic loop sensor [17]

Pressure sensors   An internal arc fault generates heat inside the switchgear compartment. A rise in temperature results in gas expansion, which means the pressure rises with temperature. Therefore, a pressure sensor can detect this change in pressure and send a tripping signal to a processing unit that controls the earthing switch. The pressure effect could also be directly used as a mechanical linkage in tripping a switching device due to the deformations from pressure rise. [16][17]

The pressure sensor may be installed on the gas tank walls and below the bursting discs of the gas-insulated switchgear, whereas in air-insulated switchgear the pressure sensor may be installed in the roof or rear wall. Both pressure sensor methods are shown in figure 3.8. Pressure sensors offer the great benefit of detecting the increase in pressure before the pressure exceeds the opening pressure threshold of the bursting discs, therefore effectively sending a signal to quench the arc so that the gas tank may remain sealed. Thus, there are no pressurized gas or hot gases that need to be evacuated and can reduce the chance of accidental exposure to working personnel. [16][17]
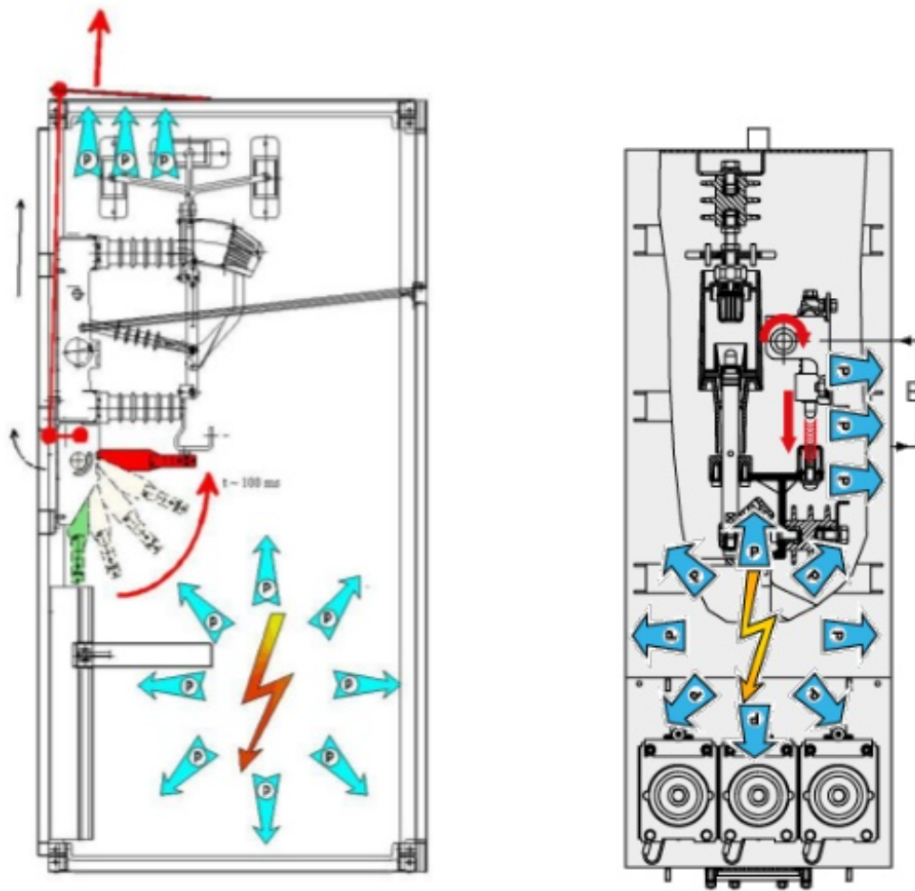
Figure 3.8: Air-insulated (left) and Gas-insulated (right) switchgear pressure sensor method protection [16]

3.5 Simplified pressure and temperature rise calculation

Internal arc fault inside the switchgear arc compartment results in a rapid increase in temperature and pressure. There exist several calculation methods for estimating the pressure rise and temperature rise inside the enclosed switchgear. The following method is a simplified calculation based on the basic model described by CIGRE A3.24 working group published in [18]. This method assumes an enclosed switchgear compartment with volume V, ideal gas conditions, and homogeneous electric arc energy input E_{arc}, which can be found with equation (2.6)

At the beginning of the internal arc fault, the switchgear operates under normal conditions, meaning the switchgear compartment is closed. By assuming ideal gas conditions, the ideal gas law and energy conservation can be applied to determine the increase in temperature and pressure. The ideal gas law is expressed with the following equation:

$$pV = mR_sT \tag{3.1}$$

where
p	:	pressure	[atm]
V	:	Volume	[m^3]
m	:	Mass	[kg]
R_s	:	Specific gas constant	[kg/m^3]
T	:	Temperature	[K]

The specific gas constant R_s is found by calculating the difference between the specific heat constant at constant pressure c_p, and the specific heat constant at constant volume c_v.

$$R_s = c_p - c_v \tag{3.2}$$

For convenience, temperature and pressure are considered independent. However, this assumption is only applicable when the temperature is under the threshold of gas dissociation (6000 K). The heat capacity ratio (κ), also known as adiabatic index, is defined as follows:

$$\kappa = \frac{c_p}{c_v} \tag{3.3}$$

substituting equation (3.2) and (3.3) in the ideal gas law equation (3.1) gives the following equation:

$$pV = mc_v(\kappa - 1)T \tag{3.4}$$

By assuming the pressure rise is only influenced by the increase of gas temperature, a simplification of equation (3.4) can be made and therefore rewritten to show the connection between temperature rise and pressure rise with the following equation:

$$\Delta T = \frac{V}{mc_V(\kappa - 1)} \cdot \Delta p \tag{3.5}$$

The energy necessary for the temperature increase is shown as:

$$E_{gas} = c_V m \Delta T = \frac{V}{(\kappa - 1)} \cdot \Delta p \tag{3.6}$$

Thus, the equation can be rewritten to define the pressure rise as:

$$\Delta p(t) = \frac{(\kappa - 1)}{V} \cdot E_{gas}(t) \tag{3.7}$$

It is important to note that these equations are only valid until the temperature of the gas exceeds 6000 K for air. That is when the molecules in the air start to dissociate, which causes pressure to rise due to the constant formation of molecular fragments. This dissociation process requires energy, which is streamlined from the heat in the air, causing the temperature rise to slow down. [15]

There are some inaccuracies and challenges in estimating the pressure rise from an internal arc fault. For example, it is unreasonable to expect that all of the energy from the internal arc fault will be transferred to the gas. Some of the energy will be lost to radiation in the enclosure walls, and some will be lost to the molecular reaction from the electrodes. The energy transmission can be defined with a ratio between the total electric energy input (2.6) and energy transmitted to heat up the gas with the following thermal transfer coefficient k_p-factor. [15]

$$k_p = \frac{E_{gas}}{E_{arc}} \tag{3.8}$$

This ratio is adjusted based on empirical data through experiments. The usual method on determining the k_p-factor is by observing the pressure rise in the arc compartment, and by substituting (3.8) in (3.7) to get a theoretical calculation that can be compared with the pressure measurements. Then adjusting the k_p-factor according to the comparison. The theoretical calculation for pressure rise is given as: [15]

$$\Delta p(t) = \frac{(\kappa - 1)}{V} \cdot k_p \cdot E_{arc}(t) \tag{3.9}$$

The k_p can be described as a factor on how much energy is needed for an ideal gas to increase the pressure. Through many experiments, the k_p have been found to be around 0.4 to 0.5. The k_p depends on several factors that are hard to measure (i.e. gas density, electrode material exothermal reactions leading to electrode evaporation, gas properties and compartment volume etc.). [15]

The results from pressure rise estimation through this method shows good correspondence to test measurements, as shown in figure 3.9. [15]
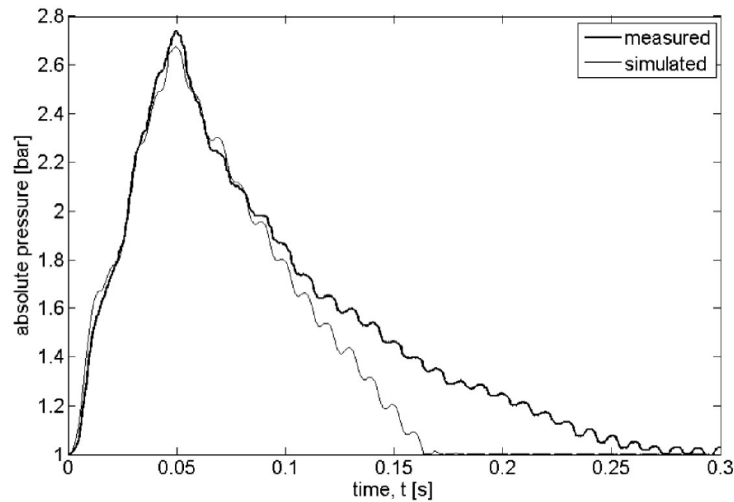
Figure 3.9: simplified pressure rise simulated compared to measured pressure rise [15]

The figure shows how fast the pressure increases from atmospheric pressure 1 atm to 2.8 atm in just 0.05 seconds. After that time, the pressure exceeds the threshold of the bursting discs, and pressure is released through the pressure relief openings. The figure shows how essential it is for the internal arc fault detection system to detect the arc fault condition within milliseconds in order to avoid the consequences of the internal arc fault. Therefore, in the work presented in this thesis, the time it takes for an arc fault detection sensor to detect the arc fault will be a key parameter due to the reasons and consequences that have been mentioned.

The calculation method corresponds to the basic model described by CIGRE A3.24 Working group published in [18]. The basic model includes the calculation of the pressure rise for the entire arc fault duration. However, this thesis will only consider the arc duration before the pressure relief disc opens. After the pressure relief disc opens, conservation of mass flow needs to be considered.

4 Ultrasonic sound propagation and application

Gas-insulated switchgear houses the power conduction components inside a hermetically sealed gas-filled tank. The pressure and flash light sensor described in chapter 3.4.2 have a standard requirement, which is to be stationed inside the switchgear tank in order to effectively detect the effects of internal arc fault (pressure increase and arc light). The drawback of this requirement is that maintenance or replacement for these sensors would consequently involve opening the sealed tanks, which is unfavorable regarding cost and downtime. A Non-intrusive sensor that can be placed outside the switchgear tank has the benefit of being easy to install and easy to maintain/replace. Ultrasonic transducers are commonly used for non-destructive evaluation of material characteristics and process flow metering. Therefore, it would be interesting to look into if the ultrasonic transducer evaluation technique could be applied for non-intrusive arc fault detection in medium voltage switchgear. The ultrasound can be used to monitor the speed of sound because it is influenced by the heat released from the burning arc fault.

Since this thesis aims to investigate the possibility of utilizing ultrasonic sound sensors for non-intrusive internal arc fault detection, it is crucial to know the theory behind the different aspects involving acoustics and ultrasonic testing. This chapter will cover the fundamentals of acoustic sound properties, wave propagation, different modes of sound waves, speed of sound, impedance mismatch, Snell's law, etc. Particular focus will be put on the generation and propagation of Lamb waves, which is essential for understanding how sound transmission through dense materials like steel is possible.

4.1 Ultrasonic testing basic principle and applications

Ultrasound is a sound wave with frequencies above the audible hearing limit for human ears, which is approximately above 20 kHz. Ultrasound is a helpful testing technique used in many industrial applications like material inspection, examination, and dimensional measurements. Ultrasonic testing can be a non-destructive testing technique (NDT) to detect material flaws, cracks, material characterization, etc. In general, ultrasonic testing is based on ultrasonic transducers that emit and capture the reflected ultrasonic sound waves for signal quantification and evaluation. A typical ultrasonic testing system is illustrated in figure 4.1. The figure shows the following equipment that is necessary for ultrasonic testing, which is a pulser/receiver, a piezoelectric transducer, and a display device. The pulser/receiver produces an electrical pulse that will be transformed to an acoustic pulse (sound wave) by the piezoelectric element in the transducer. The sound wave will propagate through the material and lose energy along its wave path due to material discontinuity. The reflected wave echo received by the transducer will convey this energy loss and material discontinuity in the form of an electrical signal. The electrical signal is displayed on the display device, where it can be quantified and processed to reveal useful information about the testing material (i.e. density, sound velocity, the distance that the signal traveled, etc.). [19]
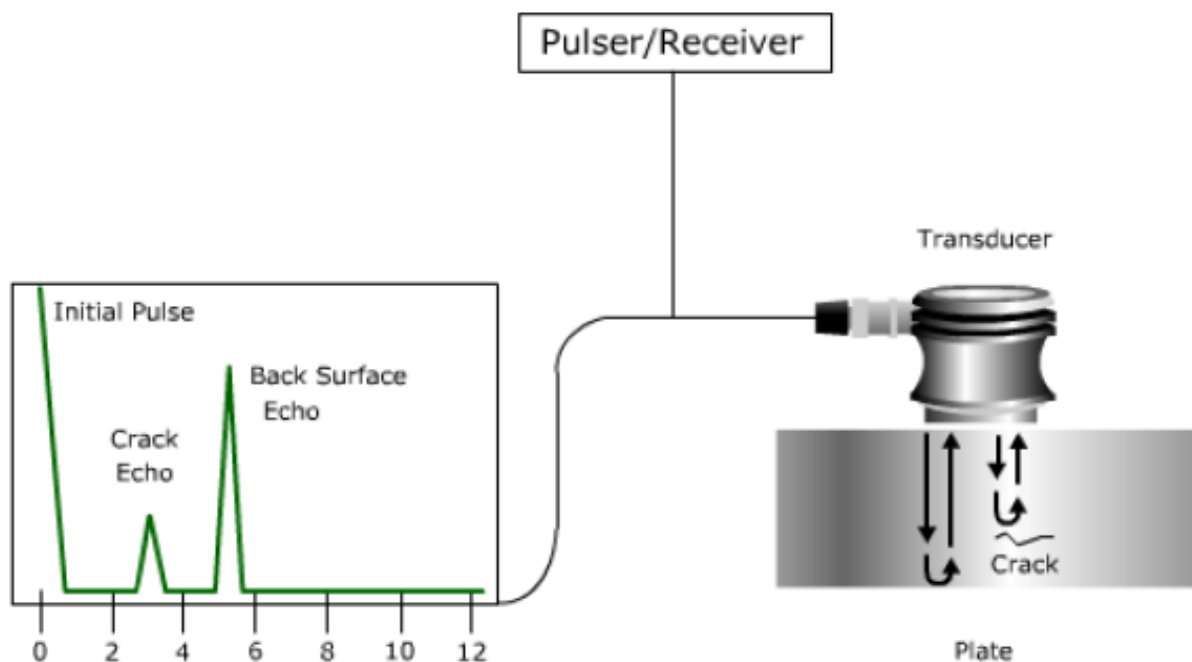
Figure 4.1: A typical illustration of an ultrasonic testing device consisting of pulser/receiver, transducer and display device. [19]

4.2 Sound pressure

Sound is vibration energy that travels through a transmission medium such as gas, liquid or solid by means of particle-to-particle interaction. All materials consist of tiny particles. The energy transfer of sound is carried out by subjecting the particles to a time-varying pressure disturbance, which forces the particles into a vibrational motion about their equilibrium positions. The vibrational motion of particles can take on many different forms, but in simple terms, sound energy transmission is possible due to the forces that arise from particle displacement. Meaning, when a particle is disturbed from rest, it will exert a force on nearby particles, which will effectively force it into a vibrational motion that will once again disturb the next particle. In doing so, the energy transfer of sound is visually similar to a wave. [19]

The pressure, velocity and displacement of the particles vary in space and time. However, it is essential to know that the particles do not follow the sound wave because internal restoring forces arise when a particle is displaced from rest. This, combined with inertia, leads to an oscillatory motion, hence the name sound *wave*. Since the vibrational motion of the particles is, essentially, an elastic oscillation in unison, the sound energy propagating through a material can be viewed upon as a mechanical wave. Particles oscillating in unison is generally referred to in physics as acoustics. [19]

4.3 Modes of sound wave propagation

There are many different modes of sound waves that can occur as it propagates through different material. The different modes of sound waves can be characterized by the different particle oscillatory patterns. However, the mode of a sound wave depends on the material because different materials allow for particle vibration in different directions. For example, solids support the sound wave modes longitudinal waves, shear waves. Additionally, thin solid plates support surface waves. However, in gases and liquids, only the shear wave is supported. Table 4.1 summarizes the wave modes and their particle vibrations that are most relevant for this thesis. [19]

Table 4.1: Sound wave modes

Wave Modes in Solids	Particle Vibrations
Longitudinal (compression)	Parallel to wave direction
Transverse (Shear)	Perpendicular to wave direction
Surface - Rayleigh	Elliptical orbit - Symmetrical mode
Plate Wave - Lamb	Component perpendicular to surface

Longitudinal wave - Compressional wave   In longitudinal waves, the particle oscillation moves in parallel to the direction of wave propagation. Both compressional and dilational forces are present in longitudinal waves. Because of this, the longitudinal wave is also generally referred to as compressional waves. Longitudinal waves are the most common type of sound wave as they are capable of being generated in liquids, gas and solids. The energy transfer of longitudinal waves is based on compression and expansion (rarefaction) movements of the atomic structure and parallel to the wave propagation direction. The upper graph in fig 4.2 illustrates the particle movement of a typical longitudinal wave. [19]

Transverse wave - Shear wave   In transverse waves, the particle oscillation moves perpendicular (or transverse) to the direction of wave propagation. Transverse waves are also commonly known as shear waves. Transverse sound waves is only supported by acoustically solid materials.   Therefore it is not possible for transverse waves to propagate effectively in materials such as gases or liquids. In general, transverse waves have a relatively weaker energy transfer capability compared to longitudinal waves. Transverse waves are usually a product of longitudinal waves, where some of the energy of the longitudinal wave are used to generate the transverse waves in solids. The lower graph illustrated in fig 4.2 illustrates the particle movement of a transverse wave. [19]
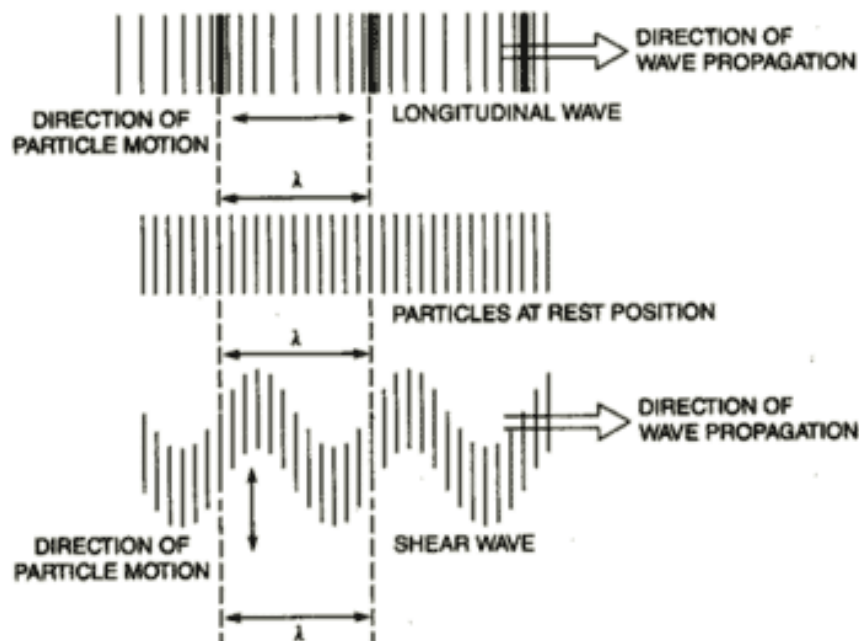
Figure 4.2: Upper graph illustrates longitudinal wave, middle graph is when the particles are at rest position, and bottom graph illustrates transverse waves [19]

Rayleigh wave - Surface wave Rayleigh waves are a type of surface wave that propagates along the surface of relatively thick solid material. The thickness required for Rayleigh surface wave propagation needs to be larger than the depth of one wavelength. Rayleigh wave particle oscillation combines the characteristic particle motion of both longitudinal and transverse waves to create an elliptical path of Rayleigh wave propagation. This elliptical particle motion is shown in fig 4.3. Rayleigh waves are generated on the surface when a longitudinal wave strikes the surface at a defined oblique angle. In general, Rayleigh waves are considered useful in ultrasonic testing for curvy areas that are otherwise difficult to reach other wave modes. [19]
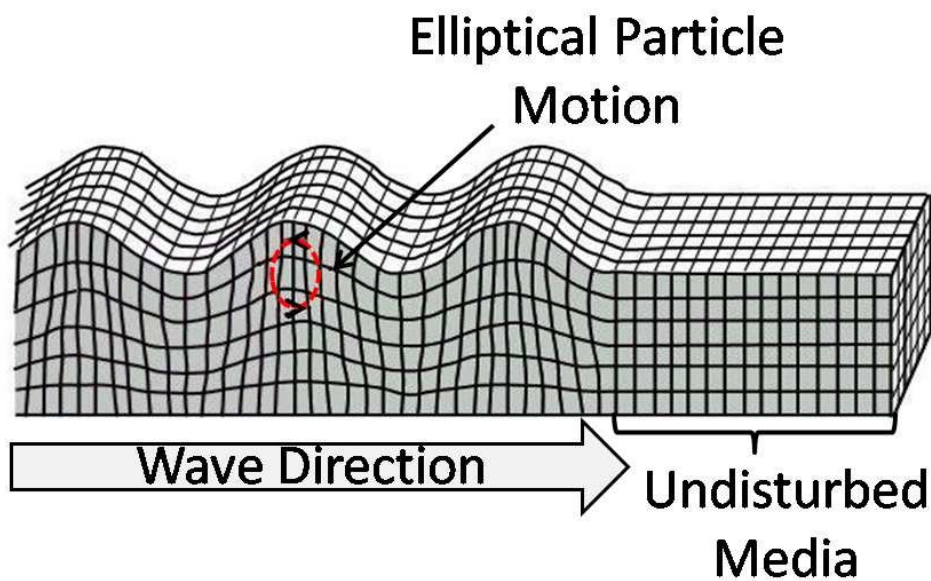
Figure 4.3: Depiction of Rayleigh wave showing elliptic particle motion [20]

Lamb wave - Plate wave   Lamb waves are a complex wave type that is similar to surface waves.   However, they can only be generated in thin plates that are only a few wavelengths thick.   Therefore, Lamb waves are generally referred to as plate waves. Lamb wave propagation is a complex combination of compressional wave and shear wave. The Lamb waves propagates moves parallel to the solid surface throughout the thickness of the material. Lamb wave propagation capabilities depends on the elastic properties and density of the material. Lamb waves are a bit more unique to the previous mentioned sound waves because they are dispersive waves, which means that the wave velocity depends on the wave frequency and material thickness. Greater detail about the velocity dispersion of Lamb waves will be covered in chapter 4.10. [19]

Lamb waves are generated from longitudinal waves when it strikes an interface at a specific angle, hence the name guided plate waves. The incident angle for Lamb wave generation in plates depends on the velocity of the incident wave and the acoustic velocity of the material through which the Lamb wave propagates. Lamb wave generation angle can be found by Snell's law, which will be described in chapter 4.9. [19]

Lamb waves consist of several particle vibrations modes, which can be classified into two subcategories; the symmetrical and asymmetrical wave modes. The velocity of the wave modes depends on frequency and plate thickness. Higher orders of symmetrical and asymmetrical modes is generated in the plate as frequency and/or thickness increases. The symmetrical and asymmetrical Lamb wave modes are illustrated in figure 4.4. [19]
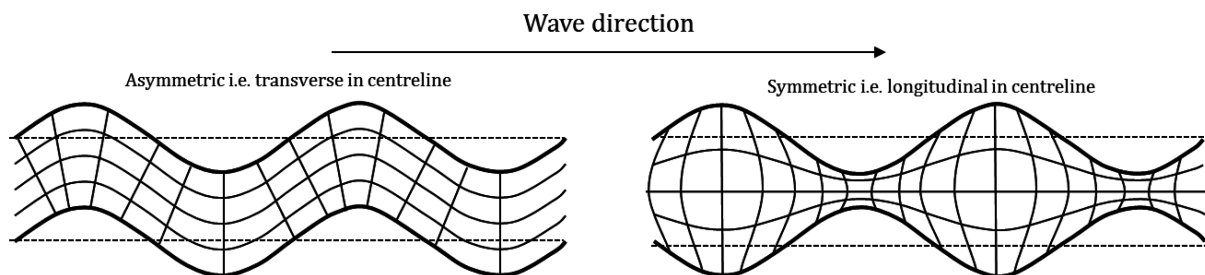
Figure 4.4: Lamb wave asymmetric and symmetric mode [21]

4.4 Basic properties of acoustic wave

An acoustic wave has several properties that describe the wave propagation ability in solid materials, liquids and gas. The simple characteristics of a plane sound wave have the generic properties listed below, and is illustrated in figure 4.5 [19]

- Wavelength

- Frequency

- Amplitude, sound pressure or intensity

- Wave velocity

- Wave direction

The wavelength of an acoustic wave has a specific relationship to wave velocity and frequency, which is expressed with equation 4.1. It is important to note that the velocity of most waves is solely dependent on the elastic properties of the material it is propagating in, and therefore not dependent on frequency. The velocity of a wave determines the wavelength based on frequency. [19]

$$\lambda = \frac{c}{f} \tag{4.1}$$

where λ : Wavelength [m]
c : Wave velocity [m/s]
f : Frequency [Hz]

PROPERTIES OF SOUND
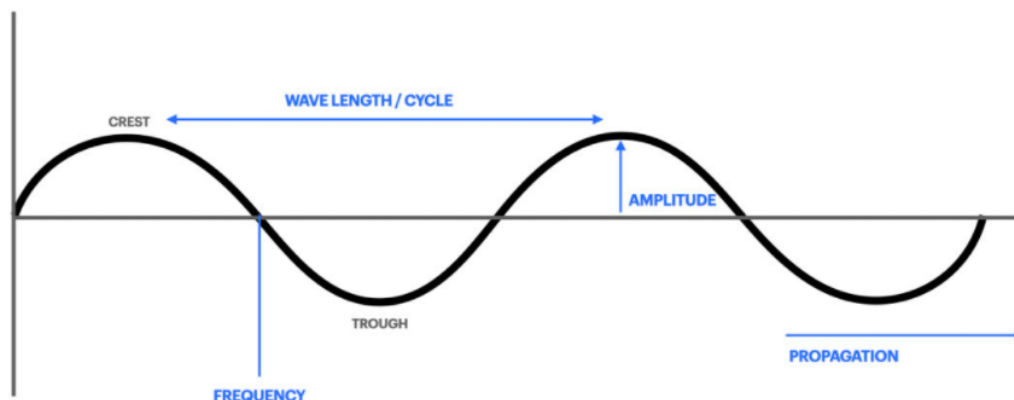
Figure 4.5: Basic properties of sound waves: crest, wavelength, frequency, amplitude, wave direction/propagation [22]

4.5 Sound propagation in elastic materials
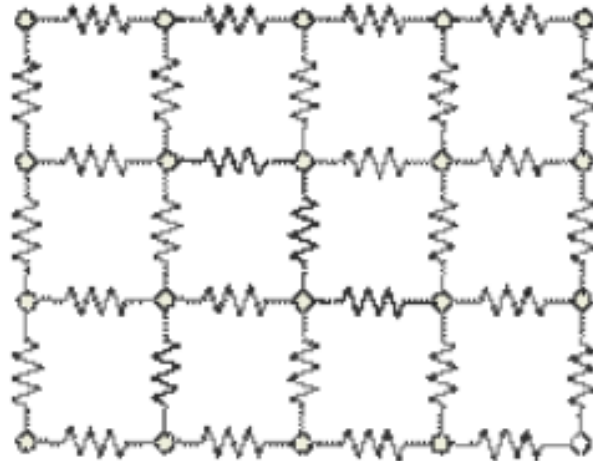
Figure 4.6: Sound propagation through a material can be visualized as a grid with infinite particles, each connected by springs with elastic and inertial properties. These properties determine sound wave velocity. [19]

It was previously explained in the beginning of this theory chapter that sound propagates by particle vibrations. Sound energy transmission through material is achieved by the oscillatory motion of the particles, visually recognized as a sound wave. An easy way to imagine how sound propagates through a material is to visualize a grid with an infinite amount of particles. This imaginative grid is illustrated in figure 4.6. Each particle is attached together by elastic springs. This way, we can imagine that when a particle is in motion, it will influence a force to the adjacent particles through their connection with the elastic springs. Therefore, the springs can be described as elastic restoring forces that act upon each particle when sound energy propagates through a material. Additionally, the springs have inertial forces. [19]

All these properties differ between materials and determine the wave velocities. The springs translate how fast sound can propagate within the material. Materials like steel have a rigid body (stiff springs) which means the bonds between the molecules is not easily compressed. Sound will therefore propagate faster in solids compared to gas, because the molecules of gas are farther apart than the molecules of steel, and those bonds are easily compressible (soft springs). [19]

The physics behind the elastic properties of sound wave propagation, and how it differs depending on the material it travels, can be easily explained through Hooke's law. Hooke's law can be expressed with the following equation: [19]

$$F_s = kx \tag{4.2}$$

Hooke's law states that a particle with a mass m can be compressed or extended within an elastic limit when the force F_s is applied to it. x is the particle displacement, and k is the spring constant. The spring constant can be regarded as a spring stiffness to deformation or particle stiffness to displacement, also known as particle inertia. Hooke's law can be seen figure 4.7. [19]
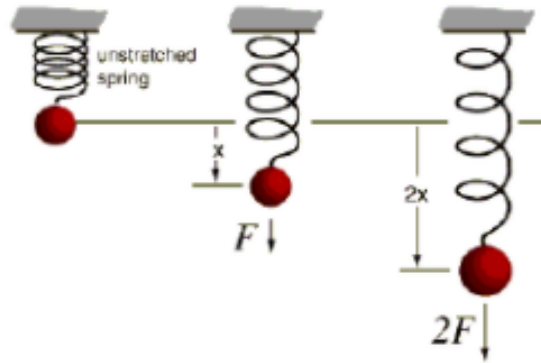
Figure 4.7: Hooke's law shows that a restoring force arises in the opposite direction of particle displacement. [19]

Wave velocity can be explained with Hooke's law in combination with Newton's second law. With the physics of Hooke's law and Newton's law, it becomes abundantly clear that the wave velocity within a material is solely a function of material properties, and is independent of wave amplitude and frequency. Mathematically, Newtons's second law is expressed as $F = ma$, which expresses that the force applied to a particle is equal to the particle's mass m and acceleration a. Hooke's law is expressed in equation (4.2), which expresses the applied force to a particle is equal to particle displacement x and the spring constant k. Combining these laws, we get the following expression: [19]

$$ma = kx \tag{4.3}$$

According to this equation, it becomes clear that the applied forces *ma* to a particle is counterbalanced by the particle displacement *x*, assuming particle mass *m* and spring coefficient *k* is kept constant. Conclusively, making the applied forces from Newton's second law equal the restoring forces from Hooke's law. [19]

When we consider mass *m* and the spring constant *k* as constants, the relationship between Newton's law and Hooke's law in equation (4.3) has only the acceleration *a* and particle displacement *x* as variables. Particle acceleration is proportional to the particle displacement. This means a particle that oscillates around its equilibrium is independent of the applied force. Therefore, sound wave velocity is independent of the applied force, and will always travel at the same speed within a material. However, this is only true as long as other variables such as temperature and density are held constant. Thus, sound wave velocity only depends on the materials restoring forces, as expressed in the equation below. Properties that affect the speed of sound are further explained in chapter 4.6. [19]

$$c = \sqrt{\frac{elastic\ property}{inertial\ property}} \qquad (4.4)$$

4.6 Material properties affecting the speed of sound in solids and gas

Sound wave velocity differs between materials. Different velocities occur within materials that have different mass of the atomic particle and different spring constants. Speed of sound is not determined by the applied force, but rather the elastic and inertial properties of the material. The density of a material is directly related to the particle's mass, which was previously established to represent the inertial property against material deformation. The elastic properties of a material is regarded as the spring constant. Therefore, the speed of sound within a material can be expressed with the following general relationship between the material density and elastic constants: [19]

$$c = \sqrt{\frac{C}{\rho}} \tag{4.5}$$

where c : Speed of sound within a material   [m/s]
        C : elastic constant in wave propagation   [N/m^2]
        ρ : material density   [kg/m^3]

The above equation can be regarded as a general equation for sound velocity where the elastic constant depends on the type of wave mode (longitudinal or transverse). The typical elastic constants *C* for materials are listed as follows. [19]

- Young's Modulus, *E*

- Poisson's Ratio, *n*

- Bulk Modulus, *K*

- Shear modulus, *G*:

4.6.1 Speed of sound in solids

Young's Modulus *E* and Poisson's Ratio *n* are the common elastic properties used for calculating the longitudinal (compressional) wave, while shear *G* Modulus is used for calculating the shear (transverse)wave. Bulk Modulus *K* is typically used for gases. Longitudinal wave speed in solids is readily derived by substituting the elastic constant *C* in equation (4.5) with Young's Modulus *E* and Poisson's ratio *n*, as follows: [19]

$$c_{Long} = \sqrt{\frac{E(1-n)}{\rho(1+n)(1-2n)}} \tag{4.6}$$

where
c_{Long}	:	speed of sound for longitudinal waves	[m/s]
E	:	Young's modulus	[N/m^2]
ρ	:	material density	[kg/m^3]
n	:	Poisson's ratio	

Shear (transverse) wave velocity in solid material is readily derived by substituting the elastic constant *C* in equation (4.5) with Shear modulus *G*: [19]

$$c_{Trans} = \sqrt{\frac{G}{\rho}} \tag{4.7}$$

where
c_{Trans}	:	speed of sound for shear (transverse) waves	[m/s]
G	:	Shear modulus	[N/m^2]
ρ	:	material density	[kg/m^3]

A few examples of longitudinal wave velocity and shear wave velocity from different materials have been given in table 4.2 The examples show that longitudinal wave is relatively faster than shear waves. This is due to the fact that materials will often have higher compressional resistance than it will have shear resistance, making the speed of sound traveling faster as a compressional wave than a shear wave. [19] The material examples in the table also show that the rigidity or sturdiness of the materials results in a greater velocity, which can be seen by comparing aluminum and copper.

Table 4.2: Examples of approximate sound velocities in solid materials

Material	longitudinal sound velocities c_{Long} [m/s]	Shear sound velocities c_{Trans} [m/s]
Aluminium	6320	3130
1020 Steel	5890	3240
Cast iron	4800	2400
Copper	4660	2330

4.6.2 Speed of sound in air

The speed of sound in solids depends on the deformation of the materials under shear stress, the density and compressibility of the material. However, gas does not support shear waves because gases do not undergo shear stress when exposed to a pressure difference like solids. Only longitudinal waves (compressional waves) are supported in gases because gas is compressible. The equation for speed of sound in air is derived by considering the adiabatic compressibility, which is directly related to pressure though the adiabatic index (heat capacity ratio). If we assume the gas is ideal, the elastic property bulk modulus K can be given as: [23]

$$K = \gamma \cdot p \tag{4.8}$$

The speed of sound in ideal gas can be expressed by substituting the elastic constant C from equation (4.5) with the bulk modulus K equation (4.8). Since we assume that the gas is in an ideal state, we can replace p with nRT/V and ρ with nM/V, so the equation for speed of sound in ideal gas becomes: [23]

$$c_{\text{ideal}} = \sqrt{\gamma \cdot \frac{p}{\rho}} = \sqrt{\frac{\gamma \cdot R \cdot T}{M}} \tag{4.9}$$

where
c_{ideal}	:	speed of sound in ideal gas	[m/s]
R	:	Molar gas constant (= 8.314 463)	[$J^{-1} \cdot mol^{-1}$]
T	:	is the absolute temperature	[K]
M	:	is the molar mass of the gas. for dry air is 0.0289	[kg/mol]
p	:	gas pressure	[Pa]
ρ	:	gas density	[kg/m^3]
γ	:	gas adiabatic index	

In an ideal gas, the molecular composition is considered fixed. Gas pressure and density are inversely and cancel each other out as temperature changes. Consequently, meaning that the speed of sound is only dependent on temperature. Therefore, equation (4.9) can be simplified to express the speed of sound as a function of temperature: [23]

$$c_{ideal} = \sqrt{\frac{\gamma \cdot R \cdot T}{M}} = \sqrt{\frac{\gamma \cdot R \cdot T}{M} \cdot (\frac{273K}{273K})} = \sqrt{\frac{(273K) \cdot \gamma \cdot R}{M}} \sqrt{\frac{T}{273K}} \approx \underline{331 \cdot \sqrt{\frac{T}{273K}}} \quad (4.10)$$

Table 4.3 shows the speed of sound increasing with temperature calculated with equation (4.10). The speed of sound in air is considerably lower than the sound velocities for solids shown in table 4.2. This is due to the elastic properties of solids being much more significant than gas.

Table 4.3: Speed of sound in air as a function of temperature

Temperature [Kelvin]	273	293	313	333	353	373	393	413
Speed of sound [m/s]	331	343	354	365	376	387	397	407

4.7 Phase velocity and group velocity
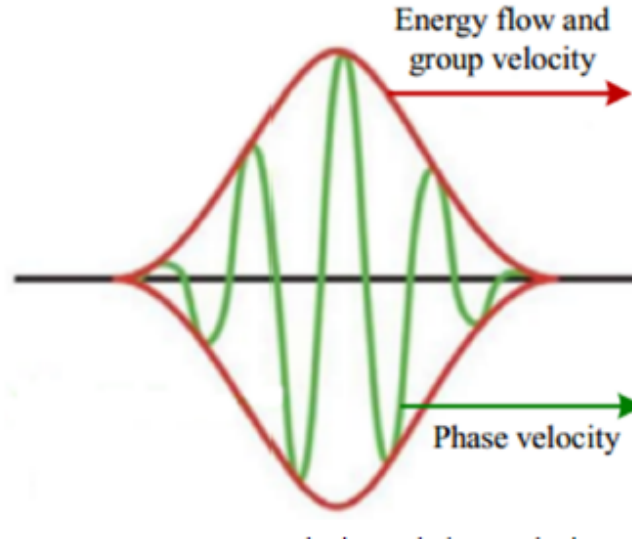
Figure 4.8: Phase and group velocity of a sound pulse envelope [24]

The velocity of a sound wave propagating in a material at a given frequency can be divided into two subgroups: phase velocity and group velocity. Figure 4.8 shows an illustration of phase velocity and group velocity of a sound pulse envelope. [24]

Phase velocity is the speed of any given phase of any one frequency component of the sinusoidal sound wave as it travels in space. In a simple terms, the phase velocity is the speed of a single frequency. For example, looking at the crest point from the beginning of the frequency wave to the end, the crest will travel a wavelength away from the source λ over the time T. Therefore, the phase velocity of that one frequency component is given as: [24]

$$c_p = \frac{\lambda}{T} \tag{4.11}$$

Equivalently, phase velocity can be given in terms of wave's angular frequency ω and angular wave number $k = 2\pi/\lambda$, which represent the proportionality between the angular frequency $\omega = 2\pi f$ and the linear speed of phase velocity c_p: [24]

$$c_p = \frac{\omega}{k} \tag{4.12}$$

43

As can be seen from the equation, phase velocity depends on the frequency of the sound wave. This is a fundamental fact that affects the generation and propagation of Lamb waves, which will be further explained in chapter 4.10. However, phase velocity alone cannot convey any information of transferred energy along with the distance, because it only keeps track of one frequency component at a time. Phase velocity cannot recognize a change in amplitude or frequency, otherwise known as modulation change. This is only possible with the group velocity equation. [24]

Sound pulse contains a group of internal waves and, therefore, a group of amplitudes, otherwise known as a wave packet. The envelope of the wave packet represents the signal content of the sound pulse. The speed of that envelope is the group velocity. This means that the group velocity is the rate of change in the shape of the wave's group of amplitudes as it propagates through space. Therefore, the group velocity is the physical expression that conveys the speed of information or the speed of energy transfer along the direction of propagation. Group velocity is expressed with the following equation: [24]

$$c_g = \frac{d\omega}{dk} \tag{4.13}$$

the group velocity can also be expressed in terms of phase velocity c_p: [24]

$$c_g = \frac{c_p^2}{c_p - f\frac{\partial c_p}{\partial f}} \tag{4.14}$$

4.8 Acoustic impedance

Every acoustic wave propagating within a material has a specific physical characteristic relating to the sound wave's ability to travel through that medium. That physical characteristic is called acoustic impedance. Acoustic impedance is similar to the analog electrical impedance, and it can be defined as: [19]

$$Z = \rho c \tag{4.15}$$

where Z :   Acoustic impedance $[\text{kg/m}^2 s]$
        ρ :   density $[\text{kg/m}^3]$
        c :   sound wave speed $[\text{m/s}]$

The acoustic impedance is an important parameter to consider in non-destructive ultrasonic testing (NDT). Materials that have different densities and sound wave velocities will have different acoustic impedance. When a sound wave propagates across the interface between two materials with different acoustics impedance, the sound wave will face an acoustic impedance mismatch. The consequence of acoustic impedance mismatch is that some acoustic waves will reflect at the interface, while some will be transmitted. The larger the acoustic mismatch between the materials, the greater amount of sound wave energy will be reflected and not transmitted. Table 4.4 shows some examples of acoustic impedance of some materials calculated by equation (4.15). [19]

Table 4.4: Examples of acoustic impedance for some materials

Aluminium	Copper	Steel	Water	air (20 °C)
17.1 x 10^6	41.6 x 10^6	46.1x10^6	1.48 x 10^6	413

The acoustic impedance of air and steel is shown in table 4.4, and it can be seen that the values present a large acoustic impedance mismatch between air and steel. The large acoustic impedance mismatch between air and steel is a great obstacle for our investigation of non-intrusive ultrasonic detection of an internal arc fault, because medium voltage switchgear walls are made out of steel or aluminum. The acoustic impedance mismatch will result in a large magnitude of the ultrasonic signal being reflected at the switchgear walls. Non-intrusive ultrasonic monitoring implies that the ultrasonic transducers are placed outside the switchgear, and therefore must be capable of transmitting the ultrasound through the switchgear walls. However, the large acoustic impedance mismatch between air and steel reveals that effective sound transmission may perhaps be physically unachievable. In spite of that, this general description of wave

reflection is mostly relevant for longitudinal waves crossing between the mediums. Because of this, the work presented in this thesis will focus on how the problem with acoustic impedance mismatch can be solved by using Snell's law to resonate the steel plates with guided Lamb waves as the ultrasonic signal. This will be described in more detail further down the chapters. [19]

4.8.1 Reflection and transmission coefficients

Ultrasonic waves that strikes the interface between two materials where there is an acoustic impedance mismatch will reflect a fraction of its energy. The greater impedance mismatch, the greater reflection of sound energy. The fraction of the incident wave energy that is reflected can be expressed with the following equation for reflection coefficient: [19]

$$R = \left(\frac{Z_2 - Z_1}{Z_2 + Z_1} \right)^2 \tag{4.16}$$

where
R : Reflection coefficient
Z_1 : Acoustic impedance in material 1 [kg/m$^2 s$]
Z_2 : Acoustic impedance in material 2 [kg/m$^2 s$]

This reflection coefficient can be multiplied by 100 to obtain the percentage of sound energy reflected. Correspondingly, the transmission coefficient T can be derived from the above reflection coefficient R above as follows: ($T = 1 - R$). [19]

Figure 4.9 illustrates an example of reflection and transmission coefficient between water and steel. By Using the acoustic impedance values shown in table 4.4, the reflection and transmission coefficients were calculated using equation (4.16) which gave the results R = 0.88 and T = 0.12, respectively. If 12% of the energy is transmitted through the water-steel interface, only 1.4% and 1.3% of that 12% will be transmitted out of the steel solid and into the water domain. The remaining energy will be reflected repeatedly, propagating along with the steel solid. Therefore, the impedance mismatch needs to be considered when doing ultrasonic measurements between materials with a great difference in acoustic impedance. [19]

The acoustic impedance mismatch between air and steel is so large that the reflection coefficient R is calculated to be 99.996%
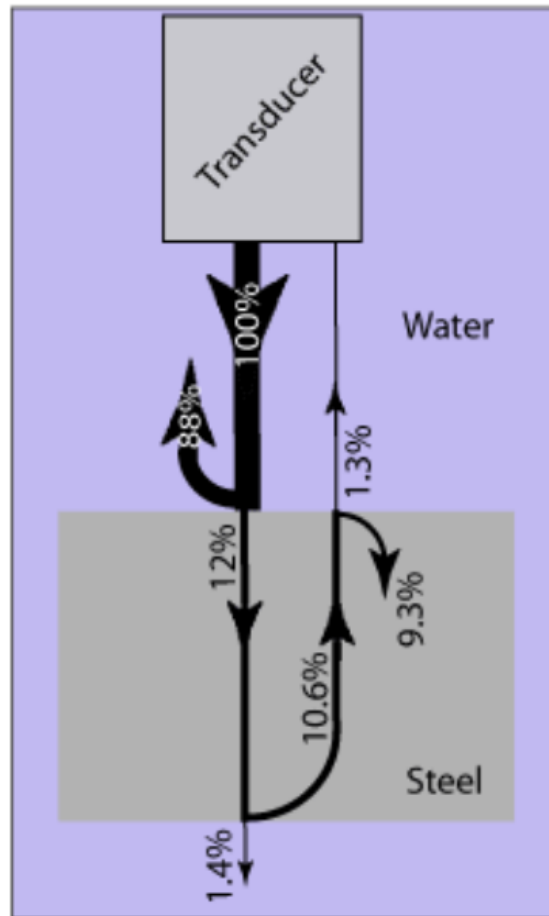
Figure 4.9: Sound wave propagation between water and steel with transmission and reflection coefficient of the sound wave energy [19]

4.9 Snell's law - Wave refraction
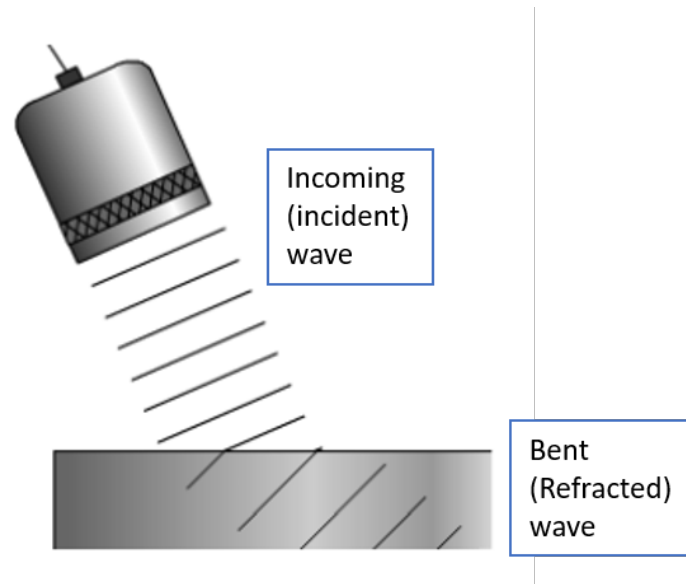
Figure 4.10: Incident wave strikes the interface between two materials of different acoustic velocities bends the wave into a refracted wave [19] [edited]

When an incident sound wave strikes a surface at an oblique angle, both a reflected and a refracted wave will be produced at the material's surface, as shown in figure 4.10. The refracted wave is a "bent" wave that propagates through the material at a different angle and speed than the incident wave. This phenomenon can also be observed with light rays. [19]

Refraction of the sound wave happens at the interface between two materials that have different acoustic velocities and densities, which was previously explained as a material characteristic called acoustic impedance mismatch. The acoustic velocity varies with different materials due to the variation in density and elastic Modulus. Figure 4.10 shows how the incident wave is propagating in one material with a defined speed, but when it crosses the interface of another material, the speed of the wave changes according to the elastic properties of the material. The figure illustrates that a portion of the wave is traveling at a faster rate than the remaining portion that has yet to cross the interface. This causes the wave to bend and eventually propagate through the second material at a different direction and speed. [19]

The relationship between the angles and velocities of the incident and refracted wave can be explained with Snell's law in the following equation: [19]

$$\frac{sin\theta_1}{V_{L_1}} = \frac{sin\theta_2}{V_{L_2}}$$

(4.17)

where
θ_1 : angle of incident wave in the first material [angle]
θ_2 : angle of the refracted angle in the second material [angle]
V_{L_1} : longitudinal wave velocity in the first material [m/s]
V_{L_2} : longitudinal wave velocity in the second material [m/s]

An example of Snell's law is shown in figure 4.11. The figure shows the incoming (incident) wave with velocity V_{L_1} propagating in material 1. The incident wave strikes the interface between material 1 and material 2 and produces a reflected wave V'_{L_1} and refracted wave V_{L_2}. The reflected wave propagates in material 1 at the same angle θ_1 as the incident wave, while the refracted wave is propagating in material 2 at a different angle θ_2. [19]

Snell's law is highly relevant when modifying the incident wave angle to generate different types of wave modes in materials. Suppose the acoustic velocities of both materials are known. In that case, one can use Snell's law to find the optimal angle of the incident wave to generate a Lamb wave, thereby optimizing energy sound transmission from air to solid plate. [19]
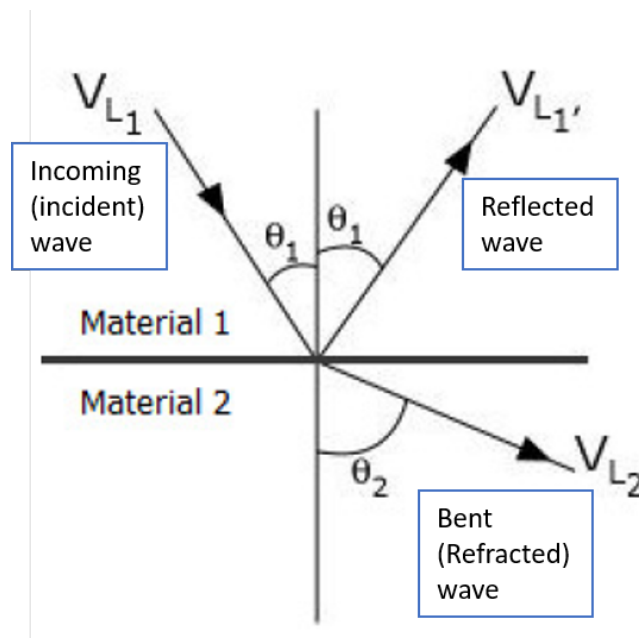
Figure 4.11: An incident wave with angle θ_1 and longitudinal wave velocity V_{L_1} strikes the interface between two materials with different acoustic materials and produces a reflected wave and refracted wave angle θ_2 and wave velocity V_{L_2}, according to Snell's law. [19] [edited]

4.10 Lamb waves and sound dispersion curves

Lamb wave is a type of wave mode frequently used in ultrasonic non-destructive testing (NDT) because it can travel long distances and are energy efficient. Additionally, Lamb waves will continuously leak some of the sound energy to the adjacent air surrounding the material, making it an optimal wave mode to use when investigating the feasibility of non-intrusive ultrasonic internal arc fault detection. However, when using the Lamb wave for ultrasonic NDT, the selected frequency must be greatly considered and adjusted according to the test material. This is because Lamb waves are dispersive, which means that the propagation velocity of Lamb waves depends on the frequency or thickness of the material it is propagating within. At very high frequencies, many modes of different Lamb wave will occur in the material. This will be described a bit further with the following text. [25]

Characteristic equations for Lamb wave modes and associated dispersion curves As was described in the earlier chapters, Lamb waves are elastic waves that propagate parallel to the plate surface with complex vibrational waves throughout the plate thickness. Lamb waves can be subdivided into two wave modes; anti symmetric and symmetric wave modes, which is labelled as A_m and S_m, respectively, where $m = 0, 1, 2, 3$ indicates the order of infinite sets of wave modes that are possible with the propagation of Lamb waves in solid materials. [25]

One must be aware of a fundamental physical characteristic when using Lamb waves for ultrasonic sound transmission because Lamb waves are dispersive. Dispersive sound waves mean that the wave velocity depends on the frequency or thickness of the material is is propagating withing. The critical parameter determining velocity dispersion in Lamb wave modes is the ratio of plate thickness d to wavelength λ. This ratio determines the stiffness of the plate, and will therefore effectively determine the velocity of the wave modes in Lamb waves. This ratio is expressed with the following equation. [26]

$$f \cdot d = \frac{d \cdot c}{\lambda} \tag{4.18}$$

For an elastic plate with the physical boundaries, the characteristic equations for symmetric Lamb wave modes S_m can be expressed with the following equation: [25]

$$4k^2 pq sin(ph)cos(qh) + (k^2 - q^2)^2 sin(qh)cos(ph) = 0 \tag{4.19}$$

and for the antisymmetric Lamb wave modes A_m can be expressed with: [25]

$$4k^2 pq sin(qh)cos(ph) + (k^2 - q^2)^2 sin(ph)cos(qh) = 0 \tag{4.20}$$

where h is one half of the total plate thickness, $k = \omega/c_p$ is the wave number, $\omega = 2\pi f$ is the angular frequency. p and q can be expressed with longitudinal velocity c_L and transverse velocity c_T with the following equation. [25]

$$p^2 = \frac{\omega^2}{c_L^2} - k^2, q^2 = \frac{w^2}{c_T^2} - k^2 \tag{4.21}$$

However, numerical methods are used to find phase velocity $c_p = f\lambda = \omega/k$, and the group velocity $c_g = d\omega/dk$, as functions of d/λ or $f \cdot d$. These numerical methods are quite complex. Therefore, this thesis will refer to and use graphs from previous works that have already found the solution to the complex equations, and which fit well with the materials used in our setups of simulation models. [26]

The solutions of the characteristic equations (4.19) and (4.20), also known as Rayleigh-Lamb Equations, for the phase velocity c_p, is plotted as frequency depending function, which is called Dispersion curves. An example of phase velocity dispersion curves for a mortal plate as function of frequency (MHz) where different modes of A_m and S_m occurs are plotted in figure 4.12. The group velocity c_g can be found with the equation (4.14) with phase velocity c_p as parameter. [25]

Figure 4.12 illustrates how Lamb waves in plate material are dispersive, and different modes of Lamb waves A_m and S_m vary with frequency as material thickness is kept constant. The zero-order modes A_0 and S_0 are the first Lamb wave modes in the frequency spectrum and are the two most important modes in ultrasonic NDT. They exist in all frequencies and are the most practical modes due to them being more energy-efficient than the higher-order modes. It can be seen from the figure 4.12 that the zero-order antisymmetric modes A_0 are highly dispersive in the low frequencies. Both the A_0 and S_0 modes in the figure converge towards the Rayleigh wave velocity. [25]
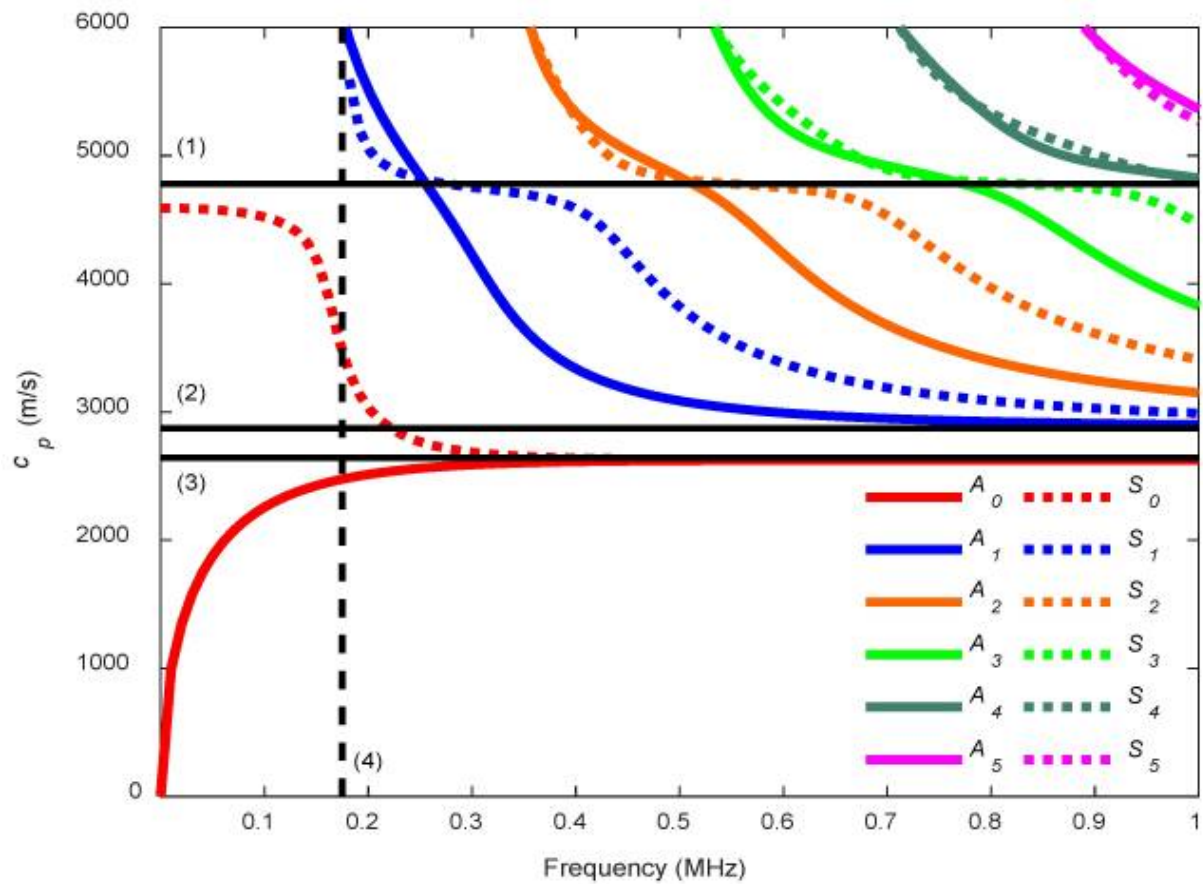
Figure 4.12: Example of phase velocity dispersion curves for a mortar plate. several modes of symmetric S_m (represented with coloured dashed lines) and antisymmetric A_m (represented with coloured solid lined) occur as frequency increases. there are three horizontal black lines that represent the non-dispersive velocities: (1) longitudinal velocity), (2) shear velocity and (3) Rayleigh velocity. The vertical black dashed line (4) is the resonant frequency of the plate material, where higher order of Lamb waves begins to occur. Graph extracted from published article [25]

When the frequency exceeds the resonant frequency of the plate material, higher order of symmetric S_m and antisymmetric A_m modes occur in addition to the zero-order modes S_0 and A_0. This type of mode conversion only exists above the resonant frequency of the plate material. It can be seen from the figure that all the higher-order modes of Lamb waves eventually converge to the shear wave (or transverse wave) velocity as frequency increases. [25]

Since Lamb wave at high frequencies generates many higher-order modes of symmetric S_m and antisymmetric A_m modes with different velocities, it can lead to difficulty in Lamb wave signal analysis. In order to avoid this and improve the interpretation of the received signal of the dispersive Lamb wave modes, it might be beneficial to follow these recommendations given by published article in [25]:

- Choose low frequencies to minimize the number of modes in the received signal. For example, one can avoid the higher-order symmetric S_m and A_m by using a frequency that is below the resonant frequency of the material. Thus only the zero-order modes S_0 and A_0 will exist in the plate. Besides, these are the signals with the most significant received signal magnitude. A_0 are beneficial for ultrasonic air borne Lamb wave detection because they present a large signal magnitude than S_0, making it easier for signal processing and filtering. [25]

- Modify the frequency to the region where the phase velocity has little dispersion, which means there is only a slight variation of phase and group velocity as frequency increases or decreases. [25]

5 Internal arc fault detection by non-intrusive ultrasonic transducers

This chapter will explain the general working principle on how the theory behind ultrasonic transducers and Lamb waves can be used for internal arc fault detection of a medium voltage switchgear. A simplified model is developed presenting the ultrasonic wave propagation path between two solid plates, and a general analytical calculation for the ultrasonic signal time delay between the transmitter and receiver at constant temperature, and as temperature increases.

5.1 The general principle on internal arc fault detection by ultrasonic transducers using Lamb waves

When an internal arc fault occurs inside a switchgear compartment, the arc energy will cause a rapid increase in temperature and pressure. Today, an internal arc fault is detected by pressure and flash light sensors. These sensors have a common requirement to be stationed inside the switchgear tank in order to effectively detect the effects from an internal arc fault (pressure increase or arc light). It would be interesting to investigate the feasibility of using an alternative sensor that can detect an arc fault without being installed inside the switchgear tank. A non-intrusive sensor placed outside the switchgear compartment has the benefit of being easy to install, maintain and replace.

Since the speed of sound is a function of temperature, and an internal arc fault causes the gas inside the switchgear to increase in temperature, a sound transducer could potentially convey that information by measuring the sound wave's velocity propagating through the switchgear gas. The time it takes for a sound wave to propagate between a transmitter and a receiver is called time delay. Naturally, the time depends on how fast the sound wave is propagating. Therefore, the objective of this thesis is to investigate the feasibility of detecting an internal arc fault by measuring the time delay of ultrasonic pulses through the switchgear, where a change in time delay is used as the triggering signal for fault detection. This concept is illustrated in a simple manner in figure 5.1
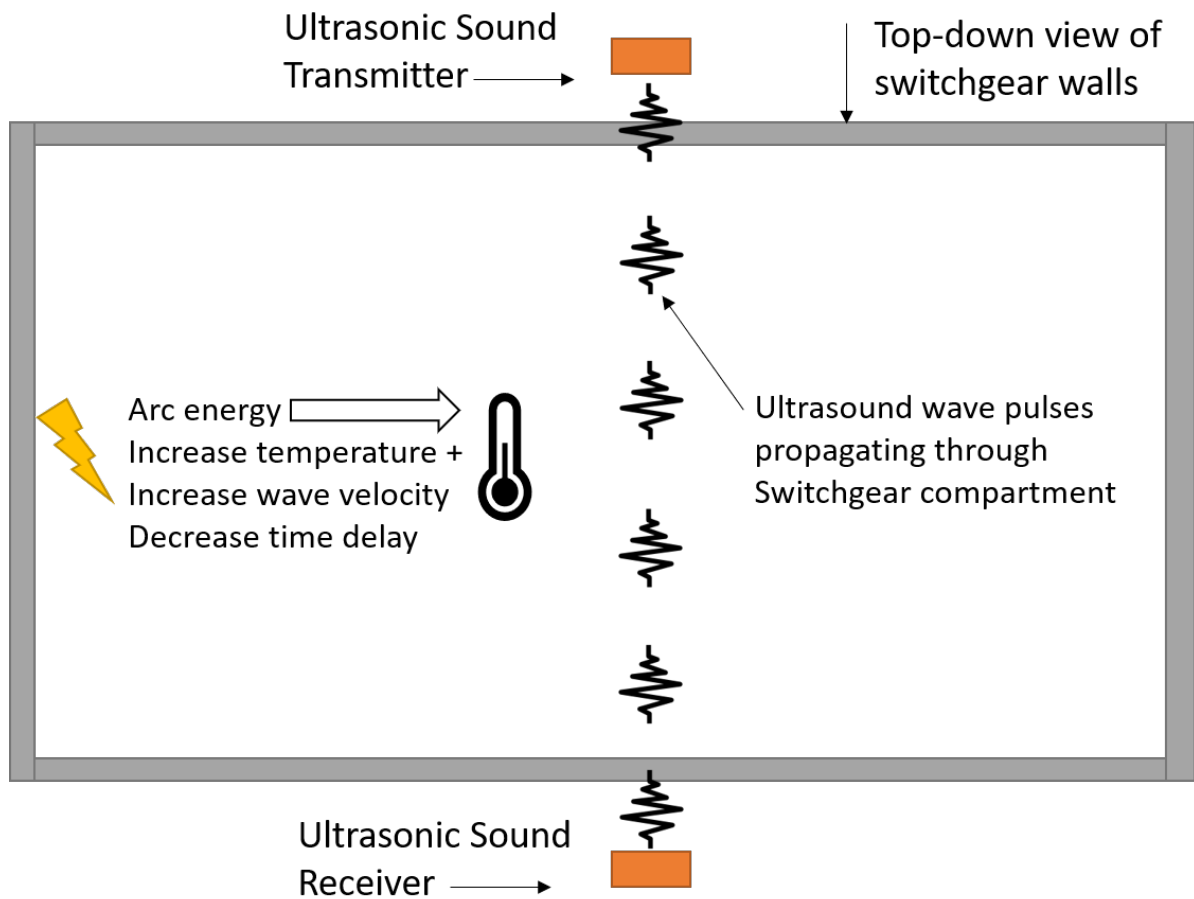
Figure 5.1: Simple schematic illustrating the concept of internal arc fault detection by non-intrusive ultrasonic sound measurement

Non-intrusive ultrasonic transducer is commonly used in the process industry, where the time delay between sent and received ultrasonic signal can be used to measure the gas flow, tank level, etc. However, these processes often involve fluids, making the acoustic impedance mismatch between tank/pipe wall and fluid sufficiently low for the ultrasonic sound to be transmitted through the wall. Therefore, ultrasonic measurement is an efficient sensor technology that has the benefit of being non-intrusive and easy to install outside the process.

However, for our setup, ultrasound needs to be transmitted through an interface of steel walls and air. It was previously shown that the acoustic impedance can be found with equation (4.15), and the values for steel and air (at 20 °C) is given in table 4.4 as $Z_{steel} = 46.1x10^6$ and $Z_{air} = 413$ respectively. Sound velocity in gas is considerably slower compared to the sound velocity in steel walls, making the acoustic impedance mismatch between gas and steel walls quite large. The consequence of a large acoustic impedance mismatch is that the ultrasonic waves will mostly reflect on the steel walls. Equation (4.16) calculates that the sound energy reflection coefficient for the air-steel interface is 99.996%, which makes non-intrusive ultrasonic measurement quite challenging.

This great challenge has been overcome and studied by the authors Z. Fan, W. Jiang and W. M. D Wright with the published article 'Non-contact ultrasonic gas flow metering using air-coupled leaky Lamb waves' published in [1]. The authors used ultrasonic leaky Lamb waves in order to measure the gas flow inside a polycarbonate pipe. Plate Lamb waves are a useful wave type for non-intrusive ultrasonic measurement because they will continuously leak energy into the adjacent air, making ultrasound transmission between steel and gas possible. The research paper showed excellent correspondence between the proposed theory and the conducted experiments. The authors also developed an COMSOL Multiphysics ® model to confirm the conducted experiments. The work presented in this thesis is greatly inspired by the models developed in the mentioned article.

Through the technique shown in the research article involving leaky Lamb waves, it may be feasible to accomplish internal arc fault detection by the use of non-intrusive ultrasonic transducers. The work in this thesis presents a simple model which investigates the fundamentals behind excitation/transmission of leaky Lamb waves between two metal plates separated with an air gap. The transducers placed on each side of the metal plate will measure the change of time delay between sent and received ultrasonic sound waves as the gas between the plates increases in temperature.
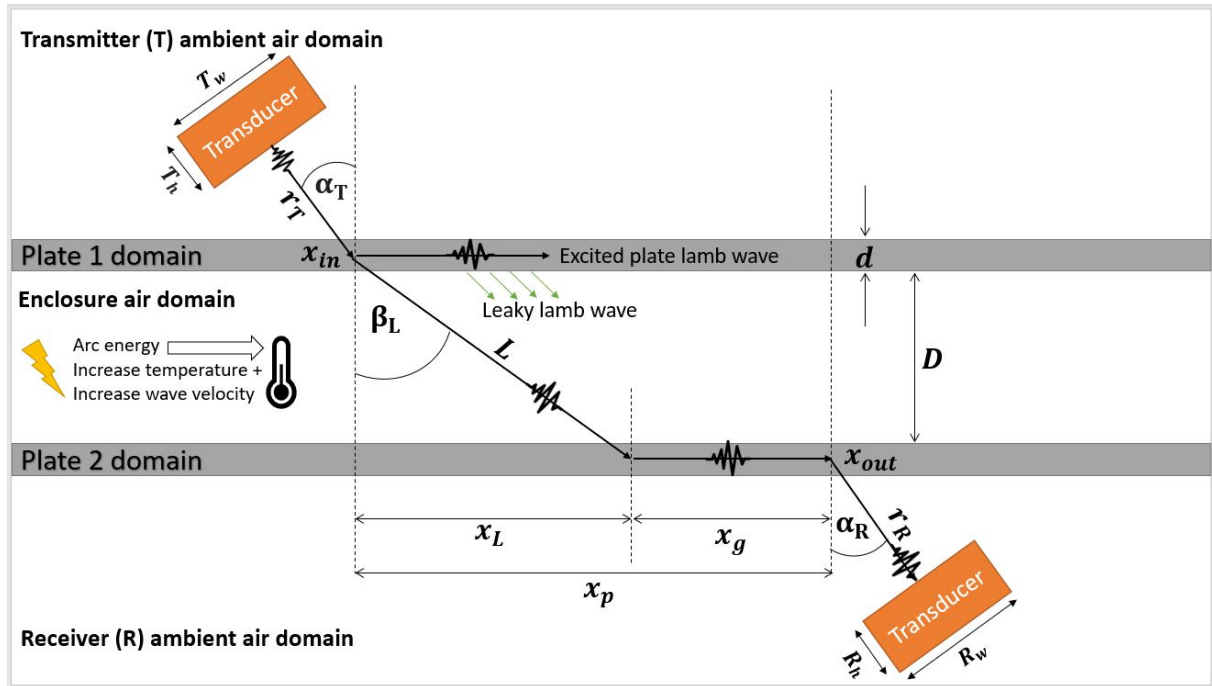
Figure 5.2: Schematic and analytical model for the ultrasound propagation using leaky Lamb waves, based on the research article published in [1]

Figure 5.2 illustrates a simplified working principle to test the concept of transmitting ultrasonic waves through plates with Lamb waves excitation. The model presents a clear representation of the ultrasonic wave propagation path. The model can also serve as an analytical model to find time delay between sent and received signal. The ultrasonic wave propagation path may be described as follows. The ultrasonic signal is generated in ambient air as a compression wave (longitudinal wave) by the transmitter. The compression wave strikes the plate and generates a plate Lamb wave within the plate. The transducers are oriented at a specific angle so that the transmission of sound energy from the incident compression wave to plate Lamb wave is optimized. Orienting the transducer at a specific angle is essential for plate Lamb wave generation. Otherwise, a large magnitude of the sound energy will get reflected instead of transmitted. If the surface of the transducer were directly facing the plate surface, as it does in figure 5.1, hardly anything of the energy will get transmitted. Therefore it is crucial to orient the transducers at an oblique angle to the surface of the plates, as shown in figure 5.2. At that specific angle, wave mode refraction occurs, and the compression wave energy will excite a Lamb wave in the plate. Once the Lamb wave is propagating along the plate it will continuously leak some of its energy in the gas between the plates. The leakage wave will occur in the gas as another compression wave that will travel between the plates. The compression wave propagates through the enclosure gas and strikes the second plate at an oblique angle. This will generate a second Lamb wave that will also

leak energy into the adjacent air. The leakage from the second plate Lamb wave occurs in the receiver air domain as another compressional wave. In time, the receiver eventually detects the compressional wave that was leaked from the second Lamb wave. When the compressional wave propagates in the gas between the plates, the wave velocity will be influenced by the increased temperature caused by the arc fault. The increase sound velocity in the gas will consequently shorten the propagation time between the plates. Thus, an internal arc fault could potentially be detected by the decreased time delay between sent and received signal.

This thesis aims to focus on the feasibility of sound propagation through metal plates using leaky Lamb waves, and if the transducers can detect a decrease in the time delay between sent and received signal as temperature increases. This feasibility study will lay the foundation for further work to prove if non-intrusive ultrasonic transducers can detect an internal arc fault. Therefore, it is not intended to be specific about transducer type, gas type, plate thickness, arc fault energy, spatial dimensions, temperature increase, temperature distribution etc. Most conditions here are considered to be ideal, thus avoiding significant complex modeling. The gas domains are considered homogeneous. The temperature increase is considered to be homogeneously distributed inside the enclosure.

5.2 Simplified analytical model for the time delay at a constant temperature

Figure 5.2 shows a schematic of the ultrasonic signal wave propagation path, and how the time delay between sent and received signal may be analytically calculated. The following analytical model is based on the models described by authors Z. Fan, W. Jiang and W. M. D Wright in the published article 'Non-contact ultrasonic gas flow metering using air-coupled leaky Lamb waves' published in [1].

The analytic model may be described as follows. The transmitter (T) has distance from plate 1 at a range of r_t. The transmitter has the angle α_T which is inclined to the surface normal of Plate 1. The transit time for the compression wave to propagate between the sender and plate 1 in the ambient air domain can be found by the following formula:

$$t_T = \frac{r_T}{c_a} \tag{5.1}$$

The speed of sound in the ambient air domain c_a is calculated using the ideal speed of sound equation (4.10). At 20 °C the speed of sound in air is found to be 343 *m/s*. When the compression wave sent from the transmitter strikes the first plate at the point of entry x_{in}, it is assumed that the first Lamb wave is instantaneously generated, and starts propagating along with the plate 1 after time t_T. The Lamb wave leaks energy into the enclosure air domain along its propagation path, generating another compression wave in the gas between the plates. This compression wave will propagate away from plate 1 at an angle β_L, which can be calculated with two acoustics velocities between the plate Lamb wave and the compressional wave according to Snell's law equation (4.17). The compression wave has the propagation path L between the plates. The transit time for the compression wave to cross the plates along path L (at constant temperature) can be found with the following equation:

$$t_L = \frac{L}{c_L} = \frac{D}{c_L \, cos(\beta_L)} \tag{5.2}$$

Where c_L is the compression wave velocity in the gas gap between the plates, and D is the gap distance. c_L can also be found using the ideal speed of sound equation (4.10). The compression wave enters plate 2 at a certain entry point which is horizontally displaced from entry point x_{in} depending on angle β_L and the distance D as follows $x_L = D \, tan(\beta_L)$. At point of entry in plate 2, mode conversion will again occur instantaneously and a second Lamb wave is generated, which will propagate along the plate 2 with a group velocity c_g. The Lamb wave leaks energy into the receiver domain as another ultrasonic compression wave. The receiver is placed horizontally at distance $x_p = x_{out} - x_{in}$ with an

inclined angle of α_R to the surface of normal plate 2. This means that the transit time for the second Lamb wave to propagate from point of entry to point of exit x_out in plate 2 can be given by:

$$t_g = \frac{x_g}{c_g} = \frac{x_p - x_L}{c_g} = \frac{x_p - D \tan\beta_L}{c_g} \tag{5.3}$$

Where c_g is the group velocity of plate Lamb wave. Finally, the transit time for the compression wave propagating across the distance between Plate 2 x_{out} and receiver r_R is given by:

$$t_R = \frac{r_R}{c_a} \tag{5.4}$$

Finally, the total time delay between sent and received signal for non-intrusive ultrasonic signal using leaky Lamb waves (at constant temperature) can be summarized with the following equation:

$$t_{delay} = t_T + t_L + t_g + t_R = \frac{r_T}{c_a} + \frac{D}{c_L \cos(\beta_L)} + \frac{x_p - D \tan(\beta_L)}{cg} + \frac{r_R}{c_a} \tag{5.5}$$

5.3 Simplified analytical model for the time delay when temperature increases

The previous analytical model considers the temperature constant, making the wave velocities and excitation angles constant. Since the speed of sound is a function of temperature, the total time delay for sent and received signal will change during an arc fault. The increase of speed of sound c_L will also affect the excitation angle β_L according to Snell's law. Therefore, the following analytical model calculates the ultrasonic signal time delay with respect to the temperature increase over time.

The total energy from the electric arc can be found with equation (2.6). Since we consider the temperature to be evenly distributed inside the enclosure, the temperature rise caused by the electric arc can be found using the simplified temperature rise calculation method described in section 3.5. We can, in a simplified manner, find the temperature rise inside a switchgear enclosure ΔT with the following equation:

$$\Delta T = \frac{E_{arc}}{c_v \cdot M} \tag{5.6}$$

Where E_{arc} is the electric arc energy input calculated from equation (2.6), c_v is the specific heat constant at constant volume and $M = Rs \cdot V$ is the molar mass calculated with the specific gas constant Rs and switchgear volume V.

As the temperature of the enclosure increases over time, the compressional wave velocity across the plate increases over time. By using the speed of sound as function of temperature, which was defined equation (4.10), we define the change of compressional wave velocity over time as follows:

$$c_L(t) = 331 \cdot \sqrt{\frac{T(t)}{273 \; K}} \tag{5.7}$$

The increase of the compressional wave velocity c_L will affect the excitation angle β_L according to Snell's law equation (4.17). Since the Lamb wave is propagating along plate 1 at 90 degrees to the plate surface normal at a constant phase velocity c_p, the change of excitation angle β_L as the compressional wave c_L increases over time can be expressed as:

$$\frac{sin(90)}{c_p} = \frac{sin(\beta_L(t))}{c_L(t)} \quad \rightarrow \quad \beta_L(t) = sin\left(\frac{sin(90)}{c_p} \cdot c_L(t)\right)^{-1} \tag{5.8}$$

The propagation path between the plates L changes with time because the excitation angle β_L changes. This can be expressed as:

$$L(t) = \frac{D}{cos(\beta_L(t))} \tag{5.9}$$

If we assume that the temperature increase is linear, which means the compressional wave velocity c_L increases with a constant acceleration a, we can find the transit time for the wave to cross the gap between plates with the displacement equation with the classical physics displacement equation. Solve the second-order equation for $t_L(t)$ to find the transit time $t_L(t)$:

$$\frac{1}{2} a t_L(t)^2 + c_L(t) t_L(t) - L(t) = 0, \quad \text{solve for } t_L(t) \tag{5.10}$$

Since the β_L may changes as the temperature increases, the entry point at plate 2 for the second Lamb wave changes, which consequently changes the transit time for the Lamb wave t_g:

$$t_g(t) = \frac{xp - D \, tan(\beta_L(t))}{c_g} \tag{5.11}$$

the transit time between the plate and transducers, (t_T and t_R) are unaffected by the temperature increase since they are located in ambient air outside of the enclosure, where the temperature is kept constant, and will therefore be calculated with equation (5.1) and (5.4) respectively.

Finally, the total time delay between sent and received signal for non-intrusive ultrasonic signal using leaky Lamb waves as temperature increases over time, can be similarly summarized with the following equation:

$$t_{delay}(t) = t_T + t_L(t) + t_g(t) + t_R =$$

$$\frac{r_T}{c_a}$$

$$+ \left(\frac{1}{2} a t_L(t)^2 + c_L(t) t_L(t) - L(t) = 0, \quad \text{solve for } t_L(t) \right)$$

$$+ \frac{xp - D \tan(\beta_L(t))}{c_g}$$

$$+ \frac{r_R}{c_a}$$

$$(5.12)$$

6 COMSOL Multiphysics® Modeling

This chapter will cover how the theory behind non-intrusive ultrasonic transducers with leaky Lamb waves was implemented, tested, and simulated using FEM-software. In this thesis, COMSOL Multiphysics ® is used to investigate ultrasonic sound propagation through metal and air, and how it is affected by temperature increase. By developing a COMSOL model, it was possible to look deeper into the theory behind Lamb wave generation in metal plates and simulate the speed of sound. Several test cases are performed where the results are analyzed and compared to the analytical model.

6.1 Introduction

Several test cases were developed in COMSOL Multiphysics® in order to test the feasibility of internal arc fault detection with non-intrusive ultrasonic transducers using leaky Lamb waves. The models developed in the test cases are built upon the fundamental model published in the research paper referenced [1], where the authors investigated the possibility of using non-contact ultrasonic transducers for gas flow measurement using air-coupled leaky Lamb waves. That model consisted of a simplified two-dimensional duct system compromising of two thin poly carbonate plates separated by an air-filled gap. It was shown through COMSOL simulations and experiments that its practically feasible for ultrasonic sound transmission between two thin plates by exciting the plates with Lamb waves. That model is used as a starting point for the first trial case. Each iteration of test cases that follows is an extension of the previous model. The expansions include an increase in temperature and steel plates.

The purpose of the first test case is to reproduce the same model from the research paper published in [1]. This was done in order to get the same results of leaky Lamb wave ultrasound transmission as presented in the paper. The following test cases are an extension of the fundamental model developed in test case 1, including temperature increase and material change from polycarbonate to steel. By this approach, the test cases will be developed logically and chronologically to get closer to the realistic conditions of an arc fault inside the steel walls of medium voltage switchgear. The simulations will show how the sound propagates through the plates, and how the received ultrasonic signal changes as the temperature increases.

The models were limited to only investigating the fundamental theory of ultrasonic sound transmission and how it is affected by increased temperature. The models and parameters used in the test cases are not intended to be specific. Gas type, transducer type, dimensions for coupling equipment, temperature increase on arc fault are non-specific. The dimensions of the models were chosen to be considerably small in order to decrease the computation time significantly. Therefore, it is important to note that the models do not represent realistic conditions for switchgear testing. That is why the work here is only meant to serve as a rough feasibility study where only transmission of sound through solid plates, and the change in speed of sound due to temperature increase, are to be investigated.

6.2 FEM-Design in Comsol Multiphysics ®

COMSOL Multiphysics® is a widely used and powerful software that allows for cross-platform finite element analysis, solver and multiphysics simulation. Comsol provides an intuitive modeling environment that solves physical problems using coupled partial differential equations (PDE). Multiphysics indicates that it is capable of solving single physical domains and a multitude of physical domains, i.e. mechanical, fluid, acoustics, electrical systems, etc. Each of the physical modules contains physical equations based on fundamental PDE that are preloaded into the model. Therefore, Comsol allows for easy modeling of the multiphysics processes without the users detailed knowledge of mathematic and numeric analysis. The general approach for developing a model in COMSOL is illustrated in figure 6.1. [27]
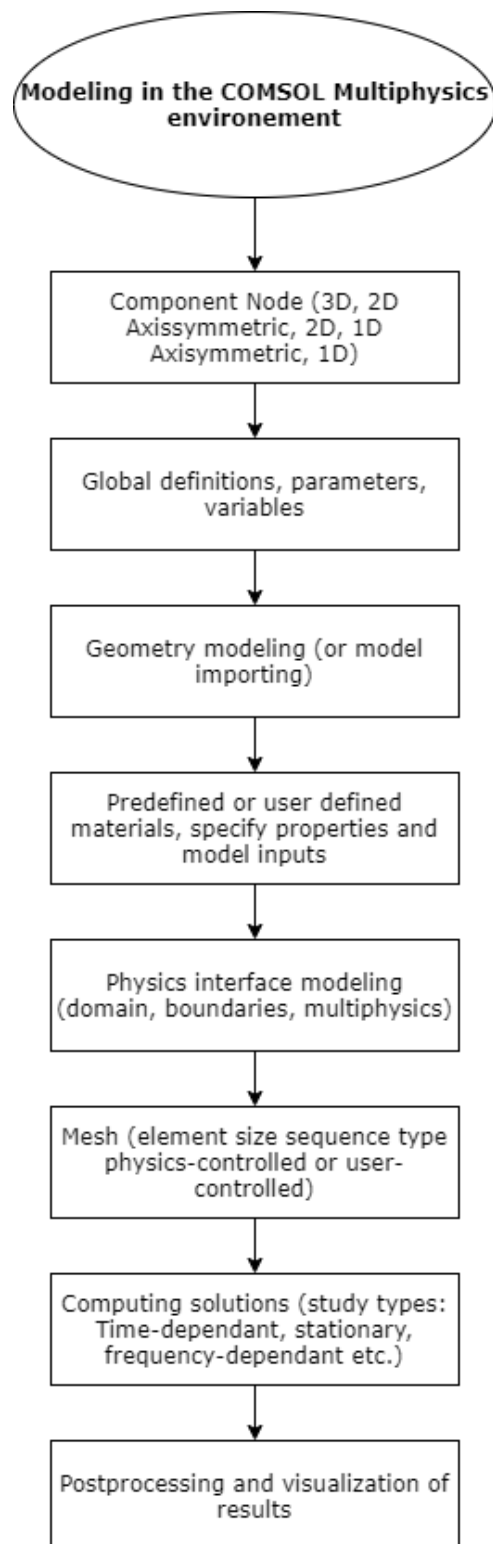
Figure 6.1: General sequence for COMSOL Multiphysics modeling [27]

6.2.1 Geometry and material parameters

The models was developed in the *2D axisymmetric* space dimension. This space dimension was beneficial to reduce the computation time and complexity of the models. The general built geometry of the COMSOL models is shown in figure 6.2. The geometry of the model is similar to the analytical model figure 5.2, where the model is subdivided into domains consisting of two solid plates spaced by an air-filled gap, with two piezoelectric transducers placed on each of the plates. Each transducer is in an ambient air domain. The first test case uses homogenous polycarbonate as plate material. Previous authors chose this material to simplify the Lamb wave propagation calculation and ensure low impedance mismatch between air, while also enhancing the detection of signals. [1] The subsequent test cases simulate stainless steel as plate material because switchgear walls are made of stainless steel. The parameter values for model geometry is shown in table 6.1 where the symbols correspond to the symbols shown in the analytical figure 5.2. The parameters for material properties of polycarbonate and steel is shown in table 6.2 and 6.3. Properties of air are shown in table 6.4
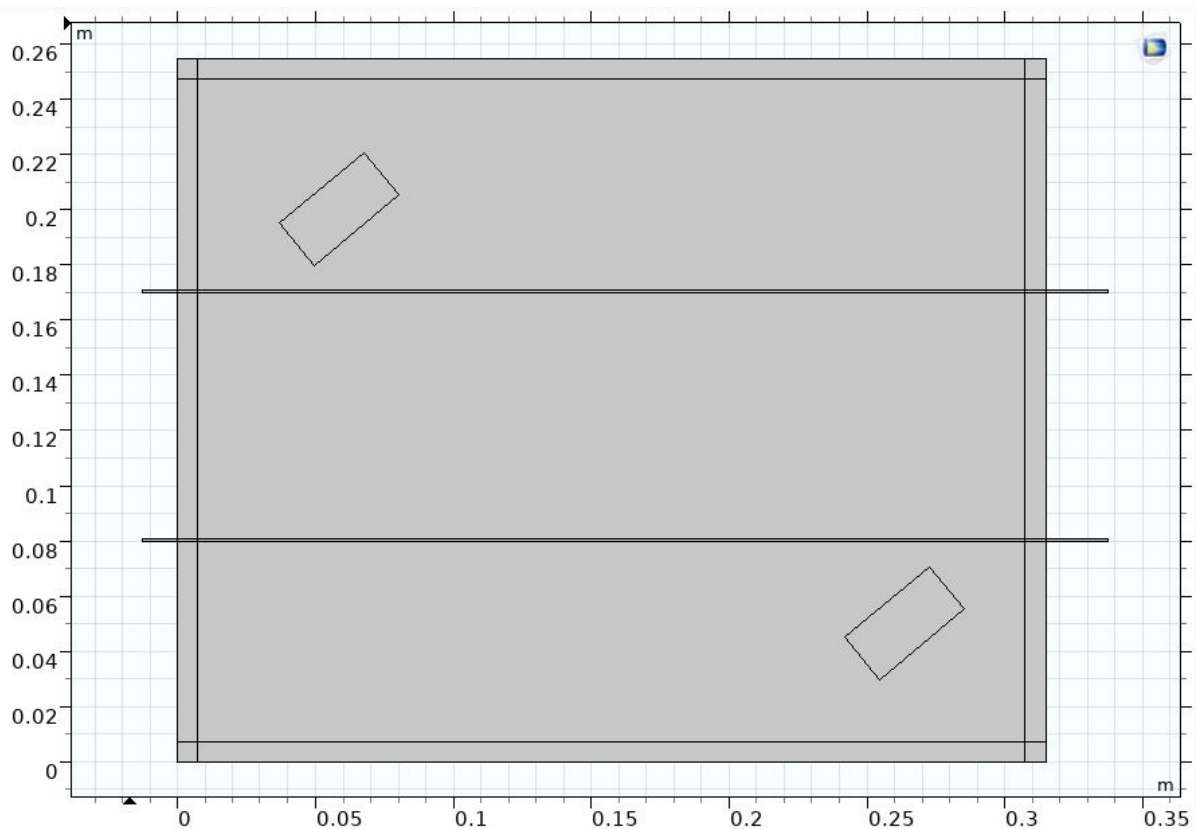
Figure 6.2: test cases geometry developed in COMSOL Multiphysics ®

Table 6.1: Geometric parameters for the different test cases

Geometric parameters	symbol	Value
Plate separation height	D	90 mm
Plate thickness for polycarbonate	d	1 mm
Plate thickness for steel	d	2 mm
Transmitter height	T_h	20 mm
Transmitter width	T_w	40 mm
Transmitter angle for polycarbonate	α_T	50°
Transmitter angle for steel	α_T	11°
Receiver height	R_h	20 mm
Receiver width	R_w	40 mm
Receiver angle for polycarbonate	α_R	50°
Receiver angle for steel	α_R	11°
Lamb wave inlet-outlet seperation	$xp = x_{out} - x_{in}$	150 mm

Table 6.2: Polycarbonate plate material properties

Material properties	symbol	Value
Young's modulus	E	2.0 GPa
Poisson's ratio	n	0.37
Density	ρ	1200 kg/m^3

Table 6.3: Steel plate material properties

Material properties	symbol	Value
Young's modulus	E	200 GPa
Poisson's ratio	n	0.30
Density	ρ	7750 kg/m^3

Table 6.4: Air properties

Material properties	symbol	Value
speed of sound	c_a	343 m/s

6.2.2 Physics modules and boundary conditions

Pressure acoustics was used with *Solid Mechanics*, *Electrostatics* and *Multiphysics* as the physics modules. The modules with the following domains and boundaries are shown in figure 6.3
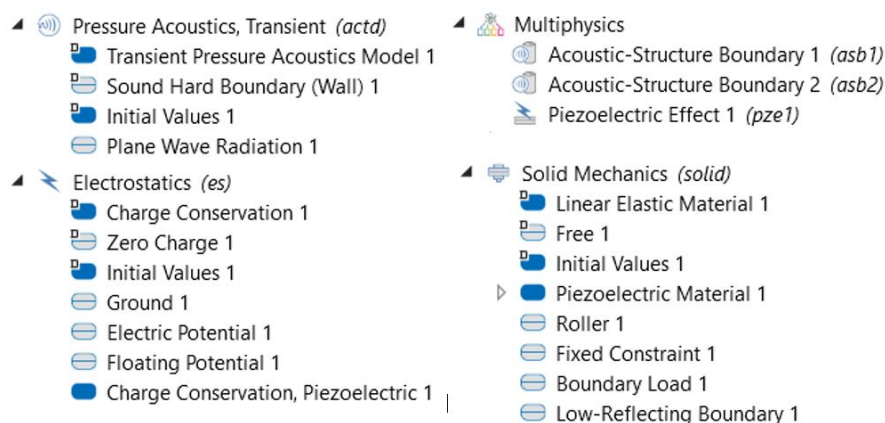
Figure 6.3: Test cases was developed with physics modules: *Pressure acoustics*, *Solid Mechanics*, *Electrostatics* and *Multiphysics* with the following domains and boundaries

The *Pressure acoustics, Transient* module simulates the pressure wave propagation in the transducer domains the enclosure domains. *Plane wave Radiation* boundary is a radiation condition that allows ultrasonic waves to leave the modeling domain with minimal reflections, thereby reducing computation time. An additional pressure acoustics module was added and applied to the enclosure domain for the temperature increases test cases.

The *Electrostatics* module was used for piezoelectric transducer operation. The boundaries *Electric potential*, *Ground*, *Charge conservation*, and *Piezoelectric-effect* enables the transducers to transform the received acoustic pressure into an electric voltage signal V, and vice versa.

The *Solid Mechanics* module was used for modeling the solid plates and the piezoelectric material in the transducers. The ultrasonic signal that is sent from the transmitter as a compression wave was simulated by applying a time-dependent *boundary load $F(t)$* (shown in chapter 6.2.3) to the transmitter surface. Reflection at plate edges were avoided by using *Low-Reflecting Boundary*.

Lamb wave energy transmission between the air domain and solid domain was made possible with the essential *Acoustic-Structure Boundary* from the *Multiphysics* module. The module connects the pressure acoustic module and solid mechanics module in order to generate a Lamb wave that leaks energy into the adjacent air domains.

6.2.3 Ultrasonic sound wave excitation signal

The models consist of two ultrasonic transducers, a transmitter, and a receiver. The transmitter sends an ultrasonic compression wave pulse, which is used to excite the plates with plate Lamb waves, and the receiver detects the signal and measures the time from when it was sent and receieved. The ultrasonic excitation signal is repeated with a 200 μs interval, creating several ultrasonic pulses over time. The ultrasonic compression wave pulse was generated in COMSOL by applying the physics boundary *boundary-load* to the surface of the transmitter. The signal is a time-dependent smooth windowed sinusoid of ten cycles in length, with a frequency f of 100 kHz and maximum $F_0 = 1000$, generated by the equation: [1]

$$F(t) = F_0 \, sin(2\pi f t) \cdot \left(sin\left(\frac{2\pi f t}{20} \right) \right)^2, \quad [t < 10/f] \tag{6.1}$$

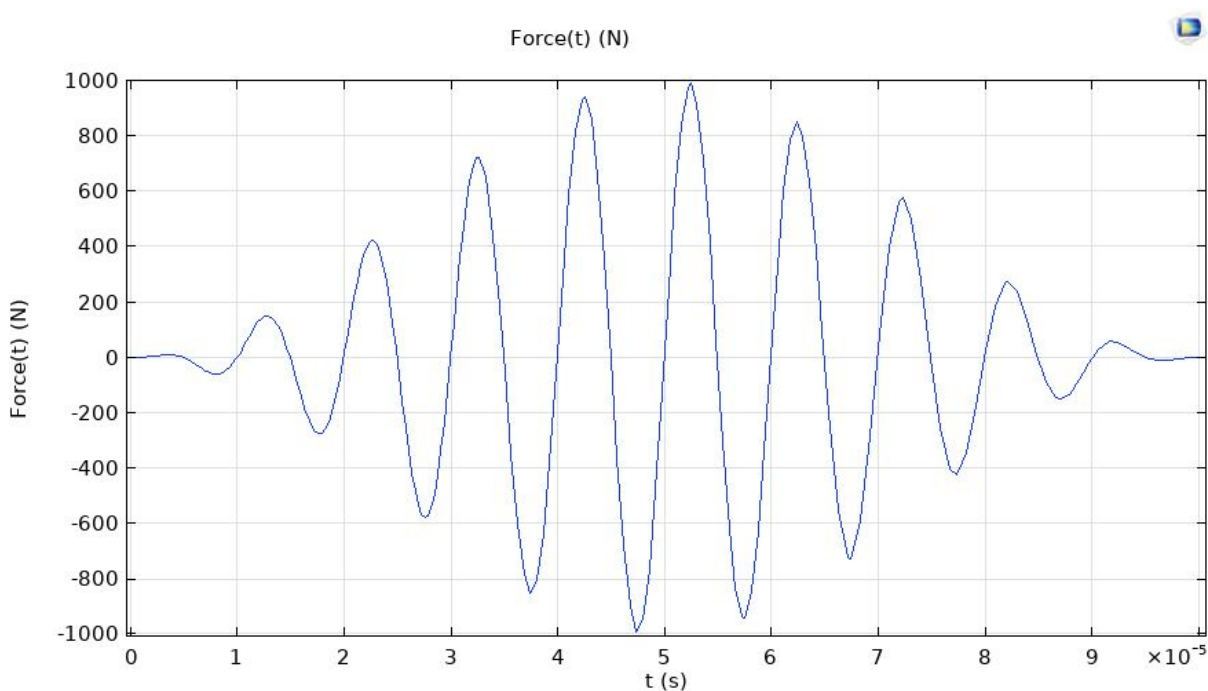Figure 6.4: The simulated ultrasonic signal from the transducer in COMSOL

6.2.4 Lamb wave modes for poly carbonate plates and steel plates

Polycarbonate plates

Lamb waves modes were described in chapter 4.10 as dispersive, which means that the propagation velocity depends on the frequency and material thickness. Specific Lamb wave modes can be determined based on the sound frequency and plate thickness, as shown from the equations in the theory. However, calculating the specific Lamb wave modes is quite complex. Therefore, this thesis will refer to and use graphs from previous works that have already found the solution to the complex equations and fit well with the materials used in our setups of simulation models. The dispersion curves for antisymmetric A_m and symmetric S_m for polycarbonate plate are readily derived and shown in figure 6.5. The resonant frequency for polycarbonate is above 0.5 MHz.mm, and the graph shows that only the zero-order modes A_0 and S_0 exist below that resonant frequency. In our test cases, the useful area for frequency-thickness phase velocities is less than 0.2 MHz.mm, because it fits the geometry of the plates (1-2 mm) in combination with the simulation frequency 100 kHz, which gives the range 0.1 MHz.mm and 0.2 MHz.mm. [1]

As described earlier, the generation and detection of Lamb waves require careful orientation of the transducers. This is essential to optimize sound energy transmission between the two different materials, air and solid plate, which minimizes reflections. Since the ultrasonic signal is produced at the frequency 100 kHz, and the polycarbonate plate has a thickness of 1 mm, we get a frequency-thickness product of 0.1 MHz.mm. From the graph it can be seen with a frequency-thickness product of 0.1 MHz.mm, the A_0 mode has a phase velocity of 430 m/s. According to Snell's law equation (4.9) and the velocity between of air ($c_a = 343m/s$) and the phase velocity of the plate $c_p = 430m/s$, the Lamb wave inside the plate will leak energy into the adjacent air at an excitation angle $\beta_L = 52.9°$. Therefore, the angle of the transducers α_T and α_R was inclined at 50 °to the surface normal of the plates. The calculation of the leaky Lamb wave excitation angle β_L (refraction angle), based on Snell's law with plate Lamb wave velocity c_p and air velocity c_a is illustrated in figure 6.6. [1]
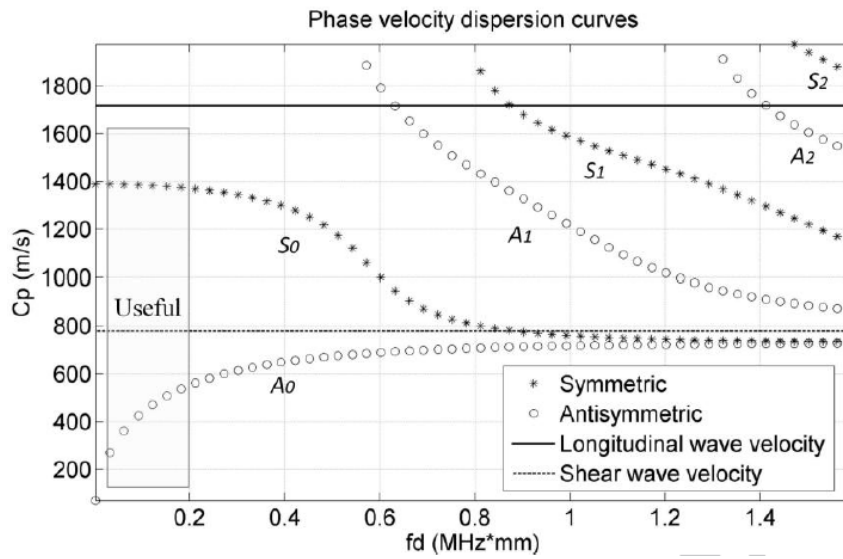
Figure 6.5: A readily derived phase velocity dispersion curve for the first three symmetric S_m and antisymmetric A_m modes in polycarbonate. Graph published in [1]
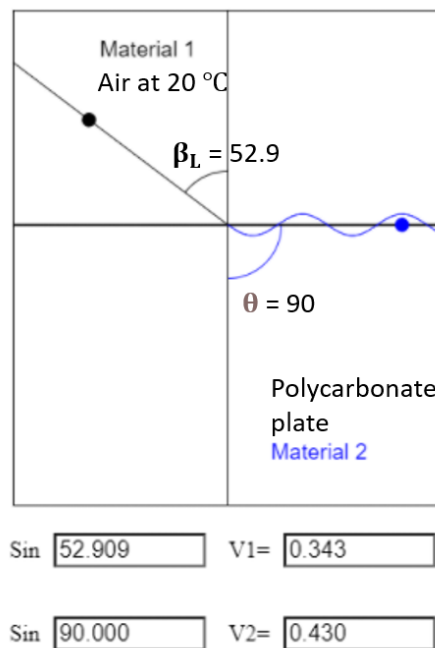
Figure 6.6: Snell's law calculates the excitation angle (refraction angle) $\beta_L = 52.9°$ between polycarbonate plate (material 2) with Lamb wave phase velocity ($c_p = 430m/s$), and air at 20 °C (material 1) with compressional wave velocity ($c_a = 343m/s$). Graph generated with Snell's Law calculator applet from [19]

Steel plates

Dispersion curves for antisymmetric A_m and symmetric S_m for steel plates are readily derived and shown in figure 6.7. The same principle for the polycarbonate plate also applies to the steel plates. The figure shows that only the zero-order modes A_0 and S_0 modes exist below the resonant frequency below 0.2 MHz.mm for steel plates. Following the same logic as above, the Lamb wave will be generated at 100 kHz in a 0.2 mm thick steel plate. We can see from the graph that the Lamb wave phase velocity for A_0 is roughly 1700 m/s. So the leaky Lamb wave will propagate at an angle of $\beta_L = 11.6°$ according to Snell's law. Therefore, the angle of the transducers are inclined at 11 °. The calculation of the excitation angle β_L (refraction angle) between steel plate Lamb waves velocity and air wave velocity according to Snell's law is illustrated in figure 6.8
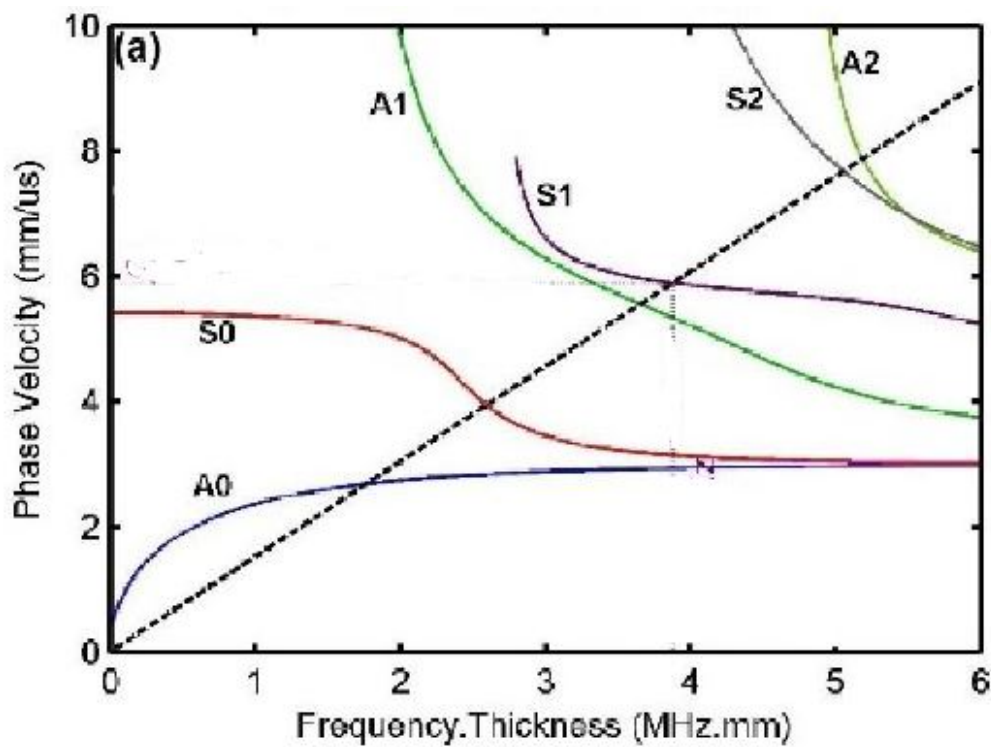
Figure 6.7: A readily derived phase velocity dispersion curve for the first three symmetric S_m and antisymmetric A_m modes in polycarbonate. Graph published in [28][edited]
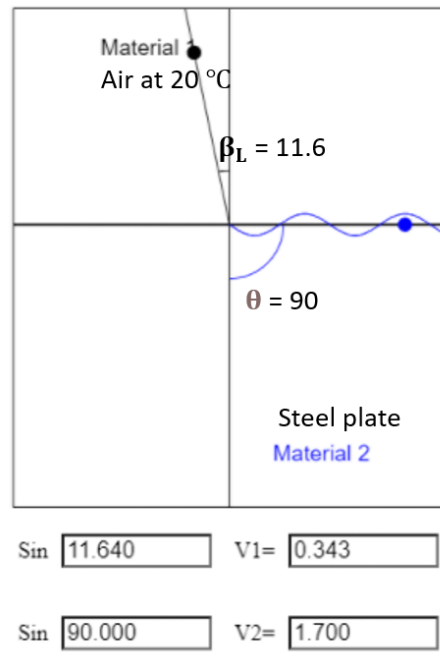
Figure 6.8: Snell's law calculates the excitation angle (refraction angle) $\beta_L = 11.6°$ between steel plate (material 2) with Lamb wave phase velocity ($c_p = 1700m/s$), and air at 20 °C (material 1) with compressional wave velocity ($c_a = 343m/s$). Graph generated with Snell's Law calculator applet from [19]

6.2.5 Mesh

In COMSOL, the mesh is a grid which divides the volume and surfaces of each model into tiny distributed elements, which should calculated accordingly to the solver algorithm. The sizes of the distributed area can be defined evenly or individually. Mesh sizing is a trade-off between the accuracy of the calculations or computation time.

Triangular mesh elements were chosen for the simulation of sound pressure waves. There is one important rule that should be followed when simulating sound waves. The maximum element size of the mesh cannot be larger than the wavelength λ of a sound wave. The wavelength of the sound waves can be found to be proportional to the velocity of the wave, and inversely proportional to the frequency, as per equation (4.1). The test models simulate the ultrasonic sound waves at a frequency of 100 kHz, and the speed of sound in ambient air is 343 m/s. Therefore, the maximum element of the mesh should not be larger than $\lambda_{max} = 3.343mm$. For better accuracy, the maximum element for the mesh grid was chosen to be five times smaller than λ_{max} in all the test cases. The small mesh size is shown in figure 6.9. The drawback with such a small mesh size is that it results in increased computation time, which cannot be modified without sacrificing the accuracy of the computed solution. This is why the model size for the test cases has considerably small dimensions because it enables the simulation process to save time while also remaining accurate.
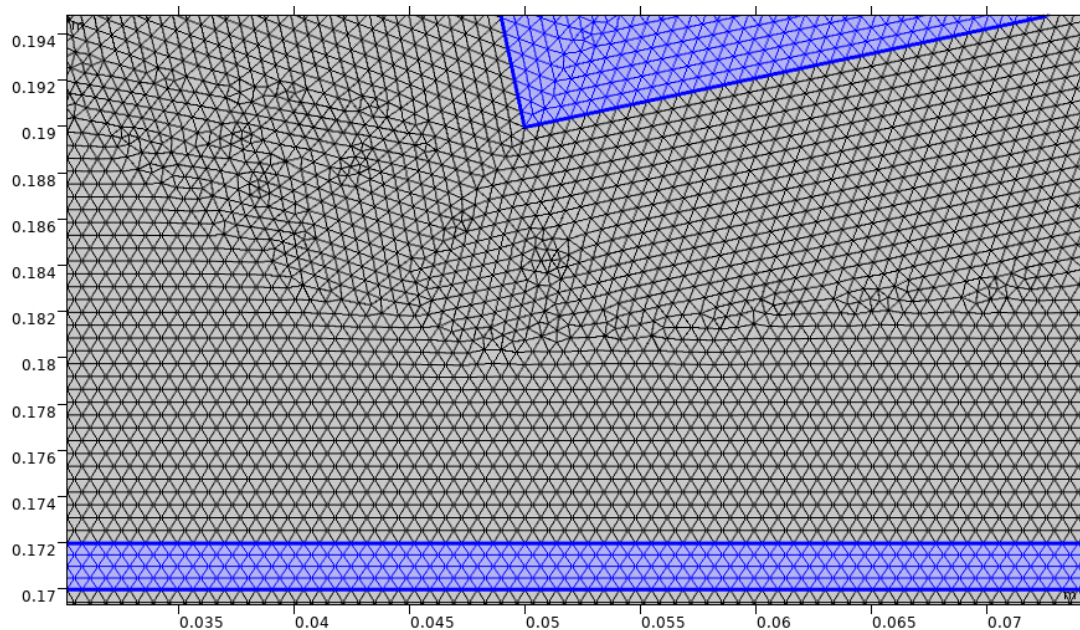
Figure 6.9: Zoomed in part of the COMSOL model showing the mesh grid for plate 1 (blue rectangle at the bottom), the surrounding air and bottom left corner of the transmitter (blue tilted rectangle at the top right corner).

7 Comsol Multiphysics® Simulations

In this chapter, several test cases are conducted in COMSOL Multiphysics ®5.4. The results from simulations are analyzed and compared with the analytical calculations based on the analytical model presented in chapter 5.2 and 5.3.

The different test cases that are to be simulated in COMSOL are as follows:

- Test case 1: Polycarbonate plate material - constant temperature

- Test case 2: Polycarbonate plate material - increase temperature

- Test case 3: Steel plate material - constant temperature

- Test case 4: Steel plate material - Increase temperature

- Test case 5: Steel box with obstacles - increase temperature

- Test case 6: Analytical calculation with switchgear dimensions

Each COMSOL model is solved by the *Time dependent Study* solver, which is commonly used for simulation models where field variables change over time. Each test case is simulated over a simulation time of 2.5 ms and with the time step size of $1/f/5 = 2\ \mu s$, where f is the sound wave frequency. The convergence tolerance for the solver is 0.01.

An average non-specific example for arc fault test conditions was chosen in order to investigate the change in sound velocity during an arc fault. Suppose we were to calculate the temperature rise with the simplified equation (5.6) where the accumulated energy E_{arc} can on average range from 10 to 60 kilo Joule over a time period of 2 ms, and with an average switchgear volume of 0.343 m^3. In that case, we would probably get an average temperature rise between 100 K and 600 K. Therefore, the enclosure domain in test cases 2, 4, 5, and 6 were chosen to be simulated with a temperature increase of 200 K, from room temperature.

7.1 Test case 1: Polycarbonate plate material - constant temperature

The model for test case 1 is built in COMSOL as described in chapter 6, where the geometric parameters for the two plates and transducers are given in table **??** and the material properties for polycarbonate are given in table 6.2. Temperature is kept constant at 20 °C.

Before we can analyze the results, it is important to simulate and show the entire ultrasonic sound propagation path between transmitter and receiver, but in order to accurately see the Lamb wave excitation in the plates, we need to zoom in closer on the plates. Figure 7.1 shows a zoomed-in snapshot of the transmitter in test case 1, where the first ultrasonic compression wave from the transmitter excites the 1st plate Lamb wave in plate 1.

The next following sequence of snapshots shown in figure 7.2 shows the entire ultrasonic sound pulse wave propagation in both airfields and plate domains at different simulation times. Each image contains color scales. The 1st and 2nd colour scales (from left to right) are von Mises Stress (N/m^2) to the surface of plate 2 and 1, respectively. The 3rd, 4th and 5th color scales are acoustic air pressure field (Pa) of the compressional sound wave in receiver domain, enclosure domain, and transmitter domain, respectively. Note that the color scales have different limits between the domains because physical quantities span several orders of magnitude as the sound wave crosses the domains.
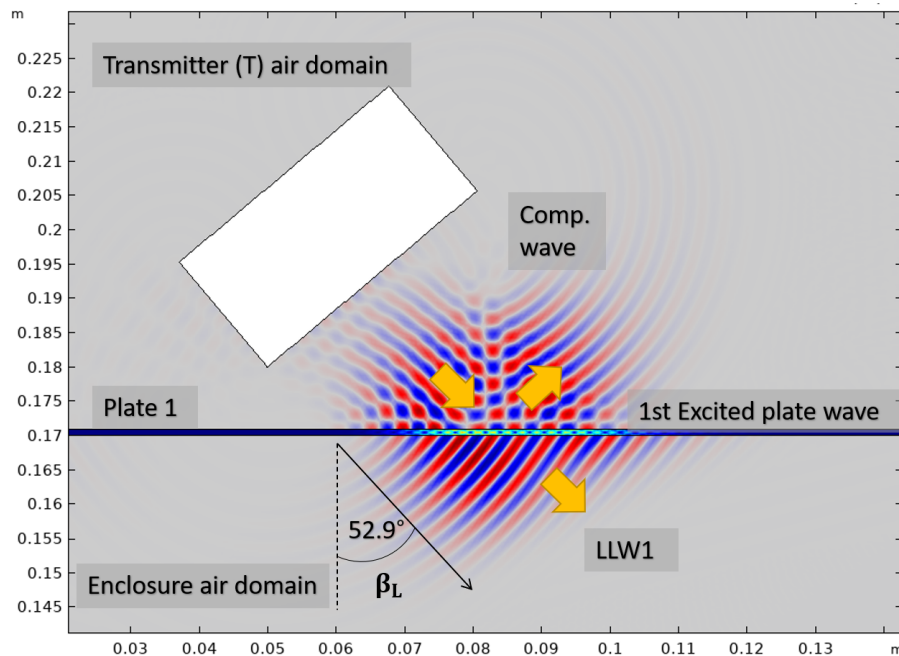
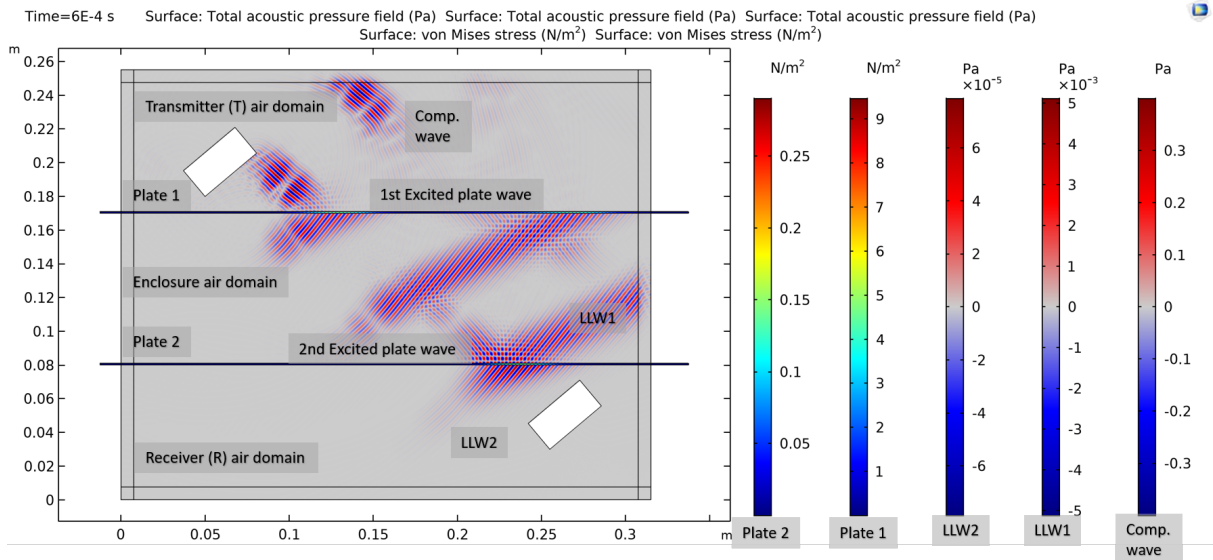Figure 7.1: Zoomed in snapshot of transmitter in test case 1 at simulation time: 1.3E-4 s
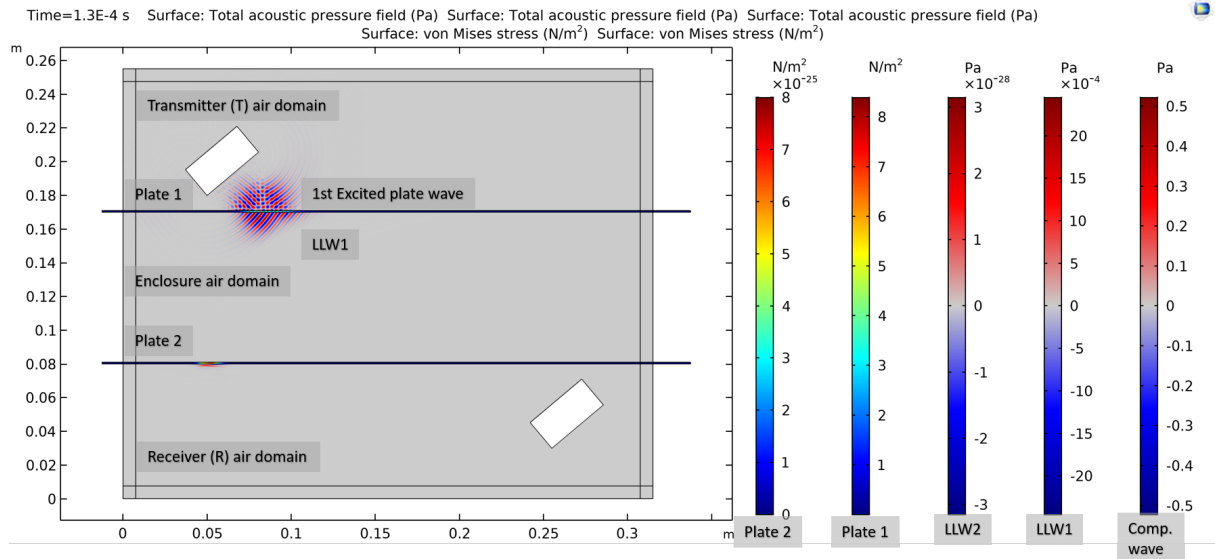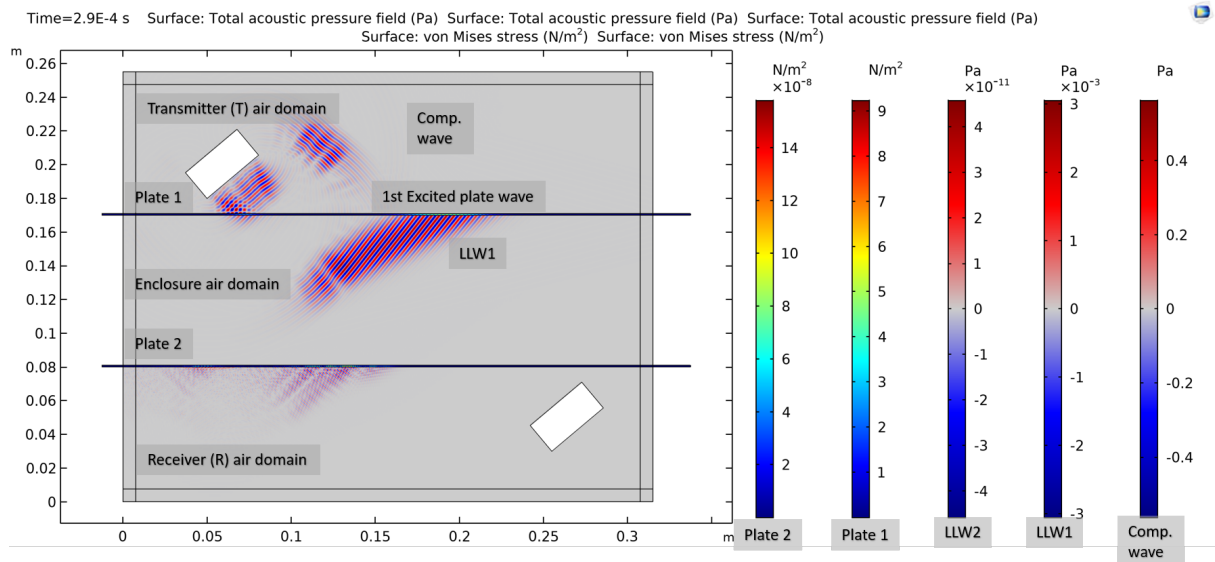
(a) Test case 1 COMSOL model at simulation time: 1.3E-4 s
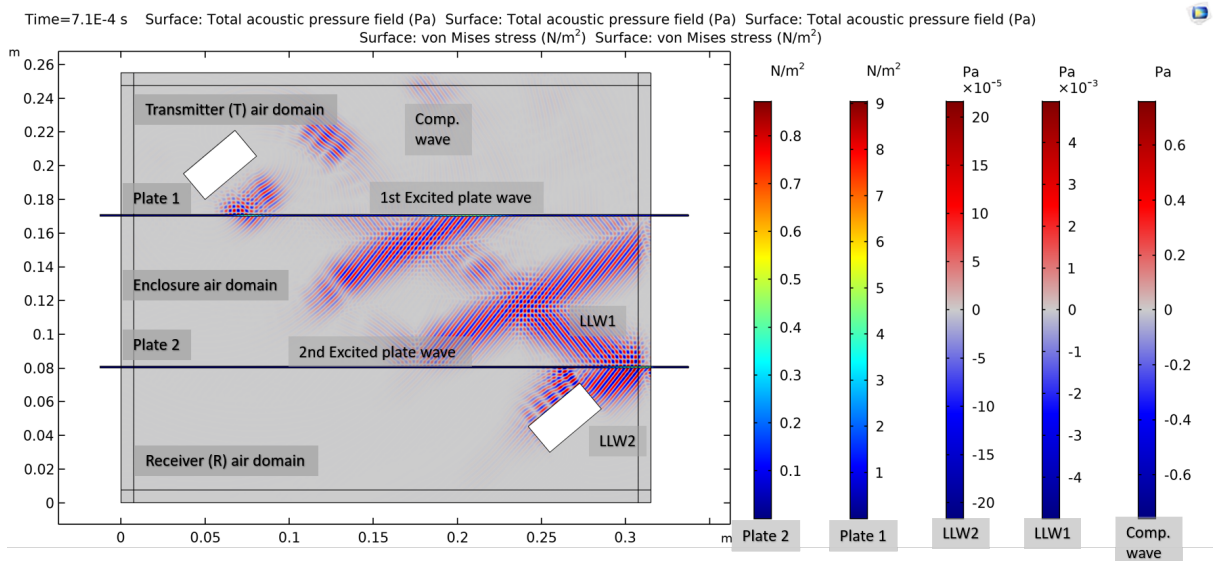

(b) Test case 1 COMSOL model at simulation time: 2.9E-4 s

(c) Test case 1 COMSOL model at simulation time: 6E-4

(d) Test case 1 COMSOL model at simulation time: 7.1E-4

Figure 7.2: Simulation of test case 1

7.1.1 Simulation results and analysis

Figure 7.1 shows the propagation of sound pressure waves by the alternating high and low (i.e., red and blue) pressure wavefronts (Pa). We can see from the figure that the incident compression wave excites a plate Lamb wave in plate 1 by the light blue color gradient in the plate. This color gradient is associated to the von Mises stress (N/m ^{2}). Some of the energy from the incident compressional wave excites the plate with a Lamb wave, while the rest of the incident compressional wave reflects away from the plate surface, as shown by the yellow arrows. The plate Lamb wave leaks energy into the enclosure air, in the form of another compressional wave, marked "LLW1". This leaky wave propagates across the gap at an angle of $\beta_L = 52.9°$ as shown in the figure. This leakage angle is determined by Snell's law and the acoustic velocities of air and solid plate, as was explained in chapter 6.2.4.

The snapshot sequence shown in figure 7.2 shows the entire ultrasound propagation path at different simulation times. Figure 7.2a is the full scale picture of figure 7.1 where the compressional incident wave excites the 1st plate Lamb wave into plate 1, which then leaks energy into the enclosure as another compression wave, marked "LLW1". In Figure 7.2b, "LLW1" travels over the gap between the plates. In this test case, the temperature is kept constant at 20 °, which means that "LLW1" has a wave velocity of $c_L = 343 m/s$ according to the speed of sound equation (4.10. Eventually, "LLW1" reaches plate 2 and excites the 2nd plate Lamb wave, as shown in figure 7.2b. Again, the sound energy from the 2nd plate Lamb wave is leaked into the receiver air domain as another compressional wave, marked "LLW2", as shown in figure 7.2c. Finally, "LLW2" reaches the receiver surface in figure 7.2d, and thereby finalizing the ultrasonic signal propagation path between transmitter and receiver.

It can be seen from the snapshot sequence in figure 7.2 that the pressure scales decrease in intensity as the sound pressure waves propagate between the transducers. This is because sound loses energy on its way reflections that occur at the surface plates. Only some of the energy is able to get through as a lamb wave. The ultrasonic pulses will reflect between the plates as the simulation time progresses. These reflections will excite Lamb waves at lower intensities. In figure 7.2b, some pressure interference can be seen on the left side of the received domain. This might be symmetric waves S_m striking the plate 2. It was previously explained that both symmetric S_0 and A_0 Lamb waves occur from Lamb wave generation at 100 kHz. Symmetric wave modes propagate faster than antisymmetric waves, but at a lower intensity. This is why it is not visible in the enclosure domain, but is in the receiver domain, because the "LLW1" has not reached plate 2 yet and has therefore not produced "LLW2", which is a A_0 wave mode.

Figure 7.3a shows the graph of the sent ultrasonic signal as the boundary load force (F) applied to the transmitter surface. The ultrasonic signal is sent as sound pulses with a 200 μ interval, as marked by the space between the red dots. Figure 7.3b shows the graph of the received ultrasonic signal as floating potential (V). Figure 7.3c shows the graph of the speed of sound inside the enclosure, which has a constant value of 343 m/s due to the constant temperature 293 K. The first ultrasonic signal is received at 640 μs, as shown by the marked red dots. Therefore, the time delay between the sent and the received signal is approximately 640 μs. We can see that the ultrasonic pulse signal is received with a consistent time delay of 640 μs and max amplitude of 35 x 10^{-10}. The red dots also show a 200 μs time interval between each and received sound pulse. On the right-hand side of the graph, there is a smaller signal disturbance with lower amplitudes. These are probably reflected sound waves from the enclosure. The decrease in signal intensity is caused by the signals losing energy each time it strikes the plate surfaces, because some of the energy is transmitted while the rest is reflected.
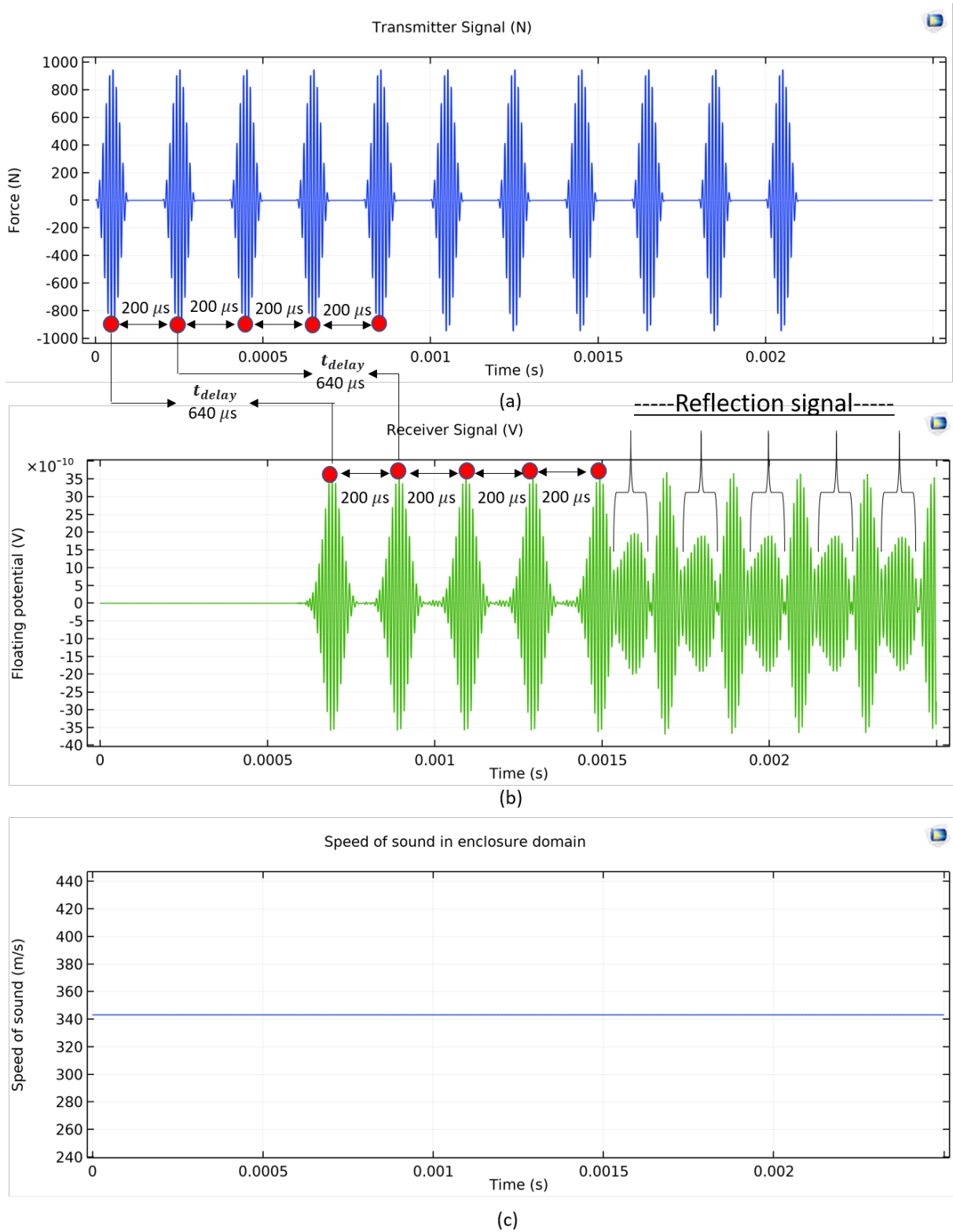
Figure 7.3: test case 1 simulation sent and received signal from transmitter and receiever, and speed of sound

7.1.2 Analytical calculation

The analytical model described in chapter 5.2 was used to calculate the time delay for test case 1. The phase and group velocities for polycarbonate materials may be found using the Rayleigh-Lamb frequency equations described in 4.10. However, it is out of scope to do the complex numerical calculation of the Rayleigh-Lamb frequency equations. Therefore the dispersion curves are readily derived by the cited source and shown in figure 7.4. When a 1 mm thick polycarbonate plate is excited with a 100 kHz sound wave (i.e 0.1 MHZ.mm), we can see from the dispersion curve figure that the A_0 Lamb wave mode will occur with a group velocity $c_g = 690 m/s$s and a phase velocity of $c_p = 430 m/s$. Since the phase velocity of the Lamb wave is 430 m/s, and acoustic velocity of air at 20 °C is 343 m/s, the leaky wave will propagate into air from the plate with the excitation angle $\beta_L = 52.9°$, according to the Snell's law (4.17).
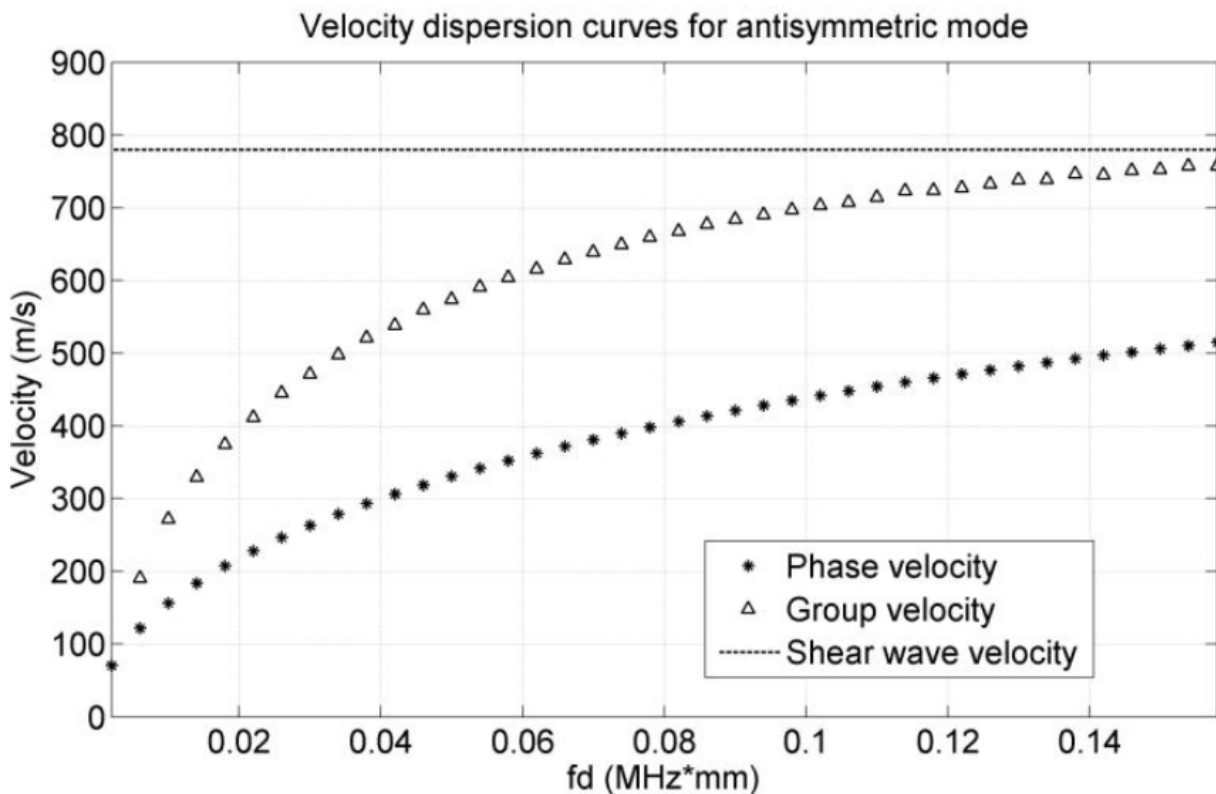
Figure 7.4: Polycarbonate material, phase and group velocity dispersion curves for the A_0 Lamb wave mode

The analytical calculation is summarized in table 7.1. The distance between the transducer and plate is $r_T = 30$ mm and $r_R = 30$ mm. the time it takes for the ultrasound to travel between transducer and plate when using equation (5.1), was found to be $t_T + t_R = 174.9\mu$s. The ultrasound travels the gap between the plate 1 and plate 2 at an angle of $\beta_L = 52.9°$ which gives the distance of $L = 149.2$ mm. The time it takes to travel from one plate to the other was found to be $t_L = 434.9\mu$s, according to equation (5.2). The excited A_0 Lamb wave in plate 2 travels a distance $x_g = 31mm$ at the theoretical group velocity of $c_g = 690m/s$, which means the time was found to be $t_g = 44.9 \mu$ s, according to equation (5.3). Summing this up gives the total time delay between sent and received signal $t_{delay} = 654.6\mu s$.

Table 7.1: Analytical calculation for the time delay, test case 1

Transit time	Equation used	Expression	Caculated value	Unit
t_T	(5.1)	$\frac{r_T}{c_a}$	87.4	$[\mu\text{s}]$
t_L	(5.2)	$\frac{L}{c_L} = \frac{D}{c_L\,cos(\beta_L)}$	434.9	$[\mu\text{s}]$
t_g	(5.3)	$\frac{x_g}{c_g} = \frac{x_p - x_L}{c_g} = \frac{x_p - D\,tan\beta_L}{c_g}$	44.9	$[\mu\text{s}]$
t_R	(5.4)	$\frac{r_R}{c_a}$	87.4	$[\mu\text{s}]$
t_{delay}	(5.5)	$t_T + t_L + t_g + t_R$	654.6	$[\mu\text{s}]$

7.1.3 Discussion

The purpose of this test case was to attempt to reproduce the same model as described in the article published in [1], which will serve as a starting point for further expansion and testing in the next test cases.

The results from the COMSOL simulations showed that the time delay between the sent and the received signal is approximately $t_{delay} = 640\mu s$. The results from the analytical calculations showed that the time delay is approximately $t_{delay} = 654.6\mu s$. By comparing the results from simulations and analytical calculations, there is a 2.26% difference. This is a reasonably low difference, and can therefore argue that the COMSOL model is in good agreement with the theory of Lamb waves, excitation angle, and acoustic velocity speeds.

The values of the results in this test case are nearly equal to the results that were found from the article published in [1], which means that this test case has somewhat successfully reproduced the same model as described in article [1]. The reason why the results from this test case is not exactly identical to the results found in the article, might be due to some boundaries missing, and minor details that may not have been fully described in the article. Nevertheless, this model shows sufficient potential for ultrasonic Lamb wave propagation, due to the theory and analytical calculation agrees with the simulations with a $100 - 2.26 = 97.74\%$ accuracy. Furthermore, the objective of this thesis is to investigate the time delay and the received ultrasonic signal. Therefore, it is not intended to comment or analyze the intensity of the pressure waves, as this can be modified/calibrated in further studies of the topic. Due to the positive results that have been mentioned above, it was decided to continue using the model developed in this test case, and further add extensions to it. The extended versions of this model will be investigated in the next upcoming test cases.

The consistent received signal shown in figure 7.3b indicates that the conditions inside the enclosure are normal and constant. A change in this signal, for example a change in the time delay, could indicate that the conditions have changed. This could potentially be used as information to detect an internal arc fault. The change in the signal can send a tripping signal to a circuit breaker or earthing switch in the switchgear. This concept will be investigated further with the next test cases, where a change in temperature is the condition that will affect the received sound wave signal.

7.2 Test case 2: Polycarbonate plate material - temperature rise

The model developed for test case 2 is identical to the one in test case 1, except that it includes an added extension involving temperature increase in the enclosure domain. The temperature increases from 293 K to 500 K over the time 1.1 - 2.5 ms, as shown in figure 7.5. The following sequence of snapshots shown in figure 7.6 shows the entire sound pulse wave propagation in both air fields and plate domains at different simulation times. The color scales are the same as the color scales in test case 1.

(a) Test case 2 COMSOL model at simulation time: 0.000104
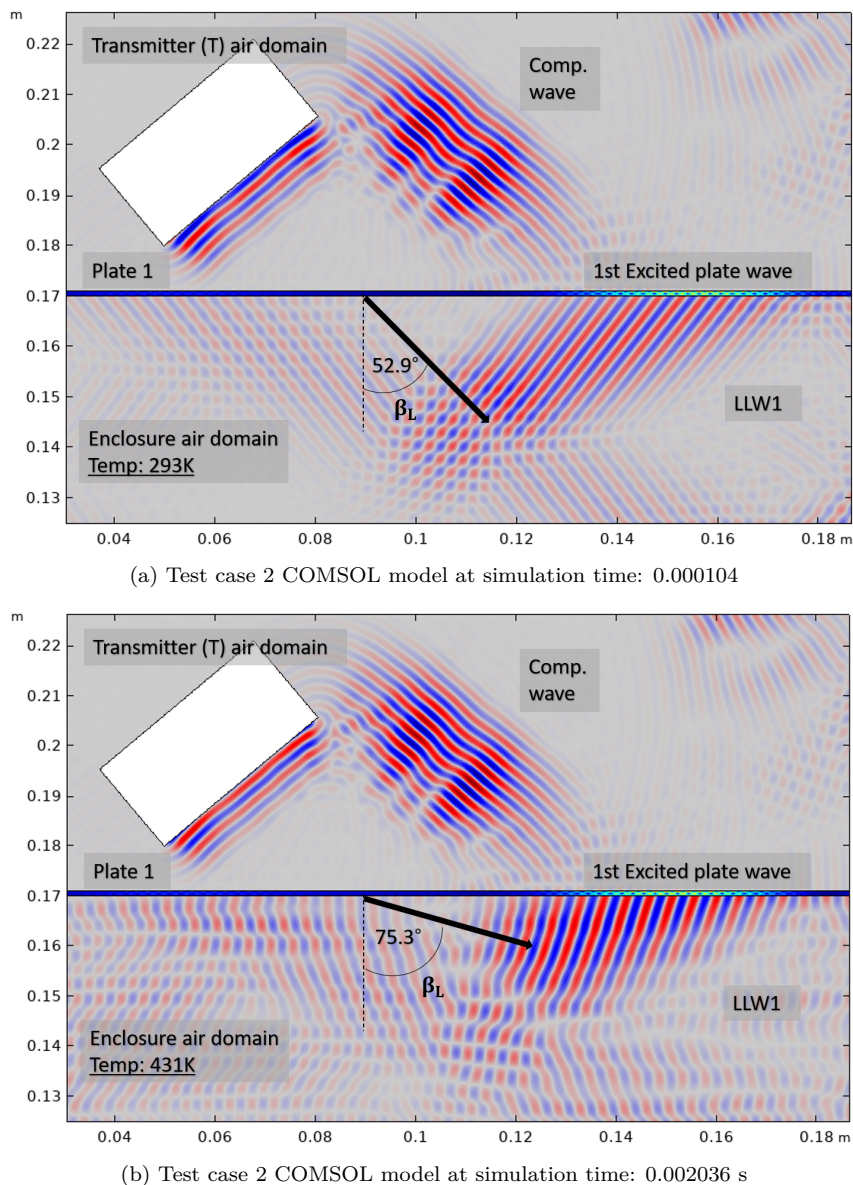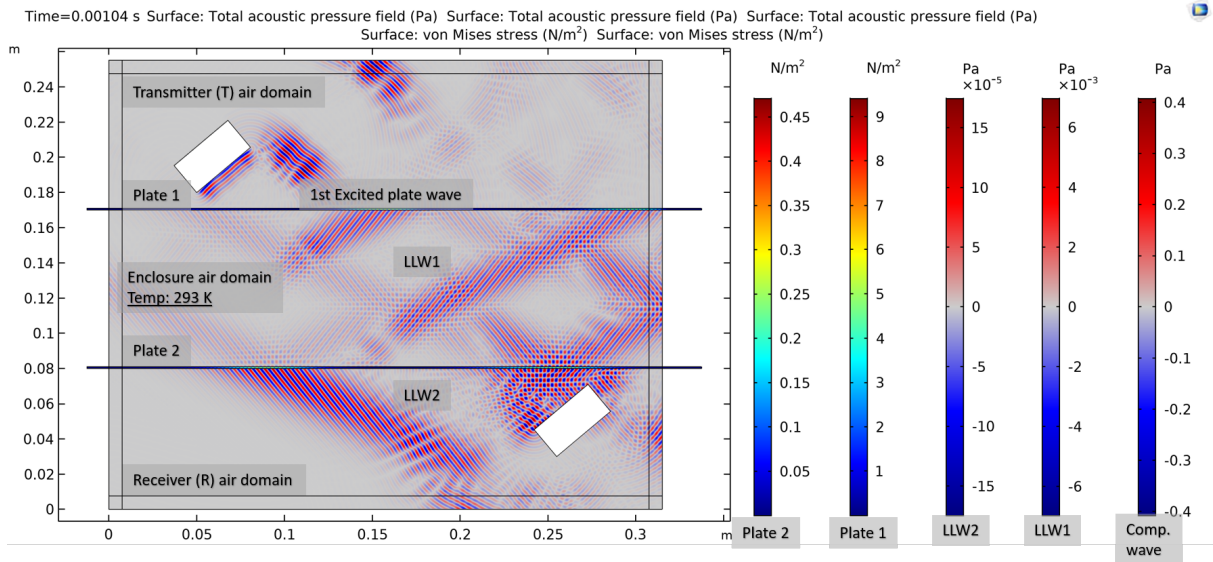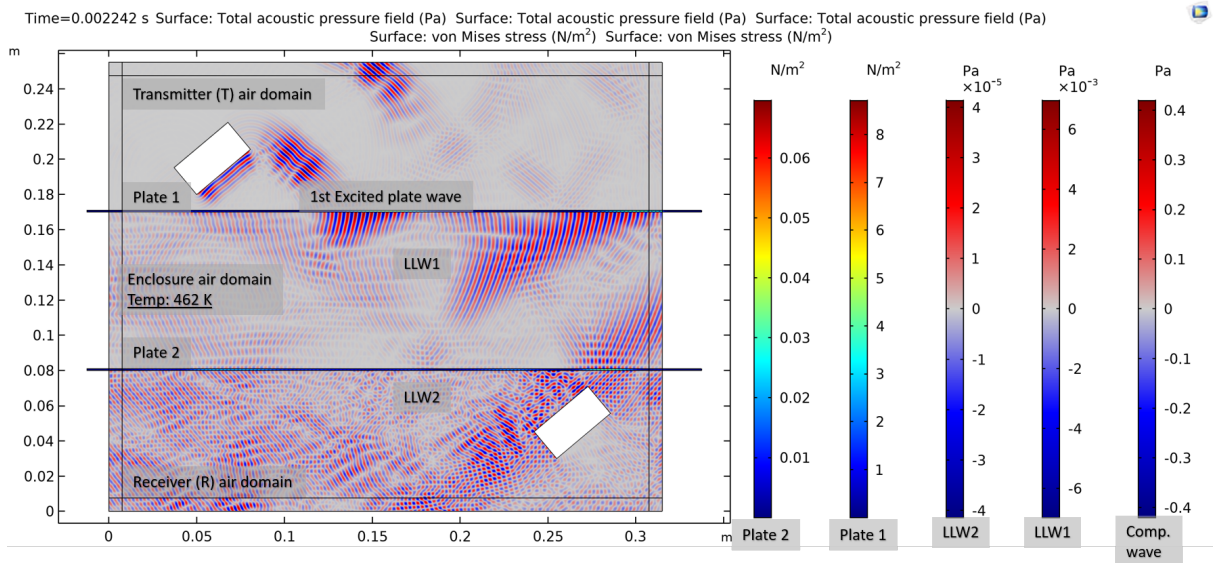

(b) Test case 2 COMSOL model at simulation time: 0.002036 s

Figure 7.5: Zoomed in snapshots of test case 4 at simulation time 0.000104 (temperature 293 K), and at 0.002036 s (temperature 431 K)

(a) Test case 2 COMSOL model simulation time: 0.00104 s

(b) Test case 2 COMSOL model at simulation time: 0.002242s

Figure 7.6: Full scale simulation of test case 2

7.2.1 Simulation results and analysis

Figure 7.5 shows two zoomed-in snapshots of the simulation from test case 2 at simulation time 0.00104 s and 0.002036 s, respectively. By comparing the figures, it becomes quite clear how an increase in temperature affects the leaky Lamb wave "LLW1" propagation.

An increase in temperature results in an increase in the speed of sound. This can be seen by the increased wavelength λ in figure 7.5b. This wavelength is wider compared to the wavelength in figure 7.5a. The wavelength λ in this model increases when the compressional wave velocity c_L increases and frequency f is kept constant, according to equation (4.1).

In addition to an increase in λ, we can also see that excitation angle β_L increases from 52.9°to 75.3°. The excitation angle is determined by the phase velocity of the plate Lamb wave (which was found by the previous test case to be $c_p = 430m/s$) and the acoustic velocity of the leaky Lamb wave "LLW1", according to Snell's law (4.17). In figure 7.5a, the temperature is 292 K, which measn that the acoustic velocity of "LLW1" is $c_L = 343m/s$, according to the speed of sound equation (4.10, where the speed is a function of temperature. In figure 7.5b the temperature is increased to 431 K, which results in the acoustic velocity "LLW1" being increased to $c_L = 416m/s$. The increase in acoustic velocity of c_L leads to an increase in excitation angle β_L, according to Snell's law (4.17).

Figure 7.6 shows two snapshots of the full-scale model where we can see the entire simulated wave propagation path of test case 2, at simulation time 0.00104 s and 0.002242 s, respectively. Here we can see at full scale how an increase in temperature affects the wavelength λ of the sound wave and the excitation angle β_L. Additionally, the figures also show a surprising fact that an increase β_L causes the propagation path between the plates L to become longer. This will have an effect on the time delay between sent and received signal.

Figure 7.7a shows a graph of the sent ultrasonic signal as a boundary load force (F) applied to the transmitter surface. Figure 7.7b shows a graph of the received ultrasonic signal as a floating potential (V). Figure 7.7c shows that the speed of sound inside the enclosure domain linearly increases from 343 m/s to 450 m/s after the time 0.0011 s, due to linear temperature increase.

The first ultrasonic signal is received at 640 *mu*s when the temperature of the enclosure domain is kept constant at 293 K. But as the temperature increases after the simulation has passed 1.1 ms, the time delay between sent and received signal increases. This is approximately measured by the max and min pulse amplitudes between sent and received signal, which is marked as red dots in figure 7.7. It is important to note that this is just an approximation of the graph, which may contribute to some sources of error.

The linear increase in speed of sound is caused by the linear increase of temperature inside the enclosure domain. From the graph in figure 7.7 we can see that the pulse intensity decreases as the temperature increases. Sound wave intensity is independent of frequency and wave velocity. Therefore, the decreased received signal might be due to the excitation angle increasing and thus shifting the propagation path away from the transducer. The entry point for the 2nd excited plate wave gets displaced farther to the right than where the receiver is located. This might mean that the wave do not reach the surface of the receiver, but instead passes far out on the right side of receiver, as temperature increases with time.

We can also see that the von Mises stress scale for plate 2 shown in figure 7.6b has decreased in value compared to the scale shown in figure 7.6a, which might indicate that the Lamb wave energy inside the plate has been reduced, and the ultrasonic signal sent from the transmitter is not transmitted through the plate 2, because it propagates out on the right side of the model. Therefore, the signals received after 2 ms might be the reflections between the transducer surface and the plate surface.
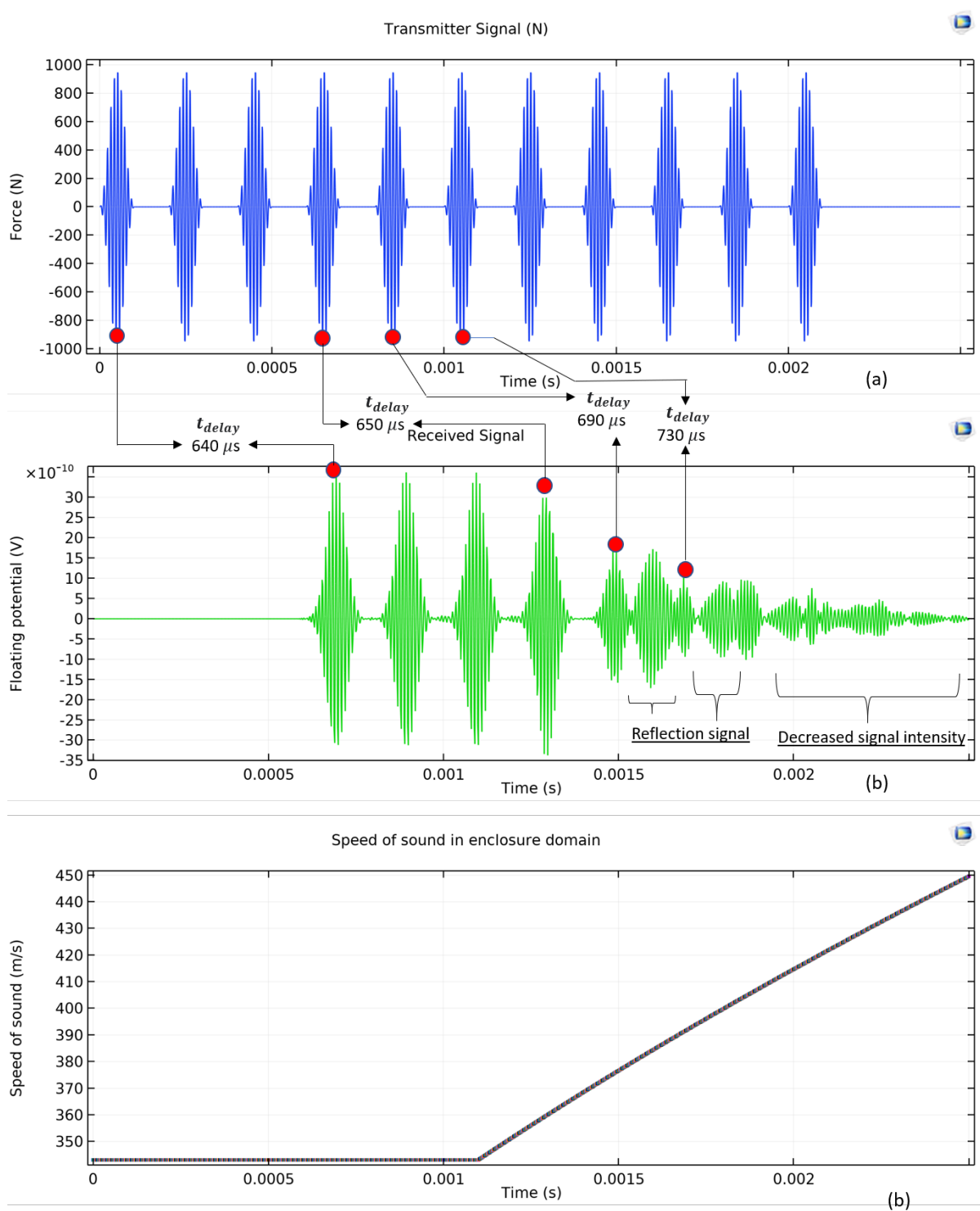
Figure 7.7: test case 2 simulation sent and received signal from transmitter and receiver, ans speed of sound

7.2.2 Analytical calculation

The analytical model described in chapter 5.3 was used to calculate the change of time delay for test case 2. The temperature increases from 293 K to 500 K over a time period of 1.1 - 2.5 ms. The phase and group velocities for Lamb waves in polycarbonate plates are the same as those found in test case 1 (which was defined by looking at the dispersion curve figure 7.4, the phase and group velocity was found to be $c_p = 430$ m/s and $c_g = 690$ m/s, respectively). Since the temperature increases over time, the acoustic velocity of "LLW1" $c_L(t)$, the excitation angle $\beta_L(t)$, and the propagation distance between the plates $L(t)$, increases over time. This will affect the sound wave transit times $t_L(t)$, $t_g(t)$, and finally $t_{delay}(t)$. Table 7.2 shows how each of these variables changes over time as the temperature increases. The multi-figure 7.8 contains graphs of the variables as a function of temperature.

Table 7.2: Analytical calculation for the time delay, test case 2

Variable	Equation used						unit
Time	Defined in simulation	1.10	1.45	1.80	2.15	2.50	[ms]
Temperature $T(t)$	Defined in simulation	293	350	400	450	500	[K]
$c_L(t)$	(5.7)	343.0	375.1	401.0	425.3	448.3	[m/s]
$\beta_L(t)$	(5.8)	52.9	60.7	68.8	81.5	—	[deg]
$L(t)$	(5.9)	149.2	184.1	249.3	612.0	—	[mm]
$t_L(t)$	(5.10)	421	489	596	1280	—	[μs]
$t_g(t)$	(5.11)	44.9	0	0	0	—	[μs]
$t_{delay}(t)$	(5.12)	640.7	663.8	770.8	1454.8	—	[μs]

Note that when the temperature exceeds 460 K, the speed of sound in the enclosure domain c_L will be faster than the phase velocity of the plate Lamb wave $c_p = 430 m/s$. According to Snell's law, if the speed of sound in the enclosure domain exceeds the phase velocity $c_L > c_p$, it will result in the plate Lamb wave stopping leaking energy into the enclosure domain. This is indicated by the empty cells in table 7.2. Consequently, meaning that ultrasonic signal will not transmit through the plate, and therefore will not be received by the receiver. As the temperature increases, the excitation angle $\beta_L(t)$ increases and shifts the entry point for the 2nd plate Lamb wave farther away from the receiver. We assume that position of the transducers is kept consistent. It can be seen in table 7.2 that the transit time $t_g(t)$ is zero. This is because the entry point of the sound wave has passed

the location of the receiver, and therefore there is no transit time in the plate between the entry point and receiver. The total time delay is the time it takes for the ultrasonic signal to travel from the transmitter until it reaches plates 2.

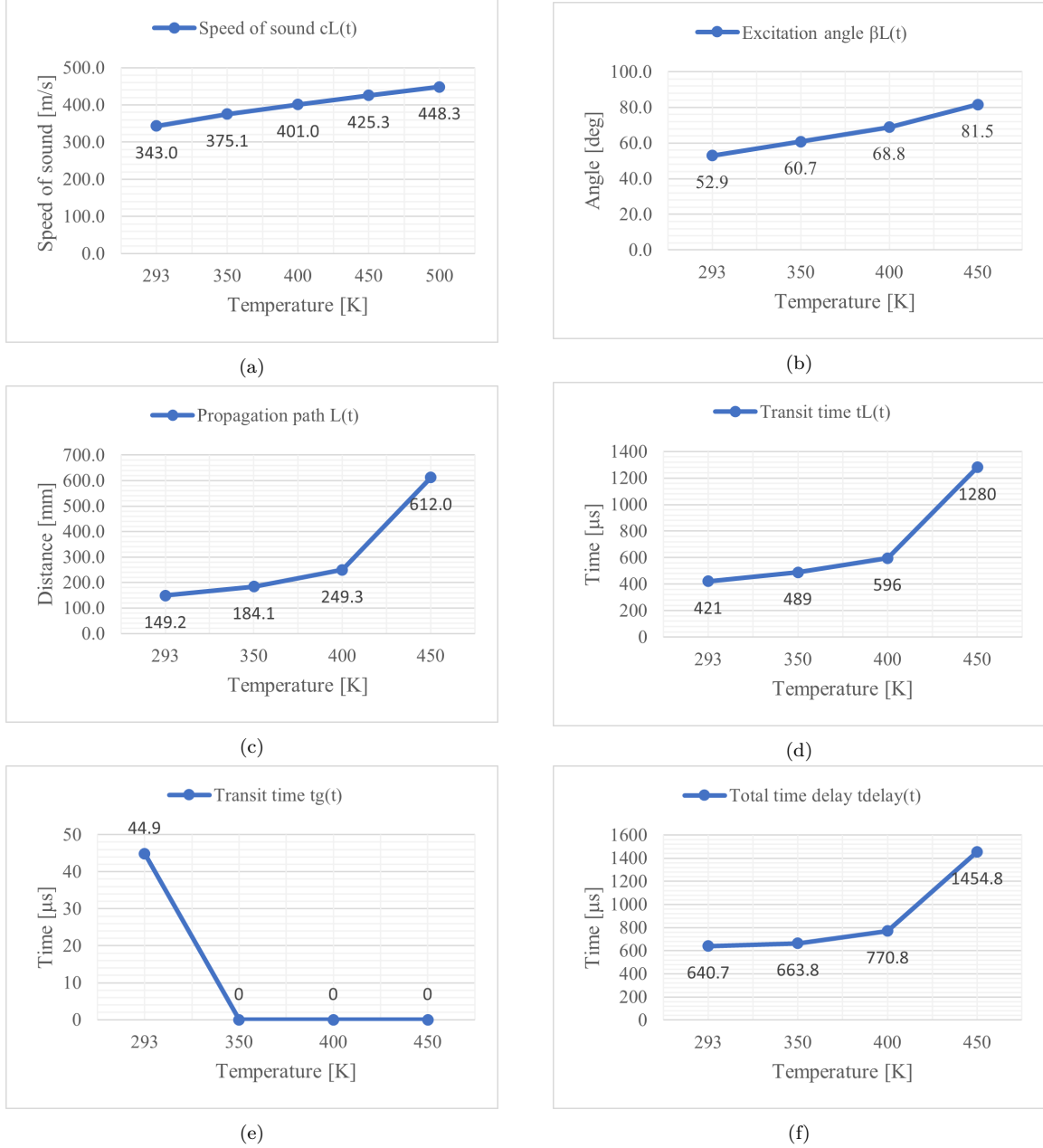Figure 7.8: Test case 2 analytical calculation of the variables as a function of temperature. (a) speed of sound inside enclosure domain $c_L(t)$, (b) excitation angle β_L, (c) propagation path distance between the plates L, (d) transit time between the plates t_L, (e) transit time of 2nd excited plate Lamb wave propagation along plate 2 t_g, (f) total time delay between send and received ultrasound signal t_{delay}

7.2.3 Discussion

The results from test case 1 showed that the received signal remained constant and stable throughout the simulation. The stability of the signal is likely due to environmental conditions like temperature and pressure being constant and not varying over time. The results from test case 2, however, shows a non-consistent received signal as the temperature inside the enclosure domain increase, which will be analyzed with the following text.

It was recently explained that an increase in temperature would result in an increase in the speed of sound. This increased velocity caused the excitation angle β_L to increase and shift the propagation path L to become longer in the distance, and effectively displacing the entry point for the 2nd plate Lamb wave farther away from the receiver. This might be the possible reason for why we can see the signal intensity in figure 7.7 decrease after the temperature increases.

The figure 7.7, also shows that the time delay between the sent and received signal increases over time as the temperature increases. The initial expectation from this test case was to observe the time delay decrease as the speed increases from the temperature rise. The decrease in time delay might be due to the relatively large increase in excitation angle β_L. The excitation angle is determined by Snell's law, and since the acoustic velocity of the compressional wave inside the enclosure domain "LLW1" are close to the value of the phase velocity of the Lamb wave excited in plate 1 (which is determined by the frequency and plate thickness according to the dispersion curve), a small change in temperature will have a huge impact on the excitation angle β_L. The propagation path L is influenced by the β_L, as can be seen from figure 7.6. Even though the speed of sound increases as temperature rises, the propagation path L distance increases at faster rate than the speed of sound, which consequently results in the time delay increasing instead of decreasing.

This explanation is also supported by the analytical calculation, where we can see from the graph figure 7.8c that the propagation path $L(t)$ increases at a faster rate than the speed of sound $c_L(t)$ shown in graph figure 7.8a, which ultimately results in the time delay t_{delay} increasing, as shown in graph figure 7.8f.

The considerably large increase in the excitation angle β_L as shown in graph figure 7.8b might be a direct consequence of the elastic properties of the polycarbonate material. Polycarbonate material has a relatively low elastic constants (Young's Modulus $E = 2.0$ GPa) compared to more dense materials like steel (Young's Modulus $E = 200$ GPa), causing the plate Lamb wave phase velocity to have small difference to the acoustic velocity of air. A small difference between the phase velocity and the "LLW1" velocity c_L results in a larger refraction angle, according to Snell's law.

A possible solution to minimize the variation in excitation angle, is to modify the frequency and thickness of the polycarbonate plate in order to increase the phase velocity, and thereby increase the acoustic velocity difference between air and plate lamb wave. This can be done according to the dispersion curves in figure 6.5. This can reduce the change of excitation angle as the temperature increases. But then the received signal may be exposed to noise from the several orders of antisymmetric A_m and symmetric S_m Lamb wave modes that may occur, as shown in the dispersion curve figure 6.5. However, polycarbonate is not used as material for switchgear walls. It would therefore be meaningless to discuss different solutions to improve the quality of the received signal, as it is inherently difficult to do due to the low elastic constants. Nevertheless, this test case proved useful to easily demonstrate the possibility of sound transmission through solid plates, and how an increase in temperature causes different effects in both the excitation of the plate Lamb waves and the received signal. It is important to be aware of these effects and how much it influences the variables $(L(t), \beta_L(t), L(t), t_L(t), t_g(t), t_{delay})$. This shows that there are alot of factors that needs to be taken into great consideration when designing a non-intrusive ultrasonic transducer for internal arc fault detection. Further investigation upon the effects and sensitivity analysis should be conducted if we were to optimize the use of ultrasonic transducers for internal arc fault detection.

In the next test cases, we will investigate steel plates, because that is the material that is used in switchgear walls. It will be interesting to see how much more or less the variables $(L(t), \beta_L(t), L(t), t_L(t), t_g(t), t_{delay})$ will vary with the same temperature and frequency conditions as this test case. .

7.3 Test case 3: Steel plate material - constant temperature

The model developed for test case 3 is built similarly to the previous test cases, meaning the geometric parameters are identical and given in table 6.1. However, this model replaces the polycarbonate plate with steel plates. The properties for steel material are given in table 6.3. The temperature in this test case is kept at a constant value of 20 degrees C.

Before we can analyze the results, it is important to simulate and show the entire ultrasonic sound propagation path between transmitter and receiver, but in order to accurately see the Lamb wave excitation in the plates, we need to zoom in closer on the plates. Figure 7.9shows a zoomed-in snapshot of the transmitter in test case 3, where the first compression is sent from the transmitter and excites the 1st plate Lamb wave in plate 1.

The next following sequence of snapshots in figure 7.10 shows the entire ultrasonic sound pulse wave propagation in both airfields and plate domains at different simulation times. The color scales are the same as the ones explained in test case 1.

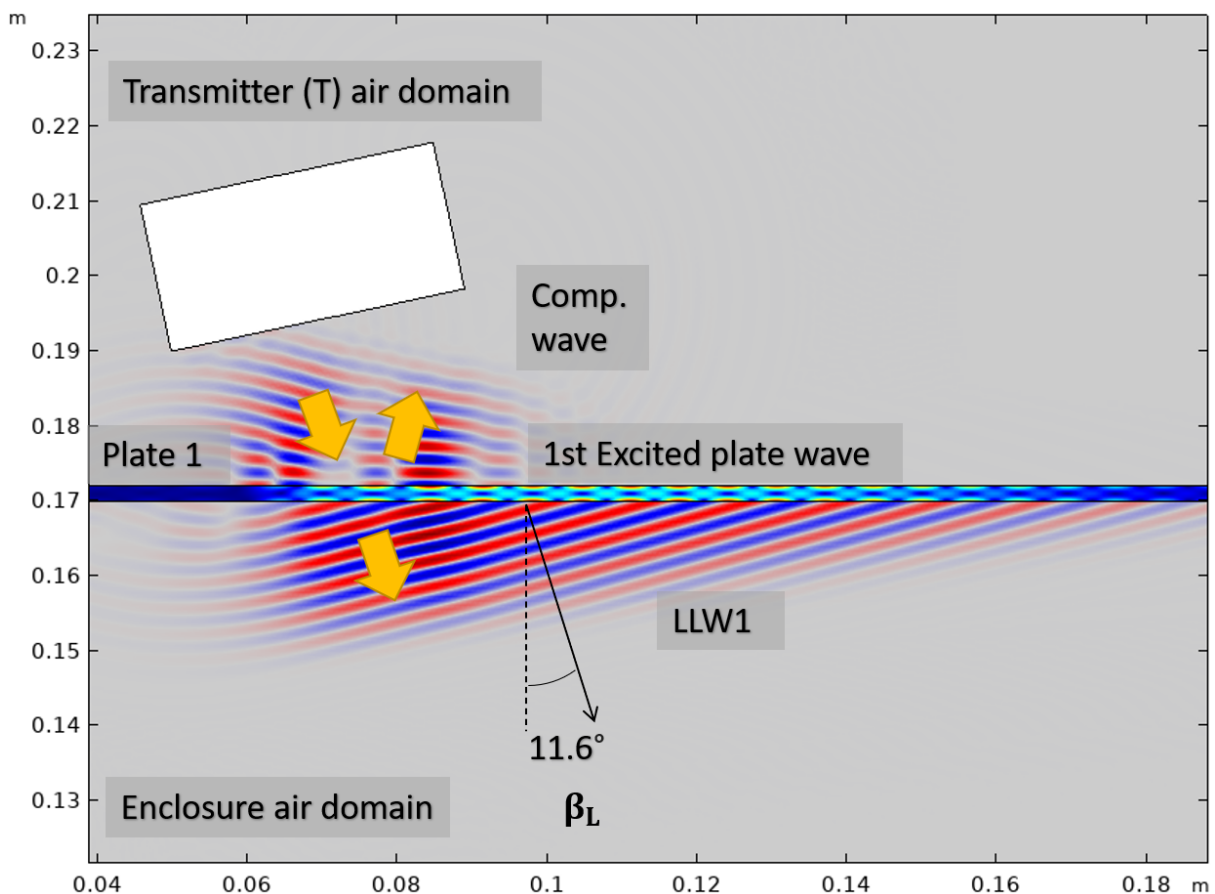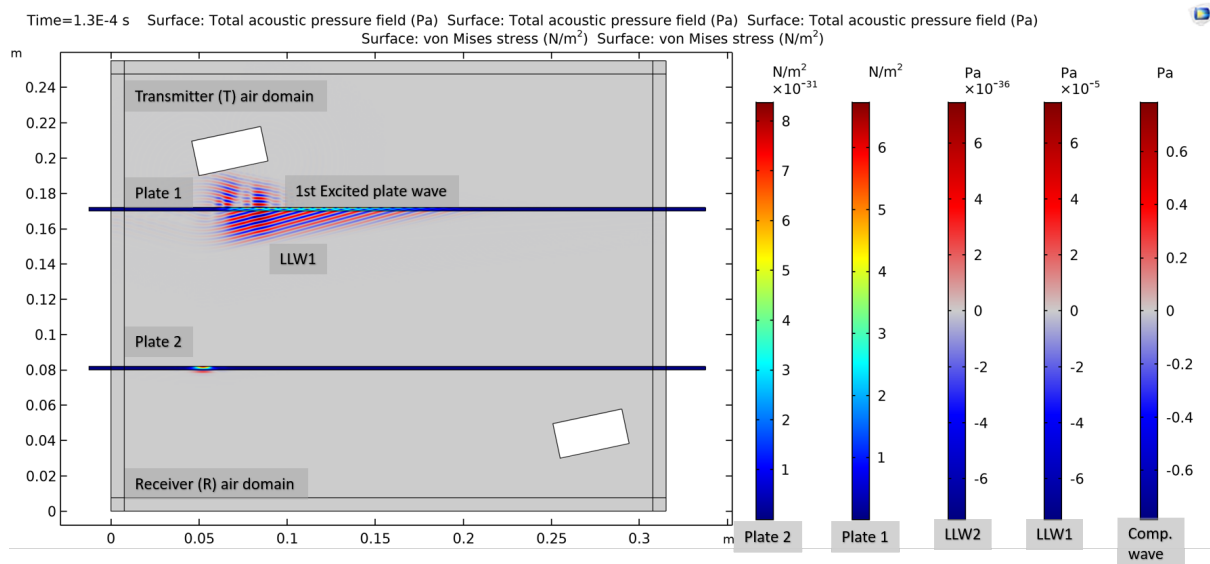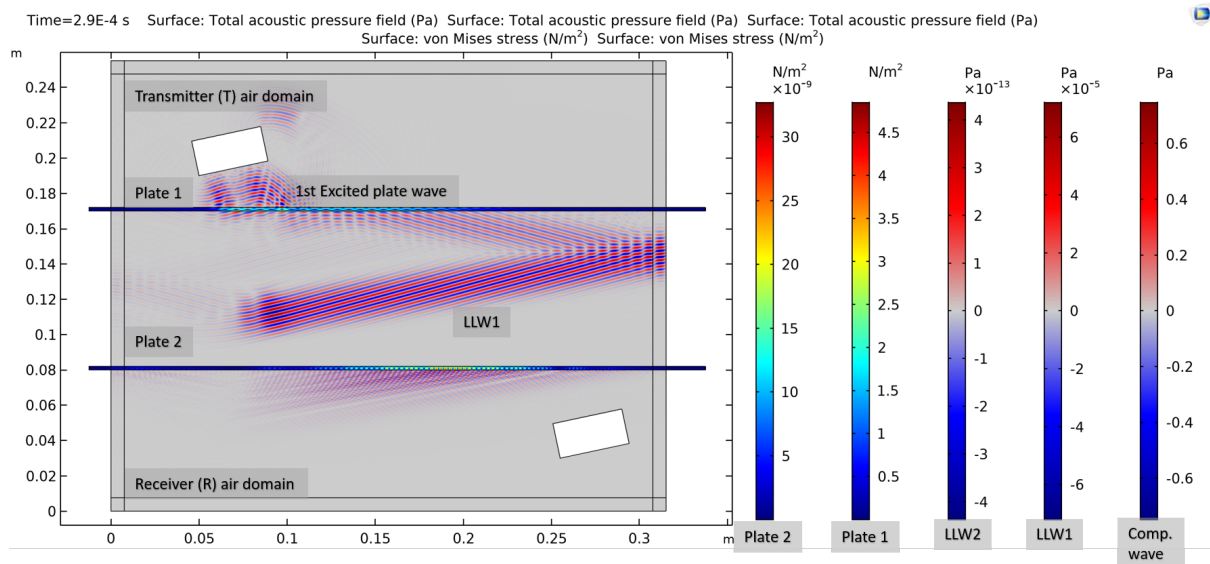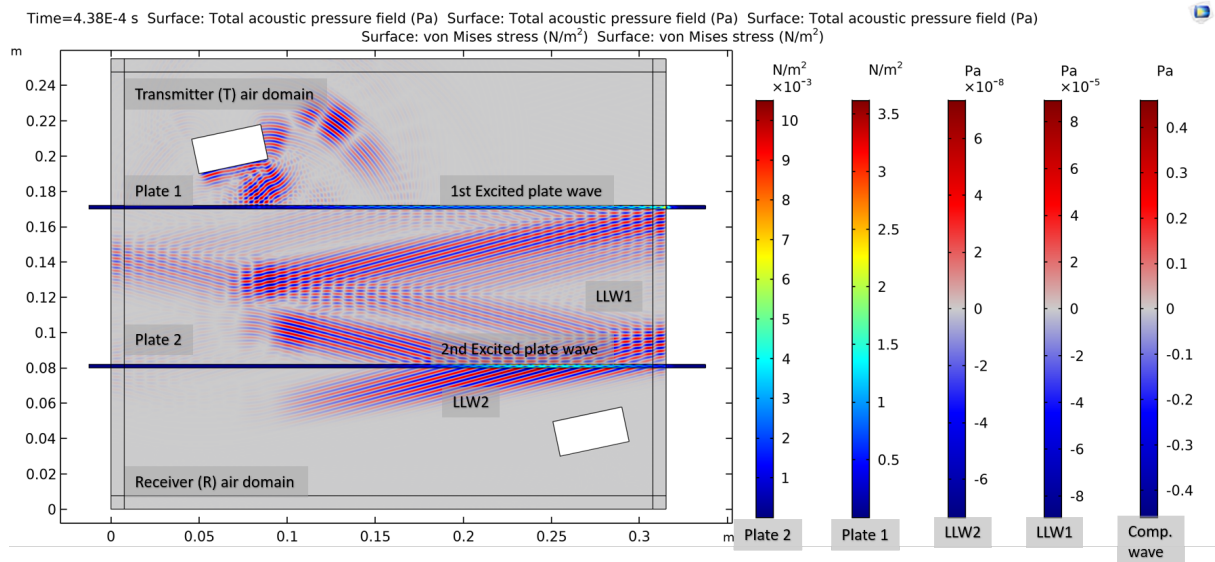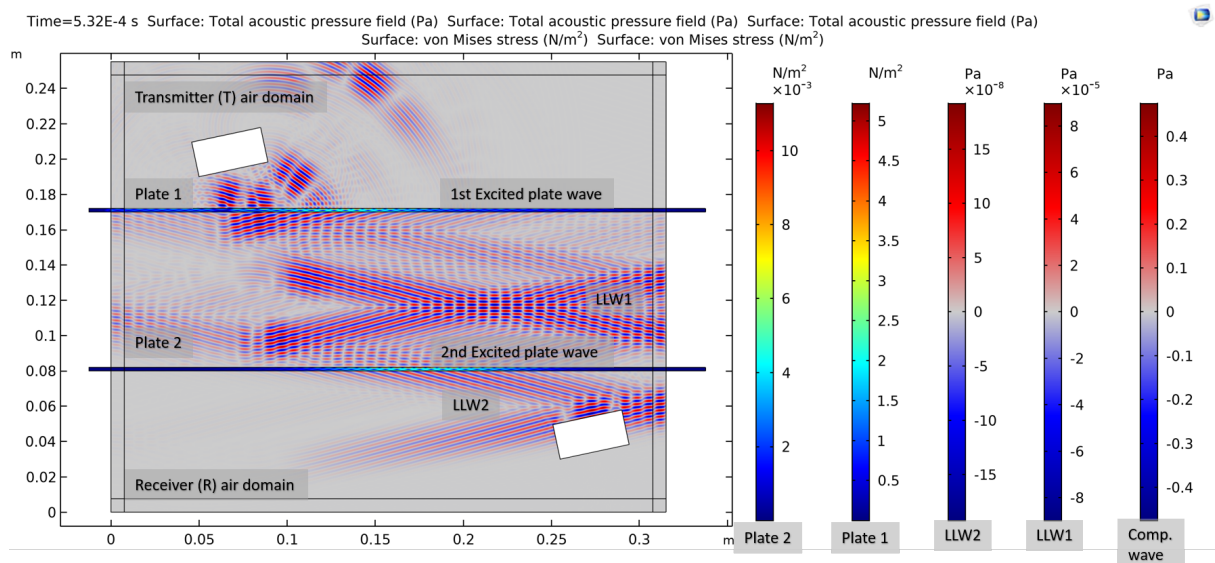Figure 7.9: Zoomed in snapshot of transmitter in test case 3 at simulation time 1.3E-4 s

(a) Simulation time: 1.3E-4 s

(b) Simulation time: 2.9E-4 s

(c) Simulation time: 4.38E-4

(d) Simulation time: 5.32E-4

Figure 7.10: Simulation of test case 3

7.3.1 Simulation results and analysis

Figure 7.9 shows a zoomed-in snapshot of test case 3 at simulation time 1.3E-4s. The transmitter produces a compression sound wave. Some of the energy from that incident compression wave is used to excite the plate Lamb wave, while the rest of the energy reflects off the plate surface, as shown by the yellow arrows. The plate Lamb wave propagates along with the steel plate, and continuously leaks energy into the enclosure air domain in the form of another compression wave, marked "LLW1". This leaky-wave propagates across the gap at an angle of $\beta_L = 11.6°$, as shown in the figure. This leakage angle (or excitation angle) is determined by Snell's law and the acoustic velocities between air and steel plate, as explained in chapter 6.2.4.

The snapshot sequence shown in figure 7.10 shows the entire ultrasound propagation path at different simulation times. The excitation of Lamb waves in the plates and propagation of leaky Lamb waves is well explained in the chapter 7.1.1 "Results and analysis" for test case 1. Therefore it is unnecessary to repeat that here. However, it is important to note that there is a noticeable change in the propagation path due to the polycarbonate material being replaced with a steel material. The steel material has more robust elastic properties, which means the excited lamb wave has faster phase velocity and group velocity compared to the previous test cases. This can be recognized by the substantially smaller excitation angle (from 52.9°in polycarbonate plate to 11.6°in steel plate), which is determined by Snell's law equation (4.17). In order to optimize the transmission of sound energy, the transmitter is inclined at an angle of 11°.

Figure 7.11a shows the graph of the sent ultrasonic signal as the boundary load force (F) applied to the transmitter surface. Figure 7.11b shows the graph of the received ultrasonic signal as floating potential (V). Figure 7.11c shows the graph of the speed of sound inside the enclosure, which has a constant value of 343 m/s due to the constant temperature 293 K. The first ultrasonic signal is received with a time delay of 500 μs between the sent signal, as marked by the red dots and arrows. The time delay is approximately consistent throughout the simulation time. The red dots also show that there is a 200 μs time interval between each sent and received signal pulse. The amplitudes of the received signal vary with time. The received signal do also contains many reflection signals with varying amplitudes.
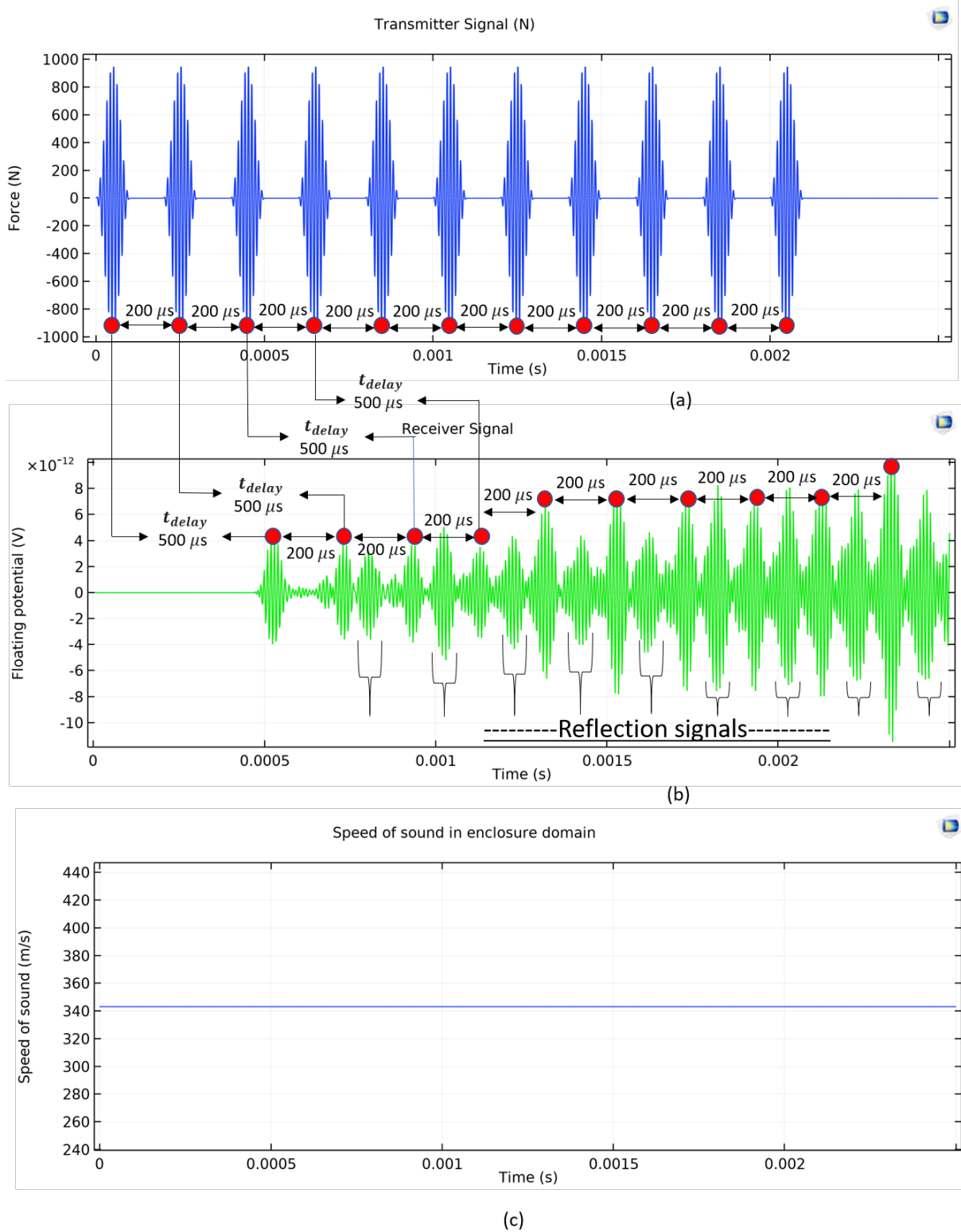
Figure 7.11: test case 3 simulation sent and received signal from transmitter and receiver, and speed of sound

7.3.2 Analytical calculation

The analytical model described in chapter 5.2 was used to calculate the time delay for test case 3. The phase and group velocities for steel material may be found using the Rayleigh-Lamb frequency equations described in 4.10. However, it is out of scope for this thesis to do the complex numerical calculation of the Rayleigh-Lamb frequency equations. Therefore the dispersion curves are readily derived by the cited source and shown in figure 7.12. If a 2 mm thick steel plate is exposed to a 100 kHz sound wave (i.e. 0.2 MHz.mm), we can see from the dispersion curve figure that the A_0 Lamb wave mode will occur with a group velocity c_g of approx, 1700 m/s and a phase velocity of c_p approx. 430 m/s. Since the phase velocity of the of the Lamb wave is 1700 m/s, and the the acoustic velocity of air at 20 °C is 343 m/s, the leaky wave will propagate into air from the plate at an excitation angle of 11.6°, according to Snell's law (4.17). The analytical calculation for time delay between send and received ultrasound signal is summarized in table 7.3
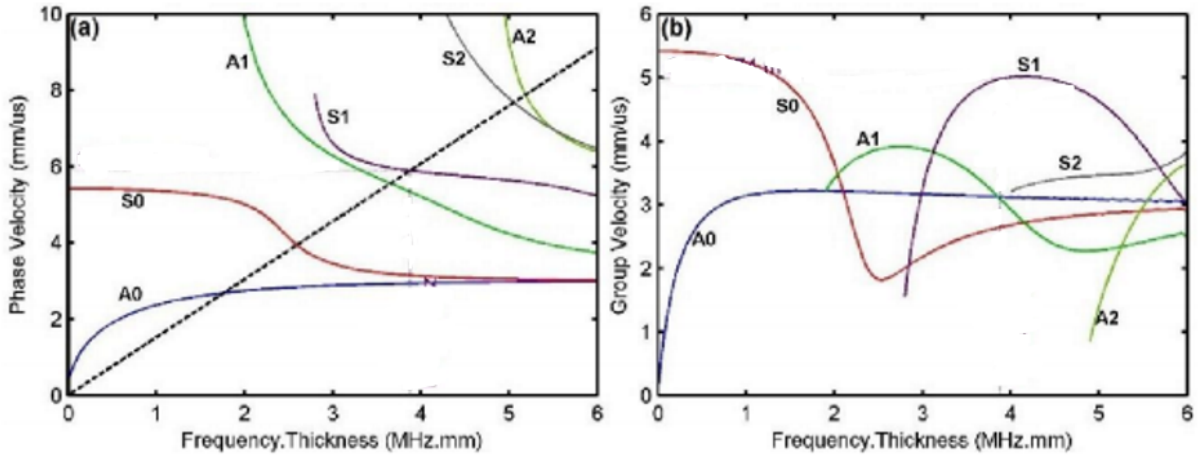
Figure 7.12: Phase and group velocity dispersion curves where several orders of antisymmetric A_m and symmetric S_m Lamb wave modes are possible at higher thickness-frequency products

Table 7.3: Analytical calculation for the time delay, test case 3

Transit time	Equation used	Expression	Calculated value	Unit
t_T	(5.1)	$\frac{r_T}{c_a}$	87.4	[μs]
t_L	(5.2)	$\frac{L}{c_L} = \frac{D}{c_L\,cos(\beta_L)}$	267.8	[μs]
t_g	(5.3)	$\frac{x_g}{c_g} = \frac{x_p - x_L}{c_g} = \frac{x_p - D\,tan\beta_L}{c_g}$	77.3	[μs]
t_R	(5.4)	$\frac{r_R}{c_a}$	87.4	[μs]
t_{delay}	(5.5)	$t_T + t_L + t_g + t_R$	523.5	[μs]

7.3.3 Discussion

The results from the COMSOL simulations showed that the time delay between the sent and the received signal is approximate $t_{delay} = 500\mu s$. The results from the analytical calculations showed that the time delay is calculated approximately $t_{delay} = 523.5$. By comparing the simulation results and the analytical calculations, there is a 4.59% difference. This is a reasonably low value and can therefore argue that the COMSOL model is in good agreement with the theory of Lamb waves, excitation angle, and acoustic velocity.

We can see there is a difference between the result from this test case compared to the previous polycarbonate test cases. All the differences and the reason behind them will be discussed in the following text.

In test case 1, the simulated time delay between the sent and the received signal was 640 μs. In this test case, the polycarbonate material has been replaced with steel material, which resulted in the time delay reducing down to 500μs, as shown in the received signal in figure 7.11. The most likely explanation for this decrease in time delay might be due to the excitation angle is $\beta_L = 11.6°$, shortening the propagation path between the plates L from 149.2 mm to only 91.9 mm. This is a direct correlation to the elastic properties of the steel plate material. Test case 1 had a 2.26% correspondence between the simulated time delay and the analytically calculated time delay, whereas this test case has 4.59%. The reduction in the accuracy between the analytical calculation in relation to the simulated results might be due to some uncertainty that is present in the analytical calculation. The dispersion curve figure 7.12 is used to find the phase and group velocities of the excited plate lamb waves, which is used to calculate the time delay in the analytical model. This dispersion curve might not have been calculated with the same steel material properties that were used in the COMSOL simulation (i.e. it might not have these properties: Young's modulus $E = 200\ GPA$, Poisson's ratio $v = 0.30$, and density $\rho = 7750\ kg/m^3$), which might be a source of error. Nevertheless, the reduction in accuracy is sufficiently low enough to argue that the simulated model is in good correspondence with the theory.

Since the steel material has a higher elastic constant and a thicker density than polycarbonate, the transducers need to be inclined at an angle of 11°in order to excite a lamb wave at 100 kHz. The drawback of this angle is that it causes sound wave reflections between the transducer and plate. From the simulation figure, we can also see that the angle causes repetitive reflections between the plates. This might be the reason why the received signal in figure 7.15b seems to be noisier with more reflection signals, compared to the received signal in test case 1. A possible solution to minimize the reflections is by strategically adjusting the frequency in accordance with the dispersion curves for steel plates. The excitation angle $\beta_L = 11°$ is determined by Snell's law and the acoustic velocities of air c_L and plate lamb wave phase velocity c_p. Since the frequency is 100 kHz, the phase velocity is $c_p = 1700m/s$, according to the dispersion

curve in figure 6.7. If we were to reduce the frequency, the phase velocity c_p would reduce, and the excitation angle β_L will increase. So by decreasing the frequency, the excitation angle can increase, and therefore potentially reduce the reflection and noise signals that are present in the received signal. Otherwise, the received signal shown in figure 7.11 may prove to be too difficult for a signal processor to evaluate regarding internal arc fault detection. This suggestion would require further studies and sensitivity analysis of the plate material with varying frequencies.

However, it is also important to remember that by increasing the excitation angle, the time delay between the sent and received signal will also increase due to the increased propagation path. An increase in the excitation angle might reduce reflections, but it would also sacrifice how fast the receiver would detect a potential internal arc fault. Therefore, again, these factors need to be greatly considered when tuning the ultrasonic transducers for internal arc fault detection.

7.4 Test case 4: Steel plate material - Temperature increase

The model developed in test case 4 is identical to the model in test case 3, except that it also includes an added extension involving temperature increase in the enclosure domain. The temperature increases from 293 K to 500 K over the time 1.1 - 2.5 ms, as shown in figure 7.13. The sequence of snapshots shown in figure 7.14 shows the entire sound pulse wave propagation in both airfields and plate domains at different simulation times. The color scales are the same as the ones explained in test case 1.
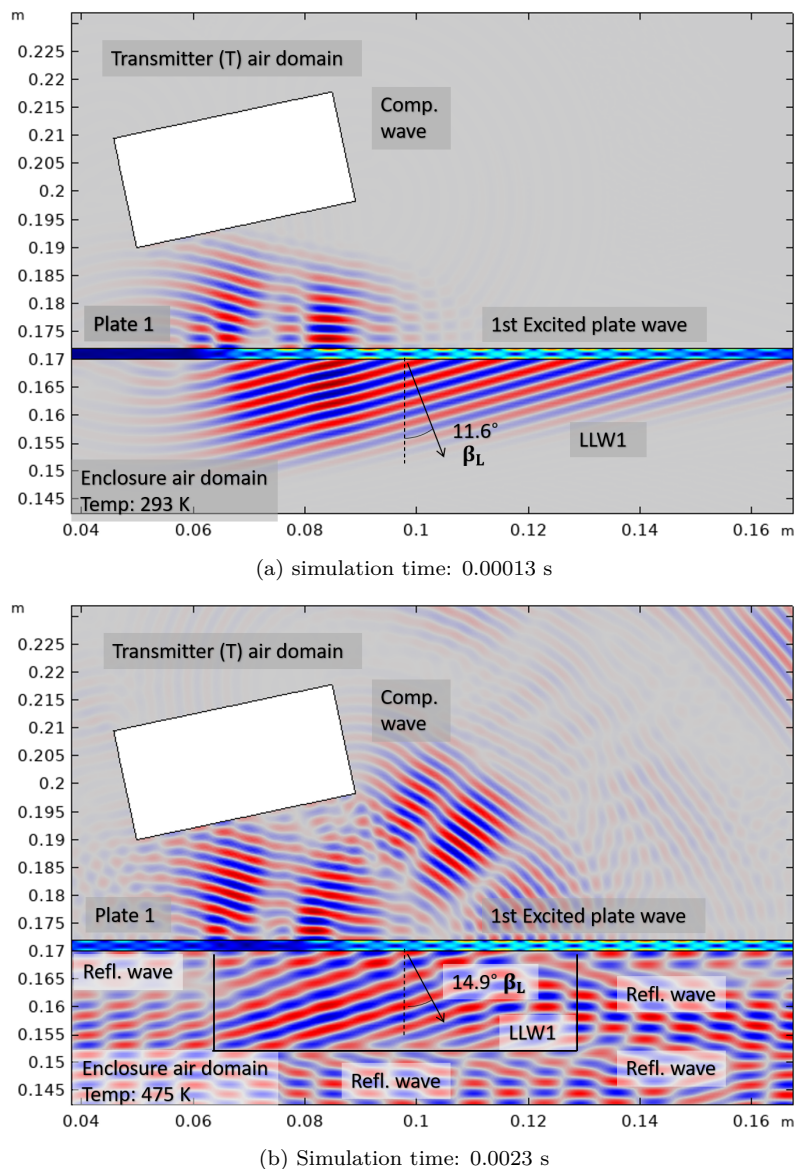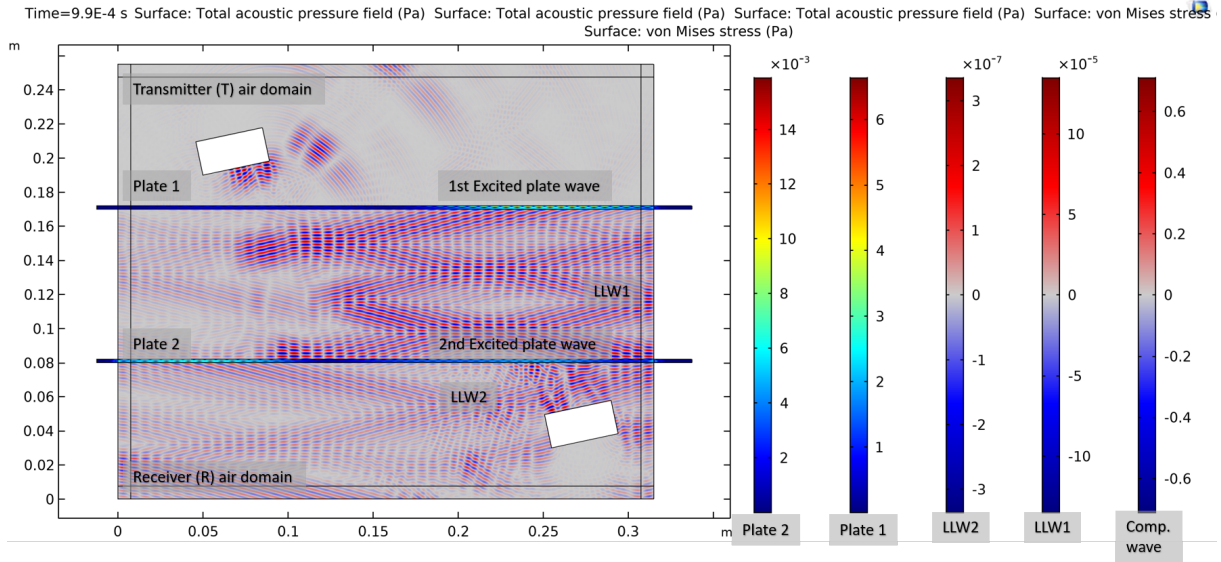

(a) simulation time: 0.00013 s

(b) Simulation time: 0.0023 s

Figure 7.13: Zoomed in snapshots of test case 4 at simulation time 0.00013 (temperature 293 K), and at 0.0023 s (temperature 475 K)

(a) Simulation time: 0.00104 s

(b) Simulation time: 0.002242s

Figure 7.14: Simulation of test case 2

7.4.1 Simulation results and analysis

Figure 7.13 shows two zoomed-in snapshots of the simulation from test case 4 at the simulation time 0.00013 s and 0.0023 s. Figure 7.13a shows the first excited plate Lamb wave and the first leaky Lamb wave "LLW1" propagating across the gap with an excitation angle $\beta_L = 11.6°$. This excitation angle is determined by the acoustic velocities between the plate Lamb wave velocity and air velocity, according to Snell's law. We can see from figure 7.13b that the excitation angle increases ever so slightly to $\beta_L = 14.9°$, due to the temperature increase from 293 K to 475 K.

Figure 7.14 shows the full scale model of test case 4 at different simulations times. Here we can see the consequence from the small excitation angle causing the sound waves to reflect repetitively between the plates. The sent ultrasonic signal may be disrupted by the reflected sound waves, as was thoroughly discussed in the previous test case.

Figure 7.15a is the graph of the sent ultrasonic signal as a boundary load force (F) applied to the transmitter surface. Figure 7.15b is the graph of the received ultrasonic signal as a floating potential (V). Figure 7.15c shows that the speed of sound inside the enclosure domain linearly increases from 343 m/s to 450 m/s after time 0.0011 s, due to the linear temperature increase. The first ultrasonic signal is received with a time delay of 500 μs between the sent signal, as marked by the red dots and arrows. After simulation time 0.0011 s, the received signal pulses in time delay and amplitude due to the temperature increase, especially after the simulation time 0.0015 s. This might be challenging differentiating between a reflected signal and a sent signal, as can be seen on the right-hand side of the graph.
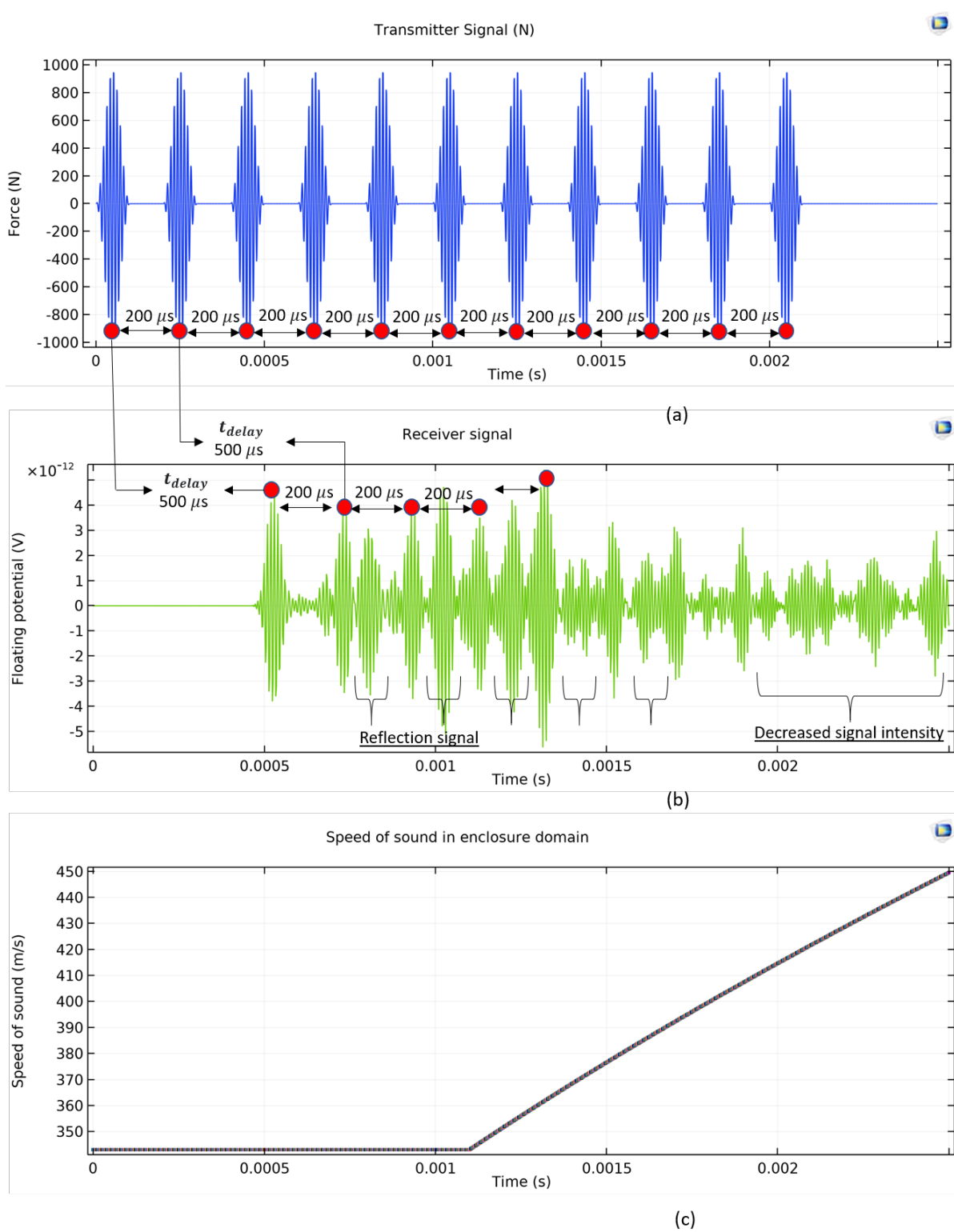
Figure 7.15: test case 4 simulation sent and received signal from transmitter and receiver

7.4.2 Analytical calculation

The analytical model described in chapter 5.3 was used to calculate the change of time delay for test case 4. The temperature increases from 293 K to 500 K over a time period of 1.1 - 2.5 ms. The phase and group velocities for Lamb waves in plates made out of steel material are the same as those found in test case 3 (looking at the dispersion curve figure 7.12, the phase and group velocity was found to approximately be $c_p = 1700m/s$ and $c_g = 1700m/s$, respectively). Since the temperature increases over time, the acoustic velocity of "LLW1" $c_L(t)$, the excitation angle β_L, the propagation distance between the plates $L(t)$ increases over time. This will affect the sound wave transit times $t_L(t)$, $t_g(t)$, and finally $t_{delay}(t)$. Table 7.4 shows how each of these variables changes over time with temperature increase. the multi figure 7.16 contains graphs of the variables as a function of temperature.

Table 7.4: Analytical calculation for the time delay, test case 4

Variable	Equation used						unit
Time	Defined in simulation	1.10	1.45	1.80	2.15	2.50	[ms]
Temperature $T(t)$	Defined in simulation	293	350	400	450	500	[K]
$c_L(t)$	(5.7)	343.0	375.1	401.0	425.3	448.3	[m/s]
$\beta_L(t)$	(5.8)	11.6	12.7	13.6	14.5	15.3	[deg]
$L(t)$	(5.9)	91.9	92.3	92.6	93.0	93.3	[mm]
$t_L(t)$	(5.10)	262.2	241.9	227.4	215.7	204.9	[μs]
$t_g(t)$	(5.11)	77.3	76.3	75.4	74.6	73.8	[μs]
$t_{delay}(t)$	(5.12)	514.3	493.0	477.6	465.1	453.5	[μs]

Figure 7.16: Test case 4 analytical calculation of the variables as a function of temperature. (a) speed of sound inside enclosure domain $c_L(t)$, (b) excitation angle β_L, (c) propagation path distance between the plates L, (d) transit time between the plates t_L, (e) transit time of 2nd excited plate Lamb wave propagation along plate 2 t_g, (f) total time delay between send and received ultrasound signal t_{delay}

7.4.3 Discussion

We can see that the received signal graph in figure 7.15b are different than the received signal from the previous test case 3 in fig 7.11b. The signal in this test case is less consistent, and the intensity of the signal decreases after some time. Therefore, it is clear that the increase of the temperature affects the ultrasonic sound wave as it propagates through the enclosure domain.

It was initially expected to see a decreased time delay between sent and received signal, as the temperature and speed of sound increases. However, after the simulation time of 0.0013, it becomes rather difficult to differentiate between the sent ultrasound pulses and the reflected pulses. Therefore, it is hard to see if the time delay decreases or increases over time. The difficulty of analyzing the signal is quite unfortunate because this complicates the logic behind how the signal can convey the information that there is an arc inside the enclosure or not. As of now, there is no clear indication in the signal that the temperature has risen or not, other than that the signal decreased in intensity.

The analytical calculation shown in figure 7.16, demonstrates in theory that all the sound wave transit times t_L, t_L and T_{delay} reduces as the temperature increases, albeit a slight reduction, it is the expected result in theory.

It was explained in the previous test cases that a possible solution to reduce the reflections is to modify the frequency. So that the Lamb wave phase velocity is similar in value to the acoustic velocity of air, this will increase the excitation angle β_L. However, it is important that the phase velocity is not too close in value to the acoustic velocity, as this causes problems with the excitation angle varying too much as the temperature increase (this consequence was observed in test case 2).

We can compare the analytical calculations between test case 2 (orange lines) and test case 4 (blue lines) by plotting the graphs together, as shown in figure 7.17. By this comparison it is easy to see how influential the material properties are to the variables, especially the excitation angle β_L. Although both test case 2 and test case 4 had the same ultrasound frequency, and the same temperature increase, the test cases gave vastly different results of the variables ($L(t)$, $\beta_L(t)$, $L(t)$, $t_L(t)$, $t_g(t)$, t_{delay}), as shown by the graph comparison figure 7.17.

The graphs in figure 7.17 truly illustrate how important it is to be aware of all the factors that influence the variables. Thus far in the report, the main factors that have been discussed to have an influence on the time delay are as follows: The frequency f, the material properties like elastic constant and density, plate thickness, propagation distance between the plates L, the increase in temperature, and more. All of these factors influence the generation plate lamb wave and its associated excitation angle β_L. All factors need to be carefully considered and tuned in order to optimize the transmission and detection of the ultrasonic signal by non-intrusive transducers.

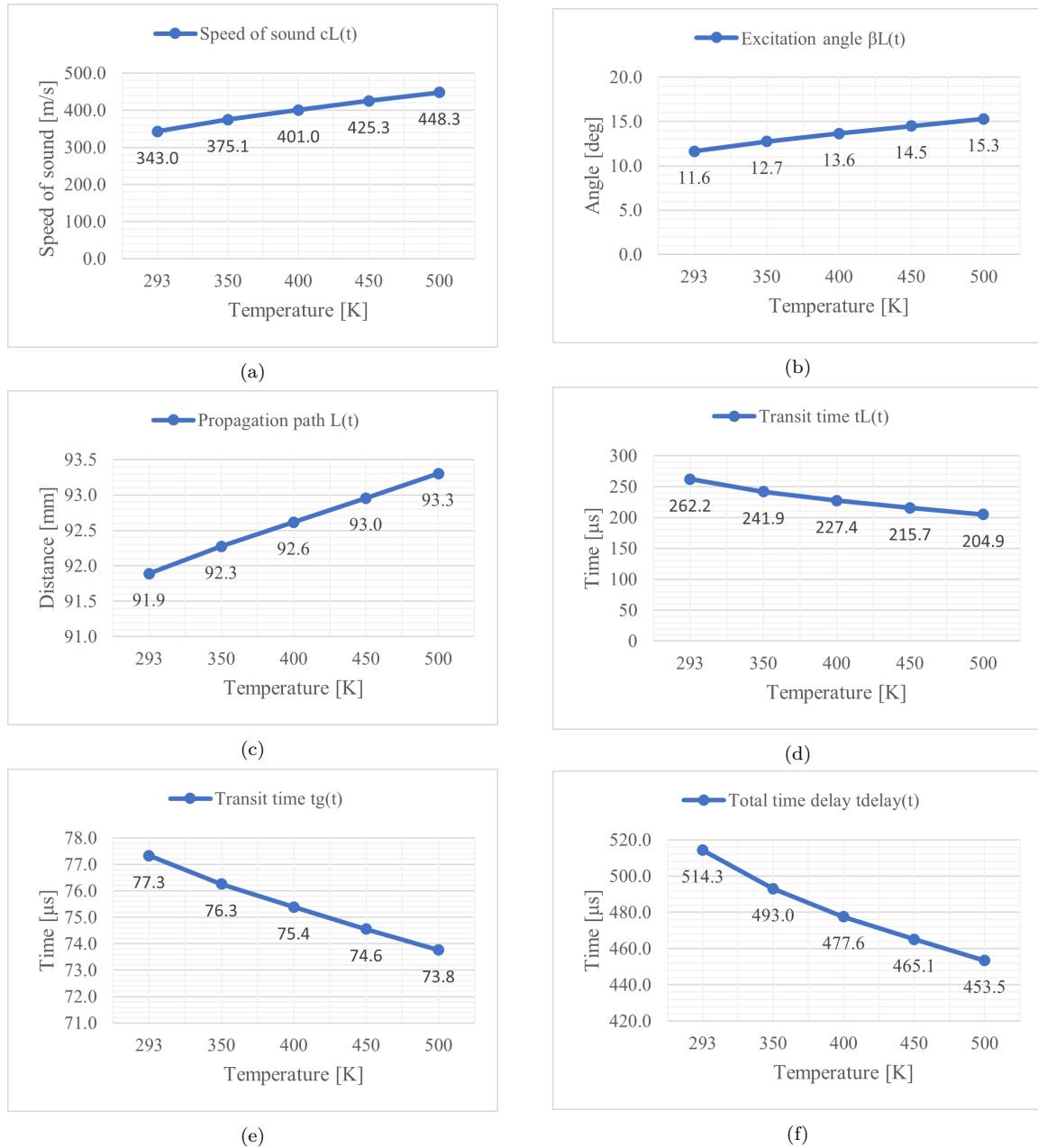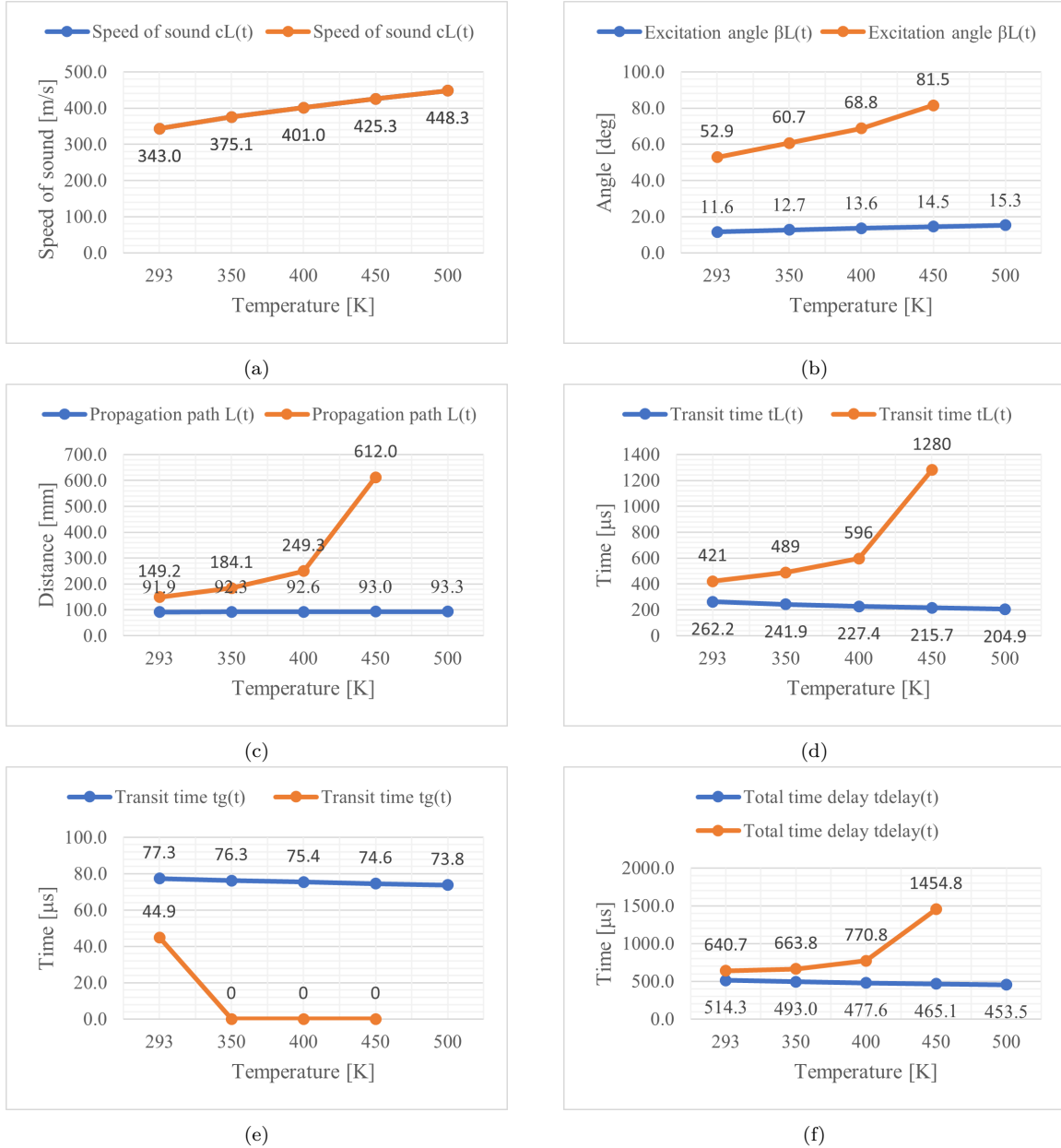Figure 7.17: Test case 4 (blue) and test case 2 (orange) analytical calculation of the variables as a function of temperature. (a) speed of sound inside enclosure domain $c_L(t)$, (b) excitation angle β_L, (c) propagation path distance between the plates L, (d) transit time between the plates t_L, (e) transit time of 2nd excited plate Lamb wave propagation along plate 2 t_g, (f) total time delay between send and received ultrasound signal t_{delay}

7.5 Test case 5: Steel box with obstacles - increase temperature

The model developed in test case 5 is an extension of the model in test case 4. This model has added sidewalls (also 2 mm thick), making it a test case where we investigate sound transmission through a steel box. In addition to the sidewalls, some objects of obstruction have been added inside the enclosure. The purpose of this test case is to get a bit closer to the realistic conditions associated with switchgear. Switchgear is built as a metal enclosure consisting of power conduction components and protection switches equipment. So naturally, switchgear contains many objects that that can cause reflections of the sound waves in all types of angles. Therefore, it will be interesting to see how the ultrasound signal will be affected when there are some obstacles in the way. Note that the obstacles are of no particular size nor shape. The plate materials are made of the same stainless steel properties as given in table 6.3. The inside the enclosure increases in temperature from 293 K to 500 K over time 1.1 - 2.5 ms, the same as the previous test cases. Figure 7.18 shows the developed COMSOL model of test case 5. The sequence of snapshots shown in figure 7.19 shows the entire sound pulse wave propagation in both airfields and plate domains at different simulation times. The color scales are the same as the ones explained in test case 1.
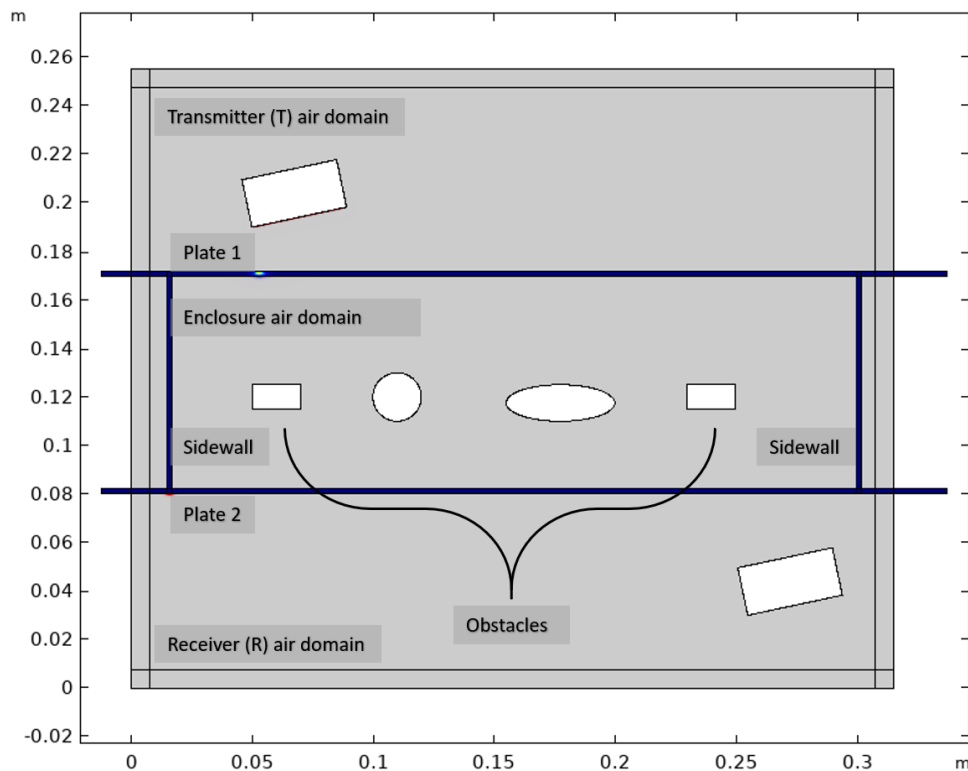
Figure 7.18: Test case 5 steel plates with sidewalls and obstacles inside the enclosure domain
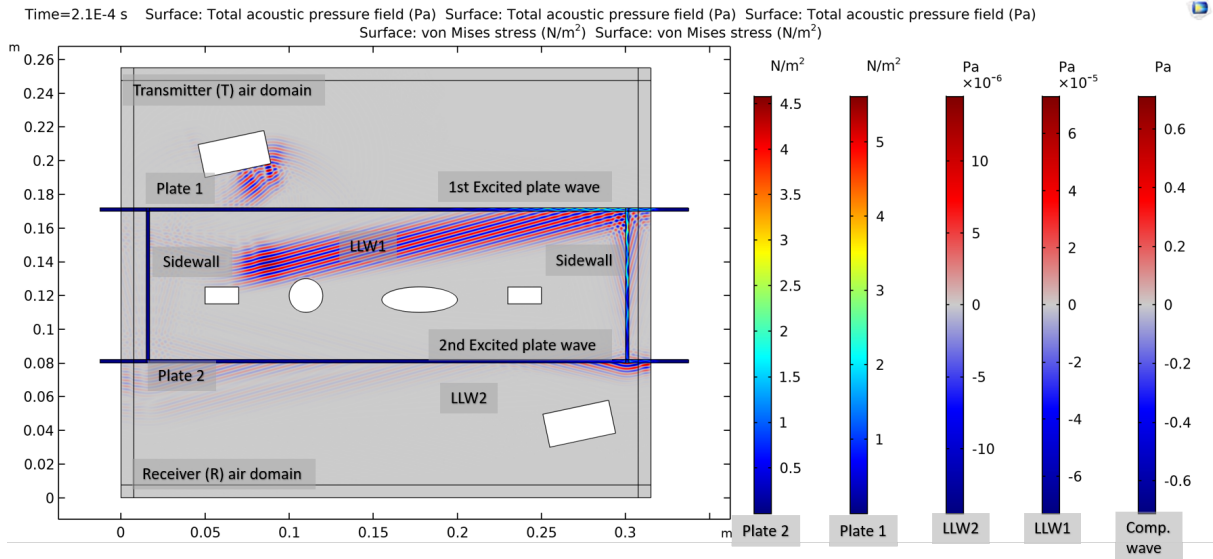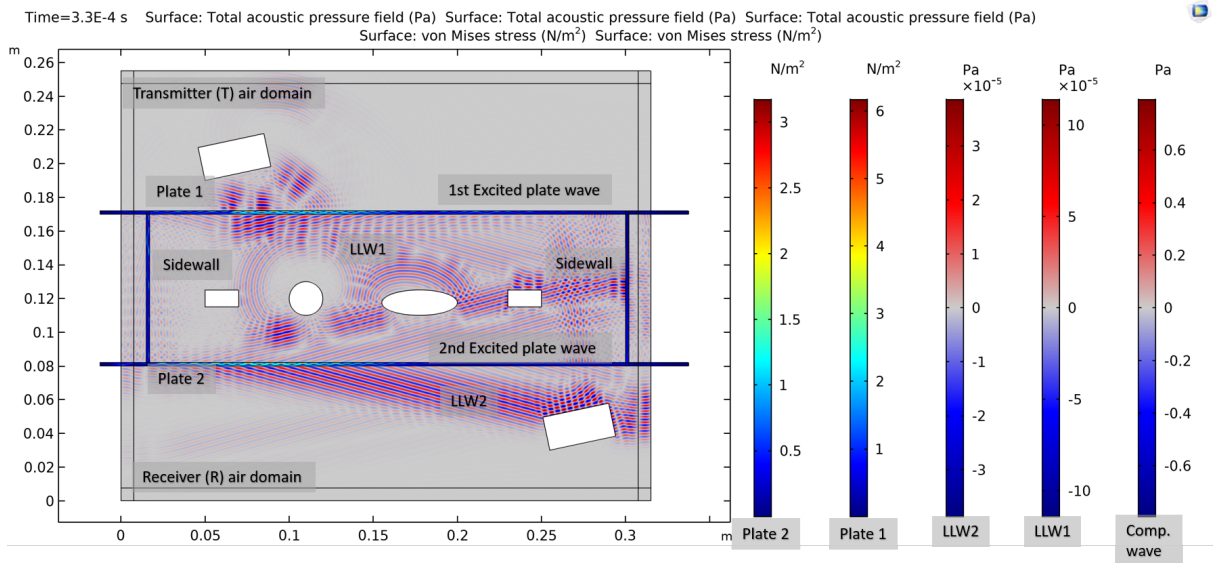
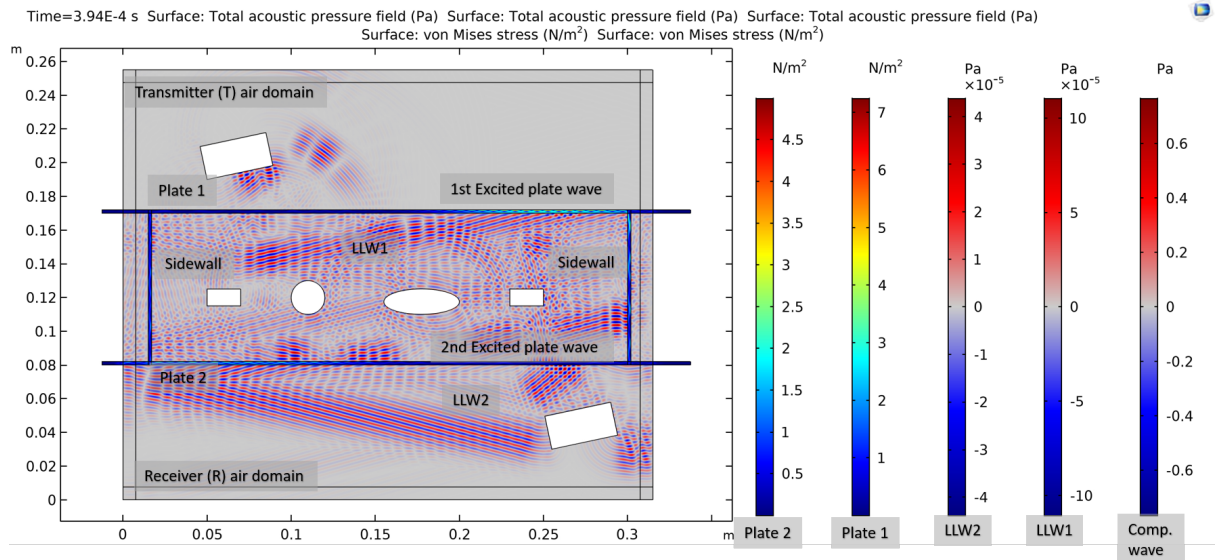(a) Simulation time: 2.1E-4 s
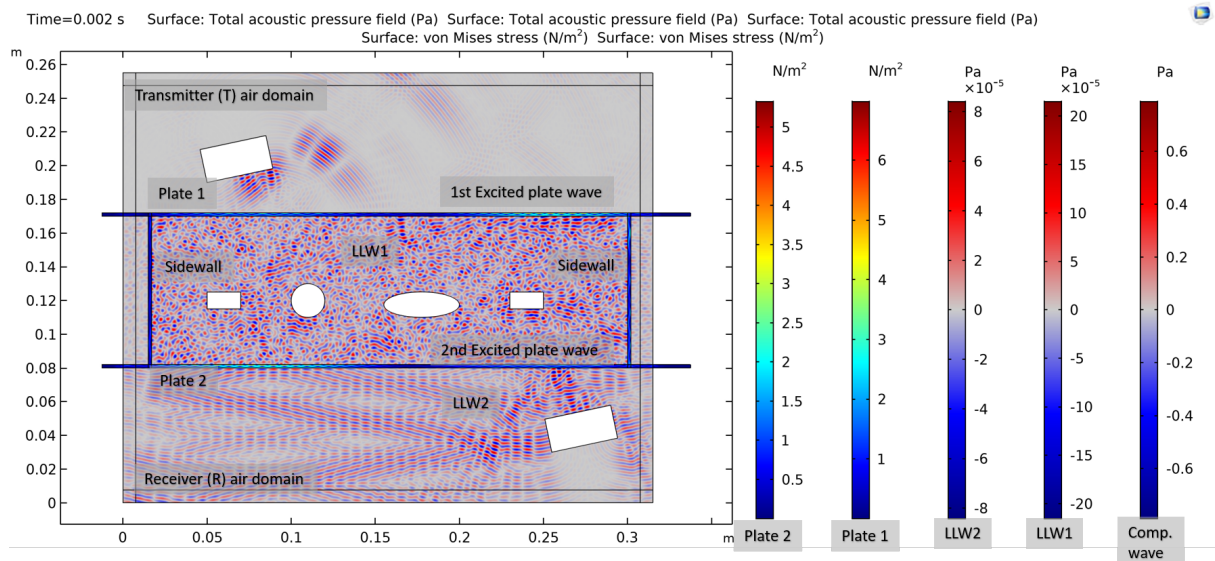

(b) Simulation time: 3.9E-4 s

(c) Simulation time: 0.00107

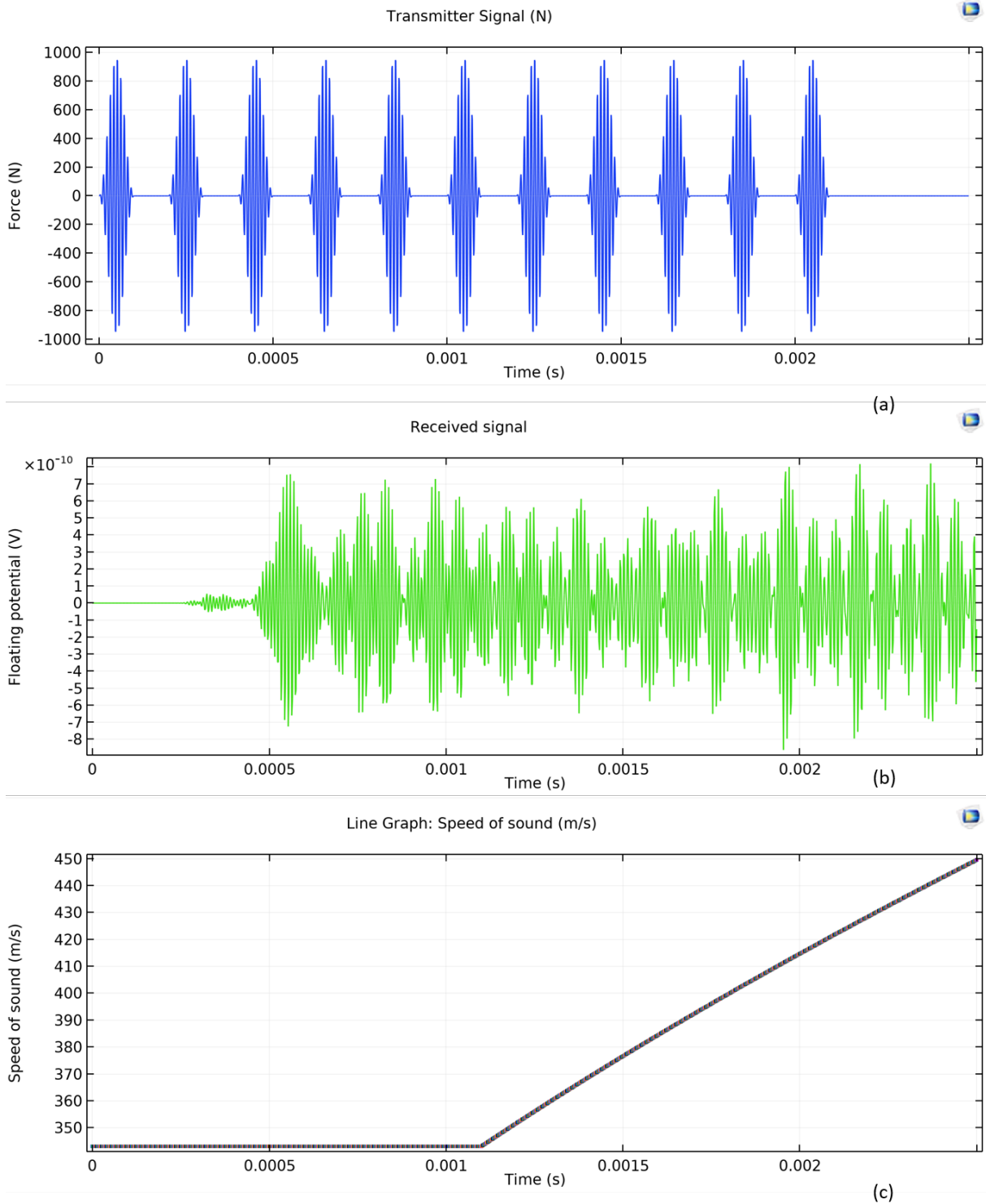(d) Simulation time: 0.002

Figure 7.19: Simulation of test case 5

Figure 7.20: Test case 5 simulation sent and received signal from transmitter and receiver, and speed of sound increase due to temperature rise

7.5.1 Simulation results and analysis

The excitation and propagation of the Lamb waves occur in the same manner as the previous test cases. However, this test case now includes the sidewalls and obstacles inside the enclosure. The simulations in figure 7.19 show how the obstacles and the sidewalls cause more reflections than the previous test cases. As the compressional wave "LLW1" travels in the direction of plate 2, some of the sound wave pulse energy gets reflected by the placed obstacles. Over time the sound waves pulses become less distinguishable due to the high number of reflected sound waves traveling inside the enclosure. It can also be seen from the figures that the sidewalls extend the plate Lamb wave propagation path. Once the Lamb wave is excited in plate 1, it will propagate along with the plate and turn the corner to propagate along the sidewall. The Lamb wave continues to propagate down the sidewall and turn the corner to plate 2. Eventually, traveling a full circle around the steel box, and simultaneously leak Lamb wave energy into the adjacent air.

Figure 7.20 shows graphs of the sent and received ultrasonic from the transmitter and receiver, and speed of sound increase due to temperature rise within the enclosure domain. The received signal in this test case is quite different from the previous test case, due to the rapid reflections exposes the receiver to a substantial amount of noise.

7.5.2 Discussion

The analytical calculation is excluded in this test case because the results would have been identical to the results from test case 4. The analytical calculation is unnecessary in this test case anyway, because the primary purpose of this test case is to see what happens to ultrasonic sound waves when the model includes sidewalls and obstacles. The simulation results showed that sidewalls and obstacles inside the switchgear walls produced more sound wave reflections than previous test cases. The reflection sound waves expose the receiver to a great deal of noisy signals. We can see from the received signal that it has become increasingly more difficult differentiating between a reflection signal and an actual sent signal from the transmitter.

From all of the test cases that have been shown so far, we can see a trend emerging from the results. The more complexity is added to the models, the more difficult it is to evaluate the signal and detect the conditions associated with an internal arc fault. The received signal from previous test cases showed some indication of an increase in temperature by either a change in the time delay between sent and received signal, or a decreased signal intensity. The received signal in this test case, however, does not show any distinct indication for neither of the conditions. By adding complexity to the model (obstacles and sidewalls) it will result in more complex received signals, that would require filtering and signal processing in order to remove the noise.

7.6 Test case 6: Analytical calculation with switchgear dimensions

So far, the test cases have been limited to test models that are minuscule in dimensions compared to the dimensions of a switchgear. The reason If COMSOL were to run a complete simulation of the entire ultrasound wave path at the length of a switchgear, then COMSOL would have spent 5-6 days on computation time. Regardless, the test cases has thus far shown the feasibility of sound transmission through the thickness of a switchgear wall, and how conditions like temperature affect the ultrasound signal, which is the main objective of this thesis. The results from test cases 1, 2 and 3 showed that there was a reasonably good agreement between the simulated time delay and analytical calculated time delay.

In any case, it would be interesting to investigate what the potential time delay between sent and received signal inside a switchgear enclosure might be. Therefore, this test case will do an analytical calculation of the typical switchgear dimension. Figure 7.21 shows a picture of a non-commercial 12 kV switchgear where most of the electrical equipment has been removed for the purpose of conducting physical testing.
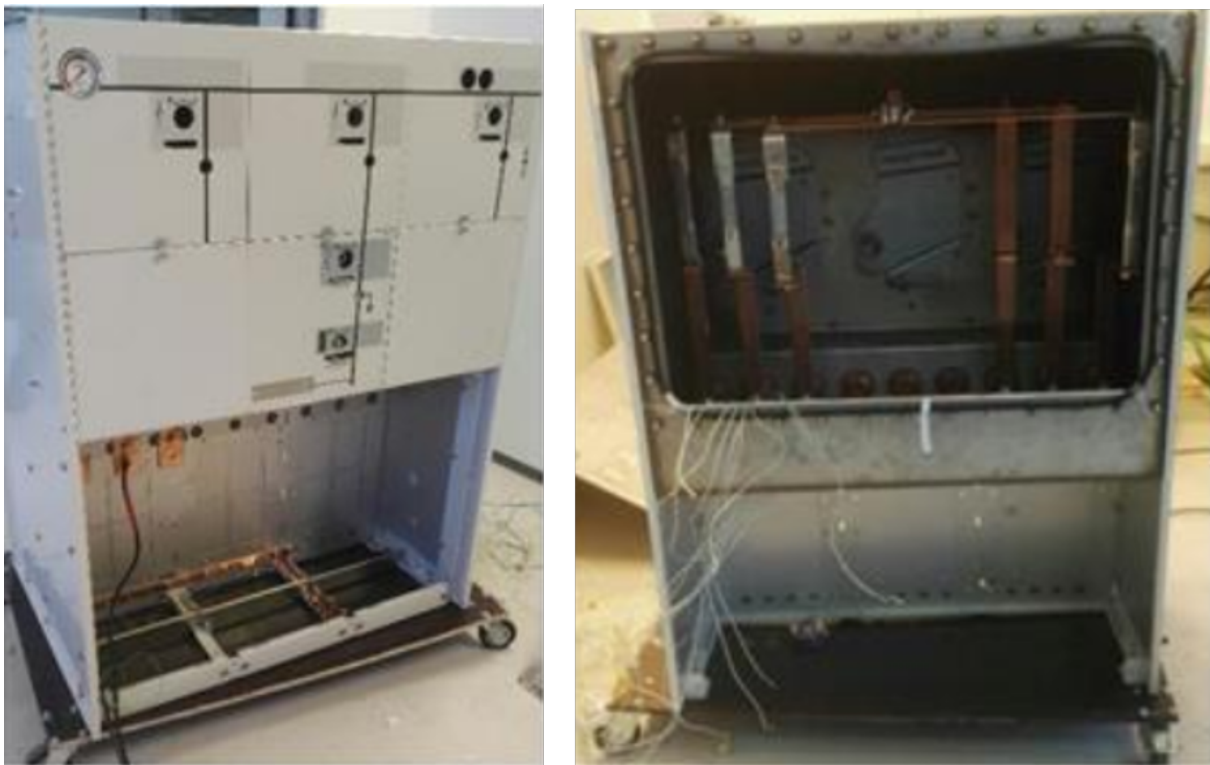

Figure 7.21: Picture of a non-commercial 12 kV switchgear, where most of the electrical equipment has been removed

Typically manufactured switchgear, like the one shown in the figure, has a height of about 1.3 meters. The width may vary depending on the number of modules that are included, and the depth of switchgear are typically 0.5 meters. Since the width of switchgear may vary, it might be more representative to do the analytical calculation based on the switchgear depth.

The analytical model described in chapter 5.3 was used to calculate the change of time delay for test case 6, where the distance between the switchgear walls is based on a typical representative switchgear depth $D = 500\,mm$. The temperature increases from 293 K to 500 K over a time period of 1.1 - 2.5 ms. The phase and group velocities in the steel plates from test case 3 and 4 is used in this model($c_p = 1700m/s$ and $c_g = 1700m/s$). Table 7.5 shows how each variable changes over time as temperature increases. The multifigure 7.22 contains the graphs of the variables as a function of temperature.

Table 7.5: Analytical calculation for the time delay, test case 6

Variable	Equation used						unit
Time	Defined in simulation	1.10	1.45	1.80	2.15	2.50	[ms]
Temperature $T(t)$	Defined in simulation	293	350	400	450	500	[K]
$c_L(t)$	(5.7)	343.0	375.1	401.0	425.3	448.3	[m/s]
$\beta_L(t)$	(5.8)	11.6	12.7	13.6	14.5	15.3	[deg]
$L(t)$	(5.9)	510.5	512.6	514.5	516.4	518.4	[mm]
$t_L(t)$	(5.10)	1346	1250	1188	1133	1086	[μs]
$t_g(t)$	(5.11)	27.6	21.7	16.8	12.2	7.8	[μs]
$t_{delay}(t)$	(5.12)	1548	1446	1379	1320	1268	[μs]

The results from the analytical model show that an ultrasound uses 1.548 ms to travel across the depth $D = 500mm$ of a switchgear. As temperature increases over time, time reduces to 1.268 ms. This change of time delay can be used as information to trip an earthing switch. These values might be acceptable in the real case of interrupting an internal arc fault. It was explained in the theory chapter active limiting systems, an arc fault detection sensor should be capable of detecting an arc fault within a general max time of 5-10 ms, which the analytical calculation results of this model indeed are within.

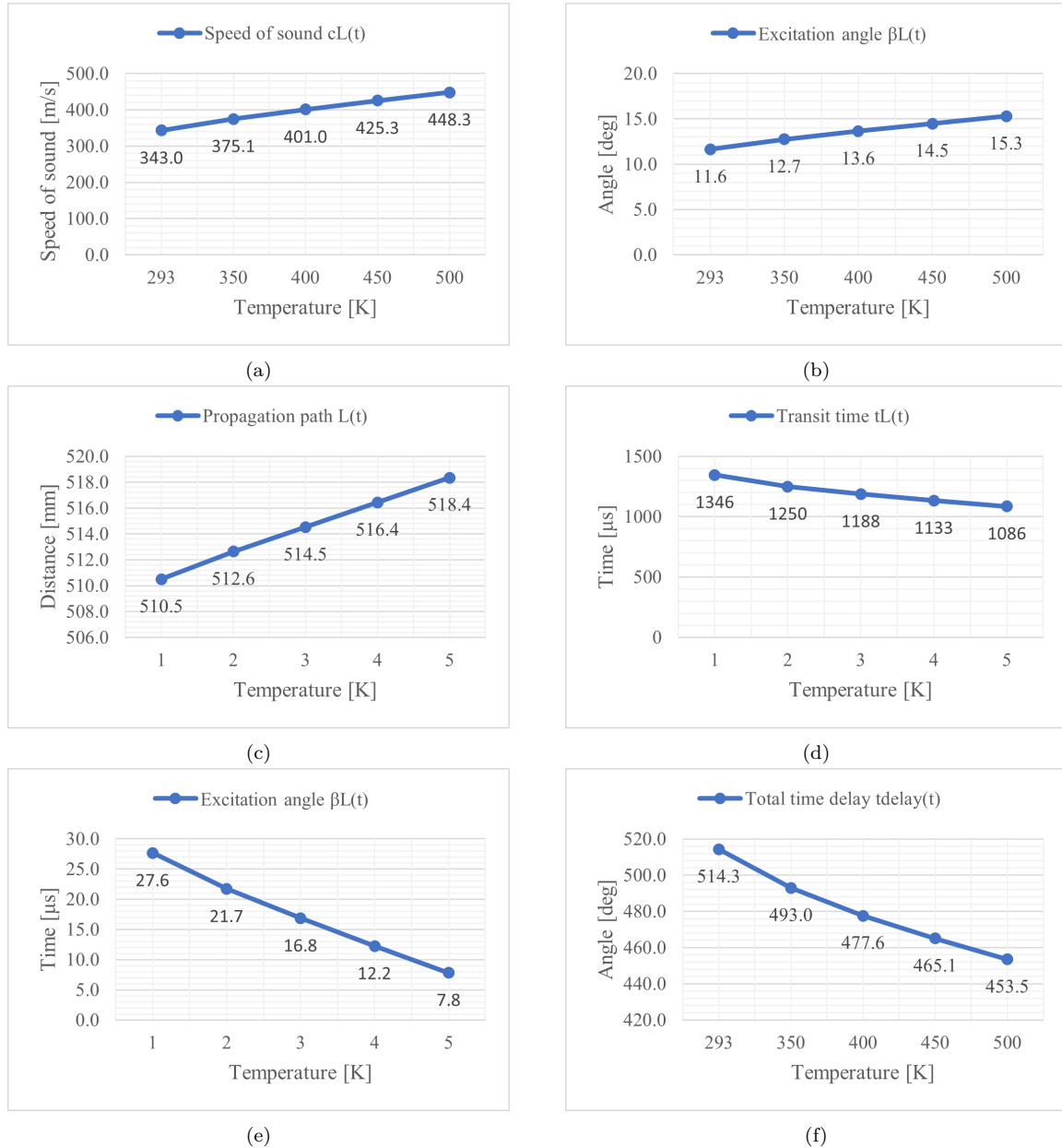Figure 7.22: Test case 6 analytical calculation of the variables as a function of temperature. (a) speed of sound inside enclosure domain $c_L(t)$, (b) excitation angle β_L, (c) propagation path distance between the plates L, (d) transit time between the plates t_L, (e) transit time of 2nd excited plate Lamb wave propagation along plate 2 t_g, (f) total time delay between send and received ultrasound signal t_{delay}

However, it is important to note that these calculations are based on ideal assumptions, and many variables have been neglected. From this it is hard to draw a meaningful conclusion on whether internal arc fault can be detected by ultrasonic transducers. There are more factors that need to be considered because they may influence the propagation of ultrasound. For example, the distribution of heat, and obstacles, in the ultrasound propagation path. It is not realistic to assume that the temperature increase is evenly distributed inside the enclosure. Heat distributes through heat transfer mechanisms like radiation, convection and conduction, which are a dynamic system that also have many factors influencing the distribution. Switchgear consist of numerous electrical equipment which can cause a substantial amount of reflections of the sound wave propagation path. In order to get a more realistic picture of the problem it would be helpful to look at studies done on switchgear heat distribution, and get an inside view of the switchgear compartment.

In 2015, E. Fjeld, W. Rondeel, K. Vaagsaether, M. Saxegaard, P. Skryten and E. Attar did an interesting study in "Thermal design of future medium voltage switchgear" published in[29], where they investigate the thermal design of a non-commercial switchgear by taking temperature measurements, calculations based on empirical guidelines given in IEC TR 60890, and running CFD simulations. The methods was used to evaluate whether the test object will pass the test criteria given by the international standard IEC 62271-1, and gain insight in improving the thermal design of a medium voltage switchgear. [29]
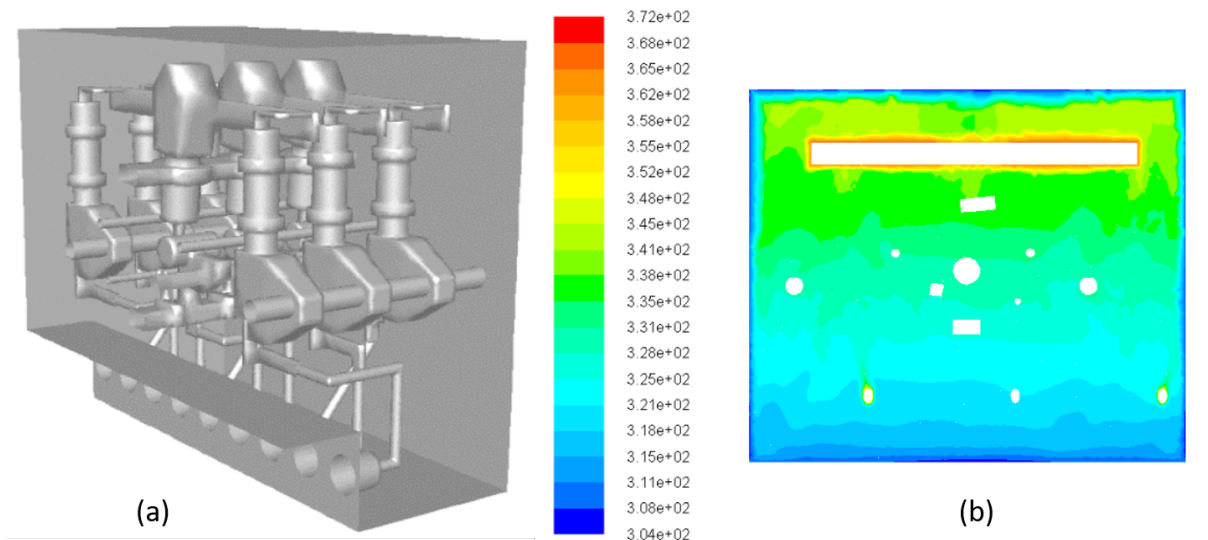

Figure 7.23: (a) The simulation domain giving an insight of the non-commercial 3 module 12 kv switchgear. (b) CFD simulations carried out by ANSYS-Fluent software shows the thermal profile of the switchgear during nominal operations [29]

The test object was a 12 kV non-commercial switchgear with three modules. Simulations were performed for thermal evaluation of the switchgear. Figure 7.23a shows the simulation domain with some outer walls removed. [29] Figure 7.23b shows CFD simulations of the thermal profile of the switchgear. The CFD simulations were carried out by the ANSYS-Fluent software. [29]

It was mentioned earlier that it would be helpful to look at studies done on the heat distribution, and what are the potential obstacle in a switchgear. This will give better insight into the problem. Figure 7.23a can be used as an example of potential obstacles that exist inside a switchgear. The figure clearly illustrates how tight it is between the electrical components, which raises a concern for the ultrasonic sound propagation path. We have seen from the previous test case 5 that obstacles produce extra noise to the received signal, which complicates the evaluation of the signal in the event of an internal arc fault. It is important for the quality of the received signal that the ultrasonic propagation path has minimal objects of obstruction on its path. Figure 7.23 illustrates the non-homogeneous nature of temperature distribution inside a switchgear. Since the speed of sound is a function of temperature, it would be beneficial if the propagation path was close to the heat source. Judging from this figure, it may be strategic for the ultrasonic signal to travel horizontally rather than vertically so that the signal may travel in an almost consistent temperature gradient. But once again, it is important to consider the obstacles before selecting a propagation path. Therefore, it is recommended to further investigate the topic by conducting proper CFD simulations and map out where the ultrasound transducers shall be pointed.

Another switchgear construction factor that is important to consider is the double sidewalls. Gas-insulated switchgear is often constructed with double walls at the width sides. The double walls consist of outer aluminum sheets and the gas-filled tank made out of steel. There is a 5 mm air gap between the double walls. It would not be recommended to install an ultrasound transducer outside the double walls, as it would be highly unlikely that any of the ultrasound can transmit through the double walls, not even if they are Lamb waves. Therefore, the ultrasound transducers need to be positioned where there are no double walls, i.e. from the front to the back of a switchgear, or top to bottom.

8 Discussion

When this master project was suggested, it was initially planned that physical experiments with ultrasonic sound transducers were to be conducted. However, during the literature research, it was quickly discovered what the main challenge of the acoustic physics of non-intrusive ultrasonic detection of an internal arc fault. When sound wave crosses over the interface between different material with a large difference in acoustic impedance, it will result in reflections, as was described in the theory chapters. So, in order to minimize the reflections and transfer as much of the sound wave energy through the metal plate, the metal plate can be excited with leaky Lamb waves. Lamb wave excitation was not possible to execute with the ultrasonic transducer that was provided at the time (Arduino ultrasonic sensor HC-SR04), as this had a considerably small voltage supply of only 5V. If the physical tests on the concept were to be conducted, one would need an ultrasonic transducer that has a voltage supply in the 100s (+ filters, pulse generator, energy supply). Therefore, it was decided that the investigation of non-intrusive ultrasonic electric arc detection was to be simulated in COMSOL Multiphysics instead.

Through COMSOL simulations, it was shown that the theory of sound transmission through dense materials like metal was possible by the use of Lamb waves. However, as the project progressed, it was discovered that the concept has several issues that raise some concerns about the reliability of arc fault detection by ultrasonic transducers. It was expected that the time delay between the sent and the received signal would reduce as the temperature increases. However, the received signal got more complex and noisy as the models expanded in complexity. Especially in test cases 3, 4, and 5, it became increasingly difficult to evaluate the received signal and find a clear indication that the temperature had increased inside the enclosure domain. A possible reason behind the challenge is that the receiver was exposed to large amounts of sound wave reflections. Sound wave reflections will be challenging to avoid in switchgear, as shown in figure 7.23a, where the compartment space is tightly filled with electrical components. Careful consideration regarding where to point the ultrasonic transducers in the switchgear must be done. In order to optimize the received signal quality, point the ultrasonic wave propagation in a direction where there is the least amount of obstacles. Nevertheless, it is also important not to direct the sound waves too far away from where an electric arc may occur because the sound waves depend on being affected by a temperature rise in order to detect an arc fault. Knowledge about how the heat distributes during an internal arc fault is also an essential factor that affects the feasibility of the concept.

This thesis assumed temperature to be evenly distributed as the temperature increased, but this is not realistic conditions.

It is well known that the heat produced from the electric arc is distributed in a non-homogeneous way. The temperature distribution over time can be simulated through CFD computation, which is out of scope in this thesis. However, it is important to know that this is a critical part in order to prove the feasibility since the speed of sound is a function of temperature. If the heat generated from the electric arc does not cover a large enough area over the sound propagation path, the sound wave will not increase in speed and will therefore imprecisely not detect the fault. Therefore, CFD simulations are necessary in order to accurately determine the time delay between sent and received ultrasonic signal, since it can accurately compute how much of the propagation path is subjected to the heat produced from an arc fault.

The difficulty of signal evaluation for the detection of temperature increase, which was expressed in test cases 3, 4, and 5, can maybe be solved with proper filtering and signal processing of the received signal, which is out of scope for this master thesis.

As described in theory, Lamb waves are dispersive. The angle of the ultrasonic transducers needs to be carefully oriented in order to optimize sound transmission. The angle used for steel plate test cases was 11.6 °. This proved to be an unfortunate angle to use as this caused reflections between the transducer and plates. The angle used in polycarbonate plate test cases was 52.9 °, which showed a better outcome with less reflection between transducer and plates. The angle can be modified by calibrating the frequency in accordance with the dispersion curves of steel. The dispersion curves of switchgear steel walls should be determined through experimental testing with different sound frequencies in order to accurately optimize sound transmission.

Although the concept of non-intrusive ultrasonic arc fault detection might work in theory, analytical calculations and COMSOL simulations cannot prove the feasibility of the concept alone. Physical experiments are needed in order to confirm the theory and simulations.

From all the uncertainties and issues that have been discovered in this thesis, it is important to consider if the concept is realistically feasible in regard to reliable arc detection. Further research and studies must be done before the method can be used as a reliable arc fault detection system. Since an internal arc fault is the most severe hazard that can happen inside a switchgear, which can cause significant damage to equipment and people, it is critical to test the reliability of the sensor by thorough studies. So far, this task has discovered problems that may indicate that the reliability of a non-intrusive ultrasound sensor may be significantly weaker compared to the pressure sensor and the light sensor. Although ultrasonic sensors might have the benefit of being non-intrusive, meaning it is easy and cheap to install/replace and maintain, it is expected that the equipment can maintain its service throughout its lifetime. An

ultrasonic transducer placed outside of the switchgear might be exposed to external hazards and disturbance that reduces the reliability of the sensor. In contrast, the pressure sensor and the light sensors are protected from any external disturbance. The thesis has described that the ultrasonic sensor is sensitive to so many factors (e.g., angle orientation of the transducer, obstacles that cause reflections, uncertain heat distribution from the arc, signal noise, placement of the transducers, and more).

Although the topic of using non-intrusive transducers on medium voltage switchgear is about the use of electrical instruments on electrical power systems/equipment, it is actually revealed through the complexity of the problem that multidisciplinary knowledge is required to solve it completely. It was shown through theory and test cases that problem that the topic deals with various fields disciplines like acoustics (Lamb waves, NDT ultrasonics, dispersion curves), signal processing (Fourier filtering for sound-to-noise ratio), material technology (Dispersion curves in steel), CFD/Ansys computation of heat distribution due to arc fault.

126

9 Conclusion

9.1 Conclusion

A literature study on internal electric arc fault generation in medium voltage switchgear, limitings systems, and non-intrusive ultrasonic transducers and their applications was carried out in this thesis.

A general working principle on how the theory behind ultrasonic transducers and Lamb waves can be used for non-intrusive internal arc fault detection of medium voltage switchgear was described. Based on the working principle and theory, a simplified model was developed for analytically calculation of the ultrasonic wave propagation path between two solid plates and the time delay between the ultrasonic transducers.

5 test case models were developed in COMSOL Multiphysics® in order to test the theory of ultrasonic sound energy transmission through the solid-air interface using leaky Lamb waves. Each model was extended from the previous in order to investigate the concept of non-intrusive ultrasonic detection of an internal arc fault. The results from the test case simulations were analyzed and compared with analytical calculations from the simplified model. Through simulations, it was revealed that in spite of the significant acoustic impedance mismatch, sound transmission through thin plates like polycarbonate and steel is possible by the method of exciting the plates with a Lamb wave at a defined angle, according to Snell's law. The simulated time delay between sent and received ultrasonic sound pulse proved to be in good agreement with the theoretical and analytical time calculations, with an approximate accuracy of 95%. However, the results also showed that the more complexity that was added with each iteration of the test cases, the more considerable increase in reflections and noise was subjected to the receiver signal, causing difficulty in evaluating the signal for an indication of temperature increase.

The results from the simulations presented several issues regarding the overall realistic feasibility of utilizing this concept as a reliable arc fault detection system. It is revealed through the complexity of the problem, and the uncertainty of the variables, that multidisciplinary knowledge is required to solve it completely. Because of a lack of detailed modeling and lack of physical experiments confirming the simulation results, the thesis is unable to draw a decisive conclusion on whether ultrasonic transducers can reliably and non-intrusively detect an internal arc fault within medium voltage switchgear.

9.2 Recommendations for further work

The following points are recommendations for further work in order to prove the feasibility of the concept completely:

- CFD or ANSYS simulations of the heat distribution produced from an internal arc should be done in order to determine how much of the sound wave propagation path will be influenced by a temperature increase, and therefore more accurately determine the time delay between sent and received ultrasonic signal.

- Signal processing and filtering of the received signal might help in effectively evaluating the complex signals that occurred in the test cases.

- Material technology research on the switchgear walls to find the optimal ultrasonic transducer frequency and angle, which can reduce reflections between transducer while also optimizing sound transmission through switchgear walls.

- Confirm simulations with physical experiments consisting of the appropriate ultrasonic transducers, pulse generator, voltage supply, and filters.

- Simulate for longer times with real switchgear dimensions.

- Conduct sensitivity analysis on all the variables and factors affecting generation and propagation of ultrasonic Lamb wave.

Bibliography

[1] Z. Fan, W. Jiang and W. M. D. Wright, 'Non-contact ultrasonic gas flow metering using air-coupled leaky lamb waves,' p. 33, Apr. 2018. DOI: `https://doi.org/10.1016/j.ultras.2018.04.008`. (visited on 13/02/2021).

[2] Wikipedia, the free encyclopedia, Electrical breakdown. [Online]. Available: `https://en.wikipedia.org/wiki/Electrical_breakdown` (visited on 23/02/2021).

[3] ——, Electrical arc. [Online]. Available: `https://en.wikipedia.org/wiki/Electric_arc` (visited on 23/02/2021).

[4] S. T. Hagen and E. Fjeld, High Voltage Technology, Course code: EPE1116. University of South-Eastern Norway, 31st May 2017.

[5] W. Rondell and E. Fjeld, 'Ch 10: The electric arc,' Lecture notes from course EPE2419 Physics of Electrical Power Engineering [unpublished], University of South-Eastern Norway, 2020.

[6] Wikipedia, the free encyclopedia, Townsend discharge. [Online]. Available: `https://en.wikipedia.org/wiki/Townsend_discharge` (visited on 10/04/2021).

[7] E. Fjeld, 'Small-scare arc fault testing of medium voltage switchgear,' Doctoral thesis, University of South-Eastern Norway, 10th Jan. 2013, 164 pp. [Online]. Available: . . .

[8] Ministry of Petroleum and Energy. (2015). 'The electricity grid,' [Online]. Available: `https://energifaktanorge.no/en/norsk-energiforsyning/kraftnett` (visited on 03/03/2021).

[9] W. Rondell and E. Fjeld, 'Ch 4: The electric arc,' Lecture notes from course EPE1116 High Voltage Technology [unpublished], University of South-Eastern Norway, 2019.

[10] ——, 'Ch 8: Thermal dimensioning of switchgear,' Lecture notes from course EPE1116 High Voltage Technology [unpublished], University of South-Eastern Norway, 2019.

[11] ABB Electrification Norway AS, Catalog safeplus 36 gas-insulated compact switchgear for ansi markets. [Online]. Available: `https://search.abb.com/library/Download.aspx?DocumentID=1VDD006344%5C%20EN&LanguageCode=en&DocumentPartId=&Action=Launch` (visited on 04/05/2021).

Bibliography

[12] E. Csanyi. (2014). 'Differences between disconnectors, load switchesm switch disconnectors and circuit breakers,' [Online]. Available: `https : / / electrical – engineering – portal . com / disconnectors – load – switches-switch-disconnectors-cbs` (visited on 03/03/2021).

[13] M. Schaak, O. Bischur and T. Stommel, <u>Resistance to intern faults</u>. [Online]. Available: `https://slideplayer.com/slide/702591/` (visited on 05/05/2021).

[14] E. Csanyi, <u>Consequences of internal arc for personal safety and mv electrical equipment</u>, Dec. 2011. [Online]. Available: `https://electrical-engineering-portal.com/consequences-of-internal-arc – for – personal – safety – and – mv – electrical – equipment` (visited on 04/05/2021).

[15] W. Rondell and E. Fjeld, 'Ch 11: Internal arc faults,' Lecture notes from course EPE2419 Physics of Electrical Power Engineering [unpublished], University of South-Eastern Norway, 2020.

[16] Cigré Working Group B3.37, 'Mitigating the effects of arc in m.v. switchgear,' Apr. 2017, ISBN: 978-2-85873-389-7.

[17] A. Sepehri, <u>Medium voltage switchgear arc flash sensors and their applications</u>, Apr. 2020. [Online]. Available: `https : / / switchgearcontent . com / 2020 / 04 / 19 / 1893 / medium – voltage – switchgear – arc – flash – sensors – and – their – applications/` (visited on 04/05/2021).

[18] Cigré Working Group A3.24, 'Tools for the simulation of the effects of the internal arc in transmission and distribution switchgear,' Cigré Tech. Brochure 602, Dec. 2014.

[19] Iowa State University Center for Nondestructive Evaluation (CNDE). (2021). 'Physics of nondestructive evaluation,' [Online]. Available: `https://www.nde-ed.org/Physics/index.xhtml` (visited on 03/02/2021).

[20] S. Jones, 'Ground vibration from underground railways: How simplifying assumptions limit prediction accuracy,' Nov. 2010. [Online]. Available: `https : / / www . researchgate . net / figure / Depiction – of – Rayleigh – wave – showing-elliptic-particle-motion_fig3_280986859` (visited on 03/04/2021).

[21] R. Marks, A. Clarke, C. Featherston, C. Paget and R. Pullin, 'Lamb wave interaction with adhesively bonded stiffeners and disbonds using 3d vibrometry published,' Jan. 2016. [Online]. Available: `https : / / www . researchgate . net / figure / A – diagrammatic – representation – of – symmetrical – and – antisymmetric – wave – modes-A_fig1_290440732` (visited on 03/04/2021).

[22] C. Zera. (). 'The 3 most important properties of sound,' [Online]. Available: `https://soundera.live/the-3-most-important-properties-of-sound/` (visited on 03/04/2021).

[23] J. S. Willam Moebs Samual j. Ling, University Physics Volume 1. Openstax, 2016. [Online]. Available: `https://openstax.org/books/university-physics-volume-1/pages/17-2-speed-of-sound` (visited on 05/04/2021).

[24] H. T. K. Tran, 'Characterization of acoustic material properties using broadband through-transmission technique,' Master's Thesis, University of South-Eastern Norway, 2016.

[25] S. Vázquez, J. Gosálbez, I. Bosch, A. Carrión, C. Gallardo and J. Payá, 'Comparative study of coupling techniques in lamb waves testing of metallic and cementitious plates,' Sep. 2019. [Online]. Available: `https://www.ncbi.nlm.nih.gov/pmc/articles/PMC6806287/` (visited on 10/04/2021).

[26] Wikipedia, the free encyclopedia, Lamb waves. [Online]. Available: `https://en.wikipedia.org/wiki/Lamb_waves` (visited on 10/04/2021).

[27] Š. P., J. Čuntala, J. Lakatoš, A. Kondelová and M. Frívaldský, 'Analysis of field of temperature of power electronic systems in comsol multiphysics environment,' 2007. [Online]. Available: `https://core.ac.uk/download/pdf/295548354.pdf` (visited on 13/02/2021).

[28] M. Soorgee, A. Yousefi-Koma and C. Lissenden, 'Damage detection in bounded fluid loaded plates using piezoelectric fiber composite generated lamb waves,' Dec. 2013. [Online]. Available: `https://www.researchgate.net/publication/292657362_Damage_Detection_in_Bounded_Fluid_Loaded_Plates_Using_Piezoelectric_Fiber_Composite_Generated_Lamb_Waves/citation/download` (visited on 04/04/2021).

[29] E. Fjeld, W. Rondeel, K. Vaagsaether, M. Saxegaard, P. Skryten and E. Attar, 'Thermal design of future medium voltage switchgear,' Proceedings Cired conference, 23rd International Conference on Electricity Distribution, Jun. 2015.

Appendix A

Master's thesis task description

FMH606 Master's Thesis

Title: Internal arc fault detection by non-intrusive means

USN supervisor: Elin Fjeld

External partner: ABB Electrification Norway AS, Skien

Task background:

ABB Electrification Norway is a large producer that offers a wide-ranging portfolio of products, digital solutions and services that improves and innovates the todays electrification technology to be safe, reliable, sustainable and energy efficient.

An internal arc fault is an unintentional discharge of electrical energy within an enclosed power system installation. The energy released from the available short circuit current flowing through the arc leads to temperature- and pressure rise within the enclosure.

Arc fault protection is becoming ever more important for all power system and process industries to maintain safety of personnel and reduce damage to expensive equipment. Since the occurrence of an arc fault is the most serious fault within a power system, and the amount of released arc flash energy is a function of time, it becomes critical to develop fast acting arc fault detection and mitigation technology which can reduce the above mentioned consequences.

Through the years, the innovation of arc fault detection technology has led the development of protection system which earths the fault very quickly (less than 10s of ms). Usually, these methods use light detecting diode fed through a glass fiber network to detect internal arc fault. The limitation of such a detection system is that the switchgear compartment must be accessible for installing the fiber or a diode. This brings lot of challenges when a sealed gas tank of a gas insulated switchgear is involved (accessibility, leakage, reliability of the electronics, cost etc.). It has become a topic of interest to investigate alternate arc fault detection which utilizes other means of sensor technology that may prove to be similar in performance without the above-mentioned limitations.

The proposal for the thesis is as follows. An internal electric arc will generate high temperature at a very fast rate, and the theory is to utilize this temperature rise detection as arc fault detection, non-intrusively. Since the sealed enclosure has its own large thermal capacitance, it needs much longer time to detect the temperature rise by a thermal sensor. But temperature is a condition that affects the speed of sound. The proposal is to use variation in speed of sound to detect few 10s or 100s of degree of temperature rise when the temperature of the arc can go into few thousand of Kelvins. Through utilization of ultrasonic sound sensor and fast acting processing unit (Arduino or RasPI), investigate if this is a potential fast and cost-effective sensor technology that can be placed outside the enclosure/switchgear.

Task description:
This thesis will explore and try to answer different issues regarding:

- Survey on temperature dependence of the speed of sound phenomena.
- Survey on internal electric arc fault and arc fault detection techniques used today.
- Get familiar with the use/programming of Raspberry PI or Arduino
- Build experimental test models of metal enclosed installations with a controlled heating source.
- Conduct an ultrasonic sound test with an ultrasonic emitter and transducer.
- If time allows it, simulate the test result in Comsol.
- If time allows it, test the concept with an arc fault test at NEFI High Power Laboratory

- Discuss the test results and how this knowledge can be used in arc detection and in a working prototype.
- The outcome of the study is intended to be suitable for conference/journal paper, if ABB and USN agrees and the Master's Thesis shall be written in LaTeX. All test results and developed simulation models shall be handed in with the report. Present the thesis work.

Student category: EPE (reserved for Tonje Tollefsen)

The task is suitable for online students (not present at the campus): No

Practical arrangements:
The student must identify what type of hardware that is best suited for the tasks and ABB/USN will contribute with the needed hardware. USN already have suitable switchgear/enclosure that could be used during the first experiments.

Supervision:
As a general rule, the student is entitled to 15-20 hours of supervision. This includes necessary time for the supervisor to prepare for supervision meetings (reading material to be discussed, etc).

Signatures:

Supervisor (date and signature): 1/2-21 *Elin [signature]*

Student (write clearly in all capitalized letters): TONJE TOLLEFSEN

Student (date and signature):

24.01.21 *Tonje Tollefsen [signature]*